



CMS-SUS-23-003

CERN-EP-2025-154
2025/08/20

A general search for supersymmetric particles in scenarios with compressed mass spectra using proton-proton collisions at $\sqrt{s} = 13 \text{ TeV}$

The CMS Collaboration^{*}

Abstract

A general search is presented for supersymmetric particles (sparticles) in scenarios featuring compressed mass spectra using proton-proton collisions at a center-of-mass energy of 13 TeV, recorded with the CMS detector at the LHC. The analyzed data sample corresponds to an integrated luminosity of 138 fb^{-1} . A wide range of potential sparticle signatures are targeted, including pair production of electroweakinos, sleptons, and top squarks. The search focuses on events with a high transverse momentum system from initial-state-radiation jets recoiling against a potential sparticle system with significant missing transverse momentum. Events are categorized based on their lepton multiplicity, jet multiplicity, number of b-tagged jets, and kinematic variables sensitive to the sparticle masses and mass splittings. The sensitivity extends to higher parent sparticle masses than previously probed at the LHC for production of pairs of electroweakinos, sleptons, and top squarks with mass spectra featuring small mass splittings (compressed mass spectra). The observed results demonstrate agreement with the predictions of the background-only model. Lower mass limits are set at 95% confidence level on production of pairs of electroweakinos, sleptons, and top squarks that extend to 325, 275, and 780 GeV, respectively, for the most favorable compressed mass regime cases.

Submitted to Physical Review D

1 Introduction

The standard model (SM) is a tremendously successful theoretical framework that essentially describes all known phenomena in high-energy physics. With the demonstration of the existence of the Higgs boson [1, 2], the field is at a crossroads. On the one hand, as of yet, there is no direct experimental evidence from colliders for new phenomena beyond the SM (BSM), such as the new fundamental particles envisaged in supersymmetry (SUSY) models [3]. On the other hand, the very existence of the Higgs boson and the presence of dark matter in the universe are compelling motivations for a model such as SUSY to be realized in nature; it can stabilize the Higgs boson mass and has the potential to provide a particle physics explanation for dark matter [4]. It is therefore crucial to confront such possibilities with experiment. Supersymmetry [5–7] has attracted much interest as a result of its perceived strong motivation, its tractability as a weakly coupled theoretical framework for perturbative calculations and thus predictions, and the rich set of potential new experimental signatures.

With a wide variety of search results from the LHC experiments based on the data sets collected in the years 2016–2018, many supersymmetric particle (sparticle) production scenarios have been constrained in their experimentally most favorable realizations [8–37]. These results are primarily in the context of simplified model interpretations. Nevertheless, there is still very strong experimental and phenomenological motivation for a focus on *compressed* sparticle mass spectra, where the mass differences (Δm) between the initially produced (parent) sparticles and the lightest sparticle (LSP) are small. Supersymmetry searches are often least sensitive in corridor regions with small mass differences; if SUSY is to be tested comprehensively, these regions must also be explored. Phenomenologically, the lowest lying states in the electroweakino sector ($\tilde{\chi}_1^0, \tilde{\chi}_1^\pm, \tilde{\chi}_2^0$) may form a nearly mass-degenerate dominantly higgsino-like triplet [38]. This scenario is particularly challenging as a result of the suppressed production cross sections in addition to the compressed mass spectrum, and is attracting much interest [39, 40]. Furthermore, probing slepton production models including those with the SUSY partners of the muon (smuons), could give insight into potential supersymmetric contributions to the muon g-2 measurements [41–43] as calculated in for example [44–46].

A general search for sparticles is performed in proton-proton (pp) collisions at a center-of-mass energy of 13 TeV by the CMS experiment at the CERN LHC. The data were collected from 2016 to 2018, with a total integrated luminosity of 138 fb^{-1} . The focus for this paper is on SUSY scenarios featuring compressed mass spectra, with the LSP expected to be the weakly interacting lightest neutralino, $\tilde{\chi}_1^0$. Only R -parity¹ conserving SUSY scenarios [47], where sparticles are produced in pairs and the LSP is stable, are considered. We target SUSY scenarios that include the associated production of a chargino and neutralino ($\tilde{\chi}_1^\pm \tilde{\chi}_2^0$) and the pair production of charginos, top squarks, and charged sleptons (selectrons or smuons). Observed event yields for various event signatures are also reported in a model-independent manner that does not assume a particular BSM particle production model.

Searching for the production and decays of such sparticles appearing in compressed mass spectra is experimentally challenging, as small mass splittings between sparticles imply that the visible products of those decays will be of low momentum, and can be difficult to reconstruct, or even detect. Normally reliable signatures of SM particles, such as the reconstructed mass of heavy vector bosons, can be significantly distorted when forced off-shell and produced in such decays, thereby degrading our ability to detect them. For decays resulting in weakly interacting massive particles, this can also mean that these invisible decay products will receive very

¹ R -parity is a multiplicative quantum number defined by $R = (-1)^{3B+L+2S}$ where B, L, S are the baryon number, lepton number, and spin, respectively, with all SM particles having $R = +1$ and all sparticles having $R = -1$.

little momentum from the decays of their parents, such that the resulting missing transverse momentum may also be small and indistinguishable from that of backgrounds. The approach taken is primarily kinematic, and a wide range of object multiplicities are used to incorporate the potential decay signatures of the targeted sparticle systems. Events are selected with significant initial-state radiation (ISR), where the high transverse momentum recoil from the ISR can often lead to measurable missing transverse momentum associated with sparticle decays in compressed scenarios, despite each invisible LSP acquiring only a small momentum in the parent rest frame from the parent sparticle decay.

The paper is organized as follows. The CMS detector and event reconstruction are described in Section 2. The SUSY signal and background process modeling and simulation are described in Section 3. The following section (Section 4) describes the selection of physics objects including electrons, muons, jets, b-tagged jets, and b-tagged secondary vertices for use in the analysis. Section 5 describes the kinematic reconstruction of events for this search considering multilepton final states, corresponding to exactly 0, 1, 2, and 3 leptons (electrons or muons) with jets. The event selection and categorization (Section 6) has two elements. Firstly, preselection criteria and event clean-up requirements are applied that remove events that are not consistent with the compressed phase space of interest for the analysis. Secondly, events are categorized into mutually exclusive analysis regions that are defined according to a combination of object multiplicities in the supersymmetric or ISR systems. A fit based on control samples in data used to constrain the background contributions in tests of various signal hypotheses is described in Section 7, including discussion of the treatment of systematic uncertainties. Results are given in Section 8 and the paper is summarized in Section 9. Tabulated results are provided in the HEPData record for this analysis [48].

2 The CMS detector and event reconstruction

A central feature of the CMS detector is a superconducting solenoid of 6 m internal diameter, providing a magnetic field of 3.8 T. Within the volume of the solenoid are a silicon pixel and strip tracker, a lead tungstate crystal electromagnetic calorimeter (ECAL), and a brass and scintillator hadron calorimeter (HCAL), each with a barrel and two endcap sections. Muons are detected using the gas-ionization chambers embedded in the steel flux-return yoke outside the solenoid. A detailed description of the CMS detector, including the definition of the coordinate system used, can be found in Refs. [49, 50].

For this analysis, physics objects, such as jets, electrons, muons, and missing transverse momentum, are considered. The reconstruction and identification of individual particles in an event is performed using the particle-flow algorithm [51] with an optimized combination of information from the various elements of the CMS detector. The energy of photons is directly obtained from the ECAL measurement. Reconstructed energies of electrons are determined from a combination of the electron momentum at the primary interaction vertex as determined by the tracker, the energy of the corresponding ECAL cluster, and the energy sum of all bremsstrahlung photons spatially compatible with the origin of the electron track. The momentum of muons is estimated from the curvature of the corresponding track. The energy of charged hadrons is determined from a combination of their momentum measured in the tracker and the matching ECAL and HCAL energy deposits, corrected for the response of the calorimeters to hadronic showers. Finally, the energy of neutral hadrons is obtained from the corresponding corrected ECAL and HCAL energy.

Hadronic jets are found from these reconstructed particles and clustered using the infrared- and collinear-safe anti- k_T algorithm [52], implemented with the FASTJET package [53]. Jets in

this analysis use the anti- k_T distance parameter of 0.4. Jet momentum is determined as the vector sum of all particle momenta clustered in the jet, and is found from simulation to be within 5–10% of the true momentum over the entire p_T spectrum and detector acceptance. Additional pp interactions within the same or nearby bunch crossings (pileup) can contribute additional tracks and calorimetric energy deposits to the jet momentum. To mitigate this effect, tracks identified as originating from pileup vertices are discarded, and an offset correction is applied to correct for remaining contributions. Jet energy corrections are derived from simulation to equalize the average measured response of jets to that of particle level jets. *In situ* measurements of the momentum balance in dijet, photon+jet, Z+jet, and multijet events are used to account for any residual differences in jet energy scale between data and simulation [54]. Additional selection criteria are applied to each jet to remove jets potentially dominated by anomalous contributions from various subdetector components or reconstruction failures. The ultimate jet energy resolution typically ranges from 15% at 10 GeV, 8% at 100 GeV, to 4% at 1 TeV [54].

The momentum resolution for electrons with p_T of 45 GeV from $Z \rightarrow ee$ decays ranges from 1.7% for barrel electrons that do not generate showers in the tracker to 4.5% for showering electrons in the endcaps [55, 56]. Muons are measured in the pseudorapidity range $|\eta| < 2.4$, with detection planes made using three technologies: drift tubes, cathode strip chambers, and resistive-plate chambers. Matching muons to tracks measured in the silicon tracker results in a relative transverse momentum resolution for muons with $20 < p_T < 100$ GeV of 1.3–2.0% in the barrel and better than 6% in the endcaps. The p_T resolution in the barrel is better than 10% for muons with p_T up to 1 TeV [57].

The missing transverse momentum (\vec{p}_T^{miss}) is defined as the negative vector sum of the transverse momenta of all particle-flow candidates in the event and its magnitude is denoted by p_T^{miss} . Anomalous high- p_T^{miss} events can occur as a result of a variety of reconstruction failures, detector malfunctions, or noncollision backgrounds. Such events are rejected by event filters that are designed to identify more than 85–90% of the spurious high- p_T^{miss} events with a mistagging rate less than 0.1% [58]. The \vec{p}_T^{miss} is modified to account for corrections to the energy scale of the reconstructed jets in the event.

Vertices are reconstructed from tracks according to the deterministic annealing algorithm [59]. The primary vertex is taken to be the vertex corresponding to the hardest scattering in the event, evaluated using tracking information alone, as described in Section 9.4.1 of Ref. [60]. Events are required to have at least one reconstructed vertex with longitudinal position $|z| < 24$ cm and radial position $r < 2$ cm relative to the nominal mean collision point.

Events of interest are selected using a two-tiered trigger system. The first level, composed of custom hardware processors, uses information from the calorimeters and muon detectors to select events at a rate of around 100 kHz within a time interval of less than 4 ms. The second level, known as the high-level trigger, consists of a farm of processors running a version of the full event reconstruction software optimized for fast processing, and reduces the event rate to a few kHz before data storage [61, 62]. The data sample for this analysis was collected in 2016–2018 using inclusive p_T^{miss} triggers with $p_T^{\text{miss}} > 120$ GeV, corresponding to a total integrated luminosity of 138 fb^{-1} of pp collisions.

3 Signal and background simulation

The SUSY signal and SM background processes are simulated using Monte Carlo (MC) event generators. Several different SUSY simplified models are used to study electroweakino, slep-

ton, and top squark production and decay [63–65].

Simulated samples are generated either at leading order (LO) or next-to-leading order (NLO) and use parton distribution functions (PDF) from either the NNPDF3.0 [66] set for 2016 data or the NNPDF3.1 [67] set for 2017 and 2018 data. Hadronization and showering of events in all generated samples are simulated using PYTHIA 8.230 [68]; these use the CUETP8M1, CP2, and CP5 tunes of the underlying-event simulation [69]. All simulations corresponding to 2016 data use the CUETP8M1 tune, the CP2 tune is used for signal simulations corresponding to the 2017 and 2018 data, while the CP5 tune is used for background simulations corresponding to the 2017 and 2018 data. The background events are passed through a full simulation of the CMS apparatus, with the response of the detector modeled using the GEANT4 [70] simulation toolkit. The detector simulation of signal samples is performed with the CMS fast simulation package FASTSIM [71, 72]. Several sets of simulations are processed so that the version of the CMS event reconstruction software used matches the run conditions of the collected data sets. Additional pp collisions from pileup interactions are simulated and overlaid on the main interaction in the MC samples, with vertex distributions that reproduce conditions observed year-to-year in data. There was a trigger inefficiency during 2016 and 2017 caused by a gradual shift in the timing of the inputs of the ECAL first-level trigger in the region $2.5 < |\eta| < 3.0$. The resulting efficiency loss is 10–20% for events containing an electron (a jet) with p_T larger than ≈ 50 (≈ 100) GeV, and is a function of p_T , η , and time. Correction factors are estimated from the data to model this effect in simulation.

For the simplified model based signal models, all SUSY particles other than the electroweakinos, sleptons, or top squarks under study are assumed to be too massive to affect the analysis observables. These simulated samples have sparticle decays with 100% branching fraction to a particular final state and always include the $\tilde{\chi}_1^0$ as the LSP. The signals are all generated using the MADGRAPH5_aMC@NLO (v2.2.2 for 2016 and v2.4.2 for 2017–2018) generator with LO precision and up to two additional partons at the matrix element level [73] and interfaced to PYTHIA for sparticle decay. The production cross sections are computed at NLO plus next-to-leading logarithmic precision with all the other sparticles assumed to be heavy and decoupled using a number of calculations and computational tools [74–81].

For the direct top squark pair production and decay three simplified models are explored: T2tt (with top squark decay via a top quark), T2bW (with the top squark decaying through an intermediate chargino that subsequently decays to a W boson and the lightest neutralino), and T2cc (with top squark decay via a charm quark). A range of top squark and LSP masses is considered with mass differences ranging from 6 to 200 GeV. For the T2tt model when $\Delta m \leq 80$ GeV, where the top quark and the W boson from the top quark decay would both be off-shell, the decay phase space is modeled as a four-body decay ($\tilde{t} \rightarrow bff'\tilde{\chi}_1^0$) whereas for intermediate mass differences, $80 < \Delta m \leq 175$ GeV, where the top quark must be off-shell but the W boson can be resonant, the stop quark decay phase space is modeled as a three-body decay ($\tilde{t} \rightarrow bW\tilde{\chi}_1^0$). For the T2bW model, the mass of the intermediate chargino is set to $\frac{1}{2}[m(\tilde{t}) + m(\tilde{\chi}_1^0)]$. Example diagrams are shown in Figs. 1 and 2.

The primary simplified models for electroweakino production and decay explored assume that a chargino-neutralino pair $\tilde{\chi}_1^\pm\tilde{\chi}_2^0$ (TChiWZ) or a chargino pair $\tilde{\chi}_1^+\tilde{\chi}_1^-$ (TChiWW) is produced. Each chargino decays to a W boson and the $\tilde{\chi}_1^0$, while the second-lightest neutralino, $\tilde{\chi}_2^0$, decays to a Z boson and the $\tilde{\chi}_1^0$, where the $\tilde{\chi}_1^0$ is the LSP. The diagrams for these production and decay processes are shown in Fig. 3. The TChiWZ model has the $\tilde{\chi}_1^\pm$ and $\tilde{\chi}_2^0$ (the initially-produced parent sparticles) with the same mass. For the TChiWW model, the $\tilde{\chi}_1^\pm$'s are pair produced. Interpretations with purely wino- and higgsino-like $\tilde{\chi}_1^\pm$ and $\tilde{\chi}_2^0$ are included for the TChiWZ

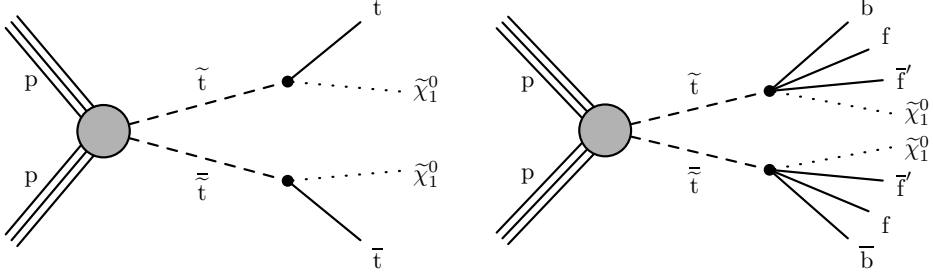


Figure 1: Diagrams for top squark pair production. The left panel shows the T2tt model with decay via top quarks and the right panel illustrates the four-body phase space used in modeling the most compressed region.

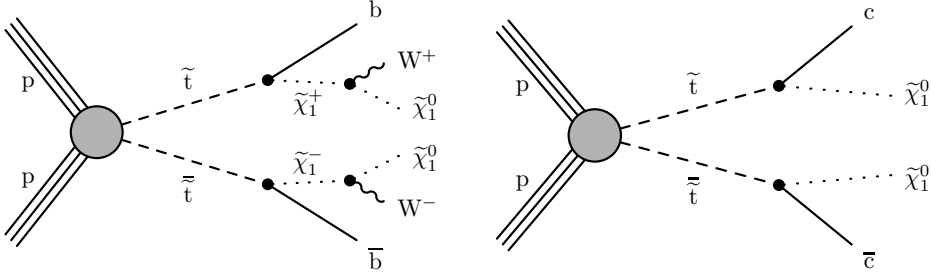


Figure 2: Diagrams for top squark pair production. The left panel shows the T2bW model with decay via an intermediate mass chargino and the right panel shows the T2cc model with decay via charm quarks.

model, while the pure wino-like interpretation is used for TChiWW. A range of $\tilde{\chi}_1^\pm$, $\tilde{\chi}_2^0$, and LSP masses is considered with mass differences ranging from 3 to 200 GeV; consequently the W and Z bosons are off-shell for much of the (mass, Δm) plane considered.

For slepton pair production, the four charged sleptons of the first and second generation (i.e., selectrons and smuons), namely, the superpartners of both lepton chiralities (\tilde{e}_L^\pm , \tilde{e}_R^\pm , $\tilde{\mu}_L^\pm$, $\tilde{\mu}_R^\pm$), are pair produced and decay with a 100% branching fraction to $\ell^\pm \tilde{\chi}_1^0$. These possibilities are illustrated in Fig. 4. The simplified model where all four states have the same mass is referred to as the TSlepSlep model. Mass differences ranging from 3 to 100 GeV are considered and the generated event samples based on the TSlepSlep model permit exploration of appropriate combinations of the four states.

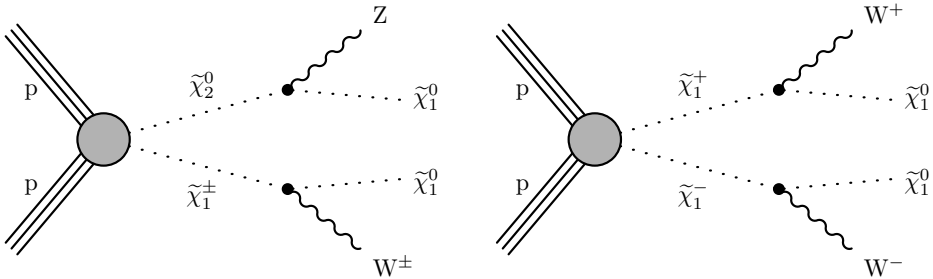


Figure 3: Diagrams for electroweakino production. The left panel shows associated production of the lightest chargino and second-lightest neutralino ($\tilde{\chi}_1^\pm \tilde{\chi}_2^0$) in the TChiWZ model and the right panel shows pair production of the lightest chargino ($\tilde{\chi}_1^+ \tilde{\chi}_1^-$) in the TChiWW model.

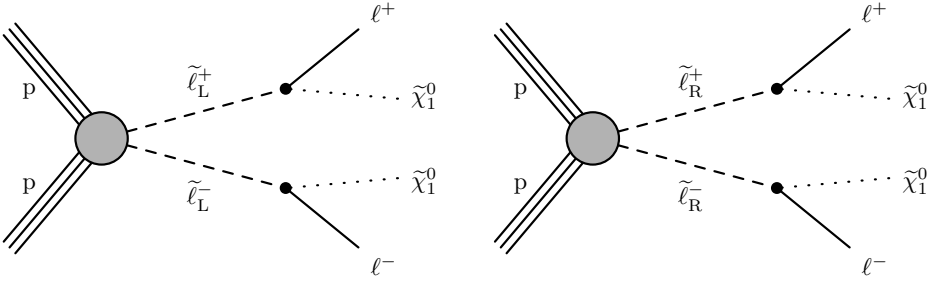


Figure 4: Diagrams for pair production of charged sleptons with subsequent decay to $\ell^\pm \tilde{\chi}_1^0$ where $\ell = e, \mu$.

An additional model for chargino pair production, denoted the TChiSlepSnu model, is studied. In this scenario, the chargino decays via an intermediate charged slepton ($\tilde{\ell}_L^\pm$) or sneutrino, as illustrated in Fig. 5. In this case, the mass of the intermediate state is set halfway between the masses of the chargino and the LSP, and it is assumed that the chargino decays with equal probability to each slepton and sneutrino flavor (branching fraction of 1/6). Mass differences between the chargino and the LSP exceeding 50 GeV are considered for this specific model.

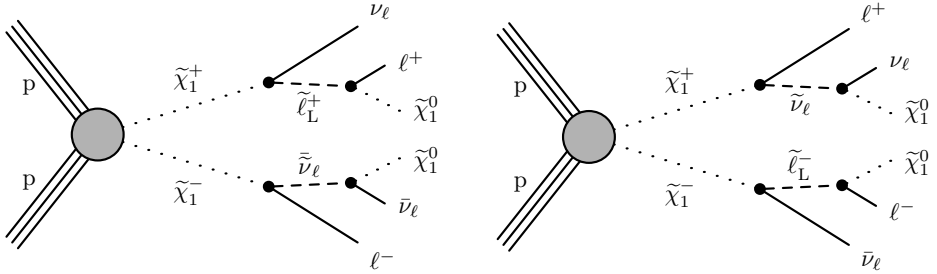


Figure 5: Diagrams for pair production of the lightest chargino with subsequent leptonic decays via an intermediate mass charged slepton or sneutrino, where $\ell = e, \mu, \tau$. In addition to the illustrated diagrams, the other two combinations where either both charginos decay to an intermediate charged slepton or both charginos decay to an intermediate sneutrino are also included in this TChiSlepSnu model.

The background samples are partitioned in seven groups:

1. $Z/\gamma^* + \text{jets}$: composed of the $Z+\text{jets}$ and Drell–Yan backgrounds and generated at LO using `MADGRAPH5_aMC@NLO`.
2. $W + \text{jets}$: generated at LO using `MADGRAPH5_aMC@NLO`.
3. $t\bar{t}X + \text{jets}$: $t\bar{t} + \text{jets}$ is generated at LO using `MADGRAPH5_aMC@NLO` with the final states separated into dilepton and single lepton. Also included are $t\bar{t} + \text{boson}$ processes generated with `MADGRAPH5_aMC@NLO`.
4. ST: this group covers the three single top quark production processes corresponding to the s -channel, t -channel, and W -associated production (tW). The s -, t -channel and leptonic tW processes are simulated using `MADGRAPH5_aMC@NLO`, while the inclusive tW samples are simulated at NLO with the `POWHEG v1` generator [82–85].
5. VV: includes diboson processes. The WW , ZZ , $W\gamma$ production and non- $b\bar{b}$ Higgs boson decays for WH and ZH production are generated at NLO precision with `MAD-`

GRAPH5_aMC@NLO using the FxFx merging scheme [86]. The WZ process, the $b\bar{b}$ Higgs boson decays for WH and ZH production, and Higgs bosons from gluon-gluon fusion are all generated with POWHEG v2 [87, 88].

6. VVV: includes triboson processes generated using MADGRAPH5_aMC@NLO at NLO.
7. QCD: quantum chromodynamics (QCD) multijet background using samples generated with MADGRAPH5_aMC@NLO. Due to shortcomings in its simulation, this background is accounted for by using an approach almost fully relying on control samples in data.

4 Physics object reconstruction

After the basic event reconstruction described in Section 2, physics objects such as electrons, muons, b-tagged jets, and tagged secondary vertices are reconstructed. Because the analysis targets compressed SUSY signatures, we prioritize the identification of objects with as low a p_T as can be efficiently analyzed.

Electrons with $p_T > 5 \text{ GeV}$ and $|\eta| < 2.4$ are identified using a multivariate discriminant based on track quality variables and the energy distribution in both the ECAL and HCAL, with the very loose selection initially applied [56]. Candidate electrons must have tracks that have a hit in every pixel detector layer and which are not associated with a reconstructed photon conversion vertex. Candidate muons with $p_T > 3 \text{ GeV}$ and $|\eta| < 2.4$ are selected based on the quality of the tracks both in the tracker and in the muon system, with the condition that they are matched to each other and satisfy the loose and soft identification criteria from Ref. [89]. Initially, loose requirements are applied on the track quality of the leptons to qualify them for the analysis. These track quality criteria include requirements on the three-dimensional (3D) impact parameter significance ($\text{IP}_{3D}/\sigma_{\text{IP}_{3D}} < 8$), the two-dimensional (2D) transverse distance of closest approach to the primary vertex ($|d_{xy}| < 0.05 \text{ cm}$), and the longitudinal distance of closest approach to the primary vertex ($|d_z| < 0.1 \text{ cm}$).

Electrons and muons that satisfy these preselection requirements are separated into three mutually exclusive categories: gold, silver, and bronze. The gold category represents the most signal-like prompt and isolated leptons, while the silver category is used to recover efficiency from isolated secondary leptons from sources such as semileptonic decays of b hadrons. The remaining leptons that do not qualify as gold or silver, but which satisfy the loose quality criteria described previously, are classified as bronze. Gold and silver electrons with $p_T > 10 \text{ GeV}$ are additionally required to pass the tight identification criteria, while muons are required to pass the medium identification selection [89]. Gold and silver leptons must also satisfy further isolation criteria. Absolute isolation requirements separate the leptons from jets using the p_T sum deposited by the particle-flow candidates in a cone of radius $\Delta R = 0.3$ around the lepton, where $\Delta R \equiv \sqrt{(\Delta\eta)^2 + (\Delta\phi)^2}$, and ϕ is the azimuthal angle measured in radians. Mini-isolation is defined as the p_T sum of charged hadron, neutral hadron, and photon particle-flow candidates within a cone in η - ϕ space around the lepton, correcting for pileup using an effective area method [90]. The cone size depends on the lepton p_T and has radius \mathcal{R} , defined as

$$\mathcal{R} = \frac{10 \text{ GeV}}{\min(\max(p_T, 50 \text{ GeV}), 200 \text{ GeV})}. \quad (1)$$

Both absolute and mini-isolation is required to be less than 4 GeV for gold and silver leptons.

Gold and silver leptons are then differentiated by their consistency with originating directly from the primary vertex, with gold categorization requiring a tighter 3D impact parameter significance, $\text{IP}_{3D}/\sigma_{\text{IP}_{3D}} < 2$, with the criterion reversed for silver leptons.

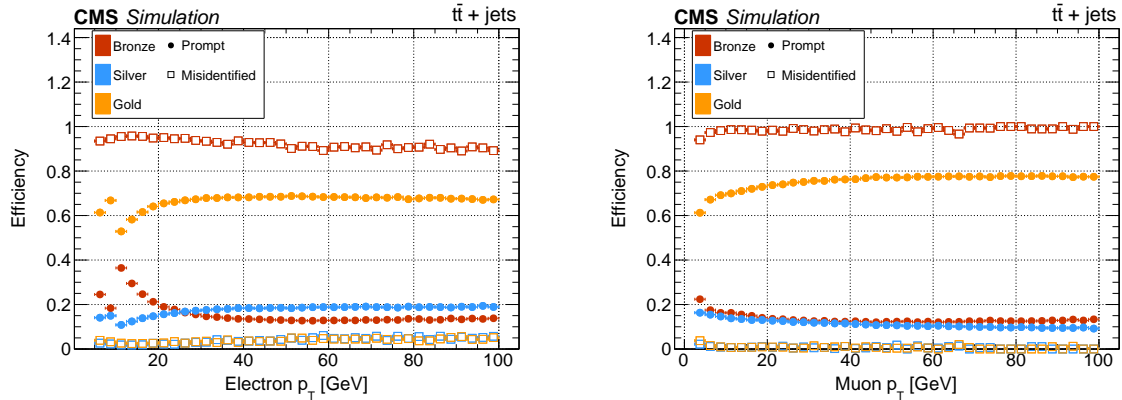


Figure 6: Efficiencies of lepton candidates satisfying baseline requirements to be identified in the gold, silver, and bronze categories for prompt leptons (solid circles) and misidentified leptons (open squares), evaluated in simulated $t\bar{t} + \text{jets}$ events. Electrons (muons) are shown in the left (right) panel. As the three categories are mutually exclusive and exhaustive for baseline leptons, these efficiencies sum to one for each source in each lepton p_T bin.

Electron identification efficiencies range from above 98% for the very loose criteria to 70% for the tight criteria. The corresponding misidentification rates range from 2 to 3% for tight identification and from 5 to 15% for very loose identification, depending on the electron’s η [56]. Loose (medium) muons have identification efficiencies above 99% (95–99%) with hadron misidentification rates below 0.5% [89]. The identification and misidentification efficiencies of these selection criteria are studied using simulated $t\bar{t} + \text{jets}$ and $Z/\gamma^* + \text{jets}$ samples. In these samples, lepton candidates are labeled as prompt if there is a generator lepton within 0.01 in ΔR of the lepton candidate and the lepton originates from the primary vertex. Lepton candidates are considered misidentified if there is no generator-level lepton within 0.01 in ΔR of the lepton candidate. Figure 6 shows these prompt and misidentified efficiencies as a function of lepton p_T . Further exploration of the sources of the leptons shows that the gold category is the most efficient at keeping genuine leptons originating from prompt sources, while rejecting most misidentified leptons as well as leptons from nonprompt sources. The silver category is also very good at rejecting misidentified leptons and accepting genuine leptons that were produced from secondary sources (primarily semileptonic b hadron and τ lepton decays). Finally, bronze leptons consist of prompt leptons that failed both the gold and silver requirements, followed by genuine leptons from nonprompt sources as well as particles misidentified as leptons.

To account for observed small differences in reconstruction, identification, and isolation efficiencies between data and simulation, the simulation is corrected by factors estimated from data using the “tag-and-probe” method [89], with both Z boson and J/ψ meson decays. These factors are derived as a function of p_T , η , and data-taking period, and take into account extrapolations of vertexing and isolation parameters. Further scale factors account for differences found between the FASTSIM signal sample simulations and the background samples generated using the full detector simulation.

Jets found with $p_T > 20 \text{ GeV}$ and $|\eta| < 2.4$ are selected if they pass criteria designed to remove jets dominated by instrumental effects or reconstruction failures [91]. Additionally, jets are required to be a distance of at least $\Delta R = 0.2$ from any identified leptons. Jets that pass the medium working point of the DEEPJET tagger [92] are classified as b jets. The identification efficiency for b quark jets ranges from 60 to 85%, depending on the jet p_T , with a misidentification rate of about 15 to 25% for charm quark jets and 1 to 7% for light-quark or gluon jets.

Differences between these efficiencies in data and simulation are corrected for as functions of jet p_T [93].

For compressed SUSY signal events, especially those originating from top squark decays, low- p_T b hadron decays are an important signature. A soft secondary vertex (SV) b-quark-finding deep neural network (DNN) algorithm was developed for this analysis to identify these decay products. The SV candidates were reconstructed using the inclusive secondary vertex finder [94]. The p_T and η of the SV are evaluated from the vector sum of the momenta of the tracks belonging to the SV. It is required that $2 < p_T < 20$ GeV, $|\eta| < 2.4$ and that the 3D displacement significance with respect to the primary vertex must exceed 3. The SV must not be matched to any jet with a p_T above 20 GeV within a cone size of $\Delta R < 0.4$, or to any lepton within a cone size of $\Delta R < 0.2$ where the cone is centered on the SV momentum.

The SV b-tagger is built using the DEEPJET framework [95, 96] and a machine-learning algorithm based on the DeepCSV tagger [97]. Eight variables are used as input for the SV b-tagger DNN: the p_T , η , mass, number of degrees of freedom, displacements from the primary vertex in both 2D and 3D, 3D displacement significance, and the cosine of the pointing angle between the primary and secondary vertices. The discriminant was trained and tested using simulated $t\bar{t} + \text{jets}$ and $W + \text{jets}$ samples.

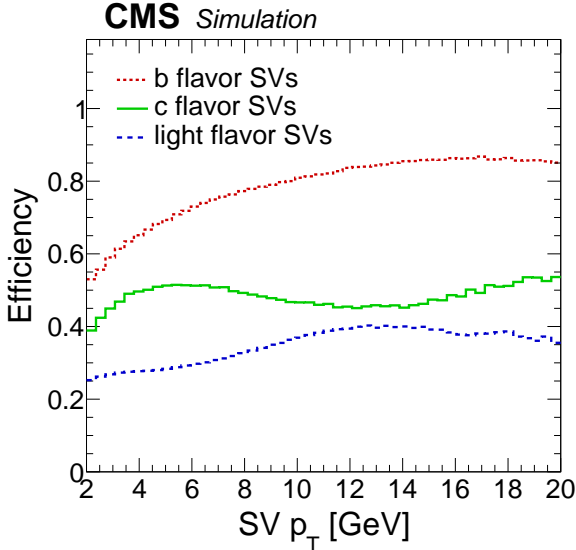


Figure 7: Distributions of the b, c, and light-quark SV tagging efficiencies, as functions of the SV candidate p_T , for the chosen working point. The SV flavor identities are determined from the generator-level flavor information and ΔR matching to SV candidates.

A working point for the training sample was chosen for the analysis, yielding a good balance between rejecting light-flavor SVs and retaining events corresponding to compressed SUSY signals. Figure 7 shows the b, c, and light-quark SV tagging efficiencies as functions of p_T . Averaged over the p_T range, the b quark SV tagging efficiency is approximately 80% with a light-quark misidentification rate of about 25%. Scale factors are derived to take into account differences between the FASTSIM signal sample simulations and the full detector simulation, with values within 5% of unity. Scale factors which take into account differences between the data and simulation are found using the fit to control samples in data described in Section 7.

5 Kinematic event reconstruction

In order to address the challenges associated with compressed sparticle mass spectra, events are selected based on significant ISR activity that causes the sparticle system to recoil resulting in observable p_T^{miss} from the momentum received by the invisible sparticles. This event topology is illustrated in Fig. 8, with $I_{a/b}$ and $V_{a/b}$ representing the systems of invisible and visible sparticle decay products, respectively, associated with the decay chains resulting from the parent particles P_a and P_b . Analyzing events according to this generic decay tree, with a variable identity and number of particles corresponding to $I_{a/b}$ and $V_{a/b}$, allows one to specifically tailor observables to exploit the features of this scenario using the recursive jigsaw reconstruction (RJR) [98–100] algorithm. Ideally, this leads to assignment of the $I_{a/b}$ and $V_{a/b}$ systems to individual candidate parent sparticle systems, $P_{a/b}$, collectively referred to as the **S** system, and an accompanying recoiling ISR system. Correspondingly, the **S** and **ISR** systems are treated as decay products of a singular center-of-mass (**CM**) system.

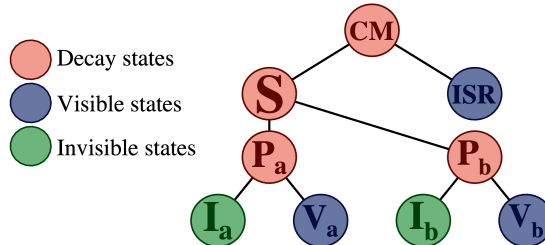


Figure 8: Decay tree diagram used to analyze events. Here **S** represents the total system of candidate sparticles, with $P_{a/b}$ representing pair-produced SUSY parent particles; $I_{a/b}$ and $V_{a/b}$ represent the systems of invisible and visible sparticle decay products, respectively. The **S** system, along with the recoiling **ISR** system, are viewed as decay products of the entire center-of-mass (**CM**) system of the colliding partons with constituent center-of-mass energy, $\sqrt{\hat{s}}$.

In the SUSY events targeted by this analysis, there are two types of unknowns: *kinematic* unknowns resulting from undetected invisible particles and *combinatorial* unknowns associated with the correct assignment and interpretation of visible particles. Within the decay tree framework, the kinematic unknowns correspond to the four-vectors of the two invisible systems I_a and I_b . The combinatorial unknowns involve determining how the reconstructed particles (leptons, jets, SVs) are assigned to the V_a , V_b , and **ISR** groups. Assuming that the combinatorial assignments have been made, such that the four-vectors $p_{V_{a/b}}^{\text{lab}}$ and $p_{\text{ISR}}^{\text{lab}}$ are measured, the kinematic unknowns associated with the invisible particles are determined by applying a combination of assumed and measured constraints, along with algorithmic *jigsaw rules* (JRs) [100], which match the structure of the decay tree shown in Fig. 8. In this case, the masses² of the individual invisible particles (M_{I_a}, M_{I_b}) are assumed to be zero, while the measured \vec{p}_T^{miss} is interpreted as the vector sum of their transverse momenta, with

$$M_{I_a} = 0, \quad M_{I_b} = 0, \quad \vec{p}_{I_a,T}^{\text{lab}} + \vec{p}_{I_b,T}^{\text{lab}} = \vec{p}_T^{\text{miss}}. \quad (2)$$

With these constraints, the remaining kinematic unknowns are the total mass of the system of all invisible particles in the event (m_I), the longitudinal momentum of that system in the

²Lower case m denotes the correct (or true) mass, and upper case, M , denotes the calculated (or measured) mass that approximates the correct mass for the system that is indicated by the subscript.

lab ($p_{I,z}^{\text{lab}}$), and the direction of the “decay axis” corresponding to how the momentum of \mathbf{I} is shared between \mathbf{I}_a and \mathbf{I}_b . The RJR algorithm proceeds by parameterizing these unknowns as components of the velocities relating the reference frames appearing in Fig. 8. As all of the measured visible four-vectors correspond to the lab frame, the first of the velocities to consider is $\vec{\beta}_{\text{CM}}^{\text{lab}}$ relating the CM frame to the lab frame. Among the kinematic unknowns, $\vec{\beta}_{\text{CM}}^{\text{lab}}$ depends only on m_I and $p_{I,z}^{\text{lab}}$, meaning these quantities can be determined independently of others.

The first JR applied is the *invisible mass rule* [100], which assigns to m_I the smallest Lorentz-invariant quantity (as a function of measured visible particles’ four-vectors) that will ensure consistency of the approximate event reconstruction (no tachyonic particles), with

$$M_I^2 = M_V^2 - 4M_{V_a}M_{V_b}. \quad (3)$$

This can be qualitatively understood as giving mass to the invisible particle system resulting from sparticle decays, based on the mass of the corresponding visible decay products. This essentially exploits the fact that the orientation of the invisible particles relative to each other is correlated with that of the visible ones, as both arise from the same decays depicted in Fig. 8. As the individual invisible particles have masses constrained to zero, M_I is adjusted for the individual visible system masses, $M_{V_{a/b}}$.

The unknown $p_{I,z}^{\text{lab}}$, or equivalently $\beta_{\text{CM},z}^{\text{lab}}$, is assigned via the *invisible rapidity rule* [100], by assigning the value of $\beta_{\text{CM},z}^{\text{lab}}$ which minimizes M_{CM} :

$$\beta_{\text{CM},z}^{\text{lab}} = \underset{\beta_{\text{CM},z}^{\text{lab}}}{\operatorname{argmin}} M_{\text{CM}}. \quad (4)$$

This choice has two important consequences. Firstly, it avoids assigning erroneously high values of M_{CM} with an incorrect choice, avoiding promoting background events to appear more interesting than they actually are. Secondly, it ensures that the analytic expression for M_{CM} (and all observables following from this choice) is independent of the true value of $\beta_{\text{CM},z}^{\text{lab}}$ and so *longitudinally boost invariant*. In fact these quantities are invariant to transverse boosts up to order $(\beta_{\text{CM},T}^{\text{lab}})^2$. The estimator for M_{CM} becomes the well-known *transverse mass* of the \mathbf{I} and \mathbf{V} systems.

With $\vec{\beta}_{\text{CM}}^{\text{lab}}$ assigned, the four-vectors of all the visible particles can be evaluated in the CM frame, and subsequently the S frame. Determining the remaining kinematic unknowns can now be viewed as assigning $\vec{\beta}_{P_{a/b}}^S$, the velocities relating the S frame to the rest frames of its children, conditioned on the previous assignments made earlier in the decay tree. Using the *invisible MinMasses² rule* [100], these velocities are determined according to the equation,

$$\vec{\beta}_{P_a}^S, \vec{\beta}_{P_b}^S = \underset{\vec{\beta}_{P_a}^S, \vec{\beta}_{P_b}^S}{\operatorname{argmin}} (M_{P_a}^2 + M_{P_b}^2), \quad (5)$$

and subject to the constraints implied by previous choices and measurements. The practical effect of this choice is similar to that of the previous longitudinal boost, in that the mass estimators (or more accurately, this sum) become independent of the true, unknown, $\vec{\beta}_{P_{a/b}}^S$. With the application of this last JR, all of the under-constrained kinematic quantities associated with invisible particles have been assigned.

The combinatorial unknowns associated with how visible objects are assigned to groups in the decay tree interpretation are determined in a manner similar to their kinematic analogs, where choices are factorized recursively according to when they appear in the decay. In this case, the

first partitioning choice is how to split the total collection of visible, reconstructed objects in the event, **VIS**, between the **V** and **ISR** systems. As for kinematic quantities, these assignments are determined by effectively picking the grouping that minimizes M_S and M_{ISR} simultaneously. Explicitly, the *combinatorial MinMasses rule* [100] prescribes

$$\{\mathbf{V}, \mathbf{ISR}\} = \underset{\mathbf{V}, \mathbf{ISR}}{\operatorname{argmax}} p_S^{\text{CM}}, \quad (6)$$

where $p_S^{\text{CM}} = |\vec{p}_S^{\text{CM}}| = |\vec{p}_{\text{ISR}}^{\text{CM}}|$ is the momentum of the **S** system in the **CM**, which, with M_{CM} fixed, will increase as M_S and M_{ISR} decrease. The maximization is over all the different ways jets can be exclusively partitioned into **V** and **ISR** groups.

The next partitioning choice is where the group **V** is split into **V_a** and **V_b** according to the *combinatorial MinMasses² rule* [100], with

$$\{\mathbf{V}_a, \mathbf{V}_b\} = \underset{\mathbf{V}_a, \mathbf{V}_b}{\operatorname{argmin}} (M_{\mathbf{P}_a}^2 + M_{\mathbf{P}_b}^2). \quad (7)$$

The practical effect of choosing partitions of objects based on mass minimization is similar to exclusive jet clustering, where the invariant mass is used as a distance metric to group objects that are traveling in similar directions.

A hierarchy of JRs is defined to remove the combinatorial dependencies on the kinematics of the invisible particles, with combinatorial decisions proceeding down the decay tree and followed by the kinematical ones. With this prescription applied, an event is fully reconstructed, as all of the four-vectors of the states shown in Fig. 8 are either measured or assigned.

Observables are constructed to be sensitive to the mass of invisible particles in the event, characteristic of the compressed signals being sought. LSPs will receive little momentum from the decays where they are produced, and the resulting p_T^{miss} will be typically negligible. The massive invisible particles (which are nearly at rest in the **S** frame) will receive an out-sized fraction of the momentum from the ISR kick among the **S** decay products, as their rest energy is largest, leading to potentially large p_T^{miss} . This mechanism introduces a correlation between the ISR system and \vec{p}_T^{miss} , such that

$$\vec{p}_T^{\text{miss}} \approx -\frac{m_I}{m_P} \vec{p}_{\text{ISR}, T}^{\text{CM}}. \quad (8)$$

This relation can be further refined using the RJR reconstructed quantities and defining the variable R_{ISR} as

$$R_{\text{ISR}} = \frac{|\vec{p}_I^{\text{CM}} \cdot \hat{p}_{\text{ISR}}^{\text{CM}}|}{|\vec{p}_{\text{ISR}}^{\text{CM}}|} \approx \frac{m_I}{m_P}. \quad (9)$$

The distribution of R_{ISR} of a selection of compressed electroweakino TChiWZ model events is shown in Fig. 9 (left), where it is observed to peak at m_I/m_P as expected. With an absence of genuine, massive invisible particles, the SM backgrounds do not exhibit the same peaking behavior, with larger values of R_{ISR} suppressed, as apparent in Fig. 9 (right). While observables sensitive to the absolute size of mass splittings in compressed scenarios can struggle to differentiate between signal and background, the resolution (and hence discriminating power) of R_{ISR} improves with increasing compression. The peaking behavior of R_{ISR} depends predominantly on the event topology and particle masses, and is observed to be largely independent of final state. Regardless of how particles in these events decay, R_{ISR} depends almost exclusively on the sparticle masses. The distribution of R_{ISR} for the SM backgrounds also behaves qualitatively similarly in different final states.

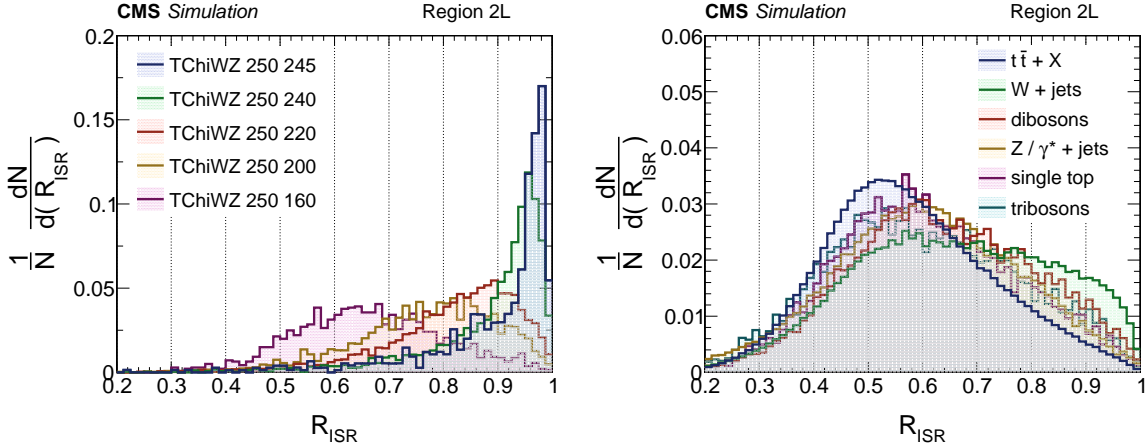


Figure 9: Distributions of R_{ISR} for simulated events in the 2 lepton final state for TChiWZ signal models with 250 GeV parent mass and various LSP masses ranging from 160 to 245 GeV (left) and the SM backgrounds (right).

The p_T^{ISR} observable quantifies the magnitude of the ISR kick to the sparticle system ($p_T^{\text{ISR}} = |\vec{p}_{\text{ISR},T}^{\text{CM}}|$). As one might naively expect, the more kick, the more distinctive the peaking behavior of R_{ISR} for signals with massive invisible particles. This behavior is illustrated in Fig. 10, where the R_{ISR} resolution improves for compressed signals with increasing p_T^{ISR} . Conversely, the SM backgrounds have increasingly suppressed R_{ISR} distributions as p_T^{ISR} grows, as seen for the $t\bar{t} + \text{jets}$ background in Fig. 10. In this analysis, p_T^{ISR} is used to define signal-enriched and control regions (CRs) by exploiting this behavior.

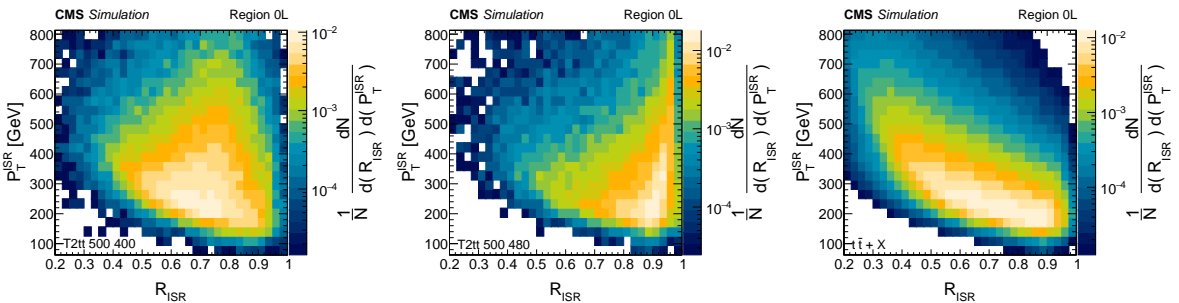


Figure 10: Distributions of p_T^{ISR} vs. R_{ISR} in events with 0 leptons for simulated top squark signals in the T2tt model with parent mass of 500 GeV and a LSP mass of 400 GeV (left), LSP mass of 480 GeV (center), and $t\bar{t} + \text{jets}$ background (right).

Additional observables sensitive to information independent from R_{ISR} and p_T^{ISR} , which reflect the R -parity-conserving decay topology, can be constructed by further resolving the decay kinematics inside the sparticle decay system \mathbf{S} “perpendicular” to the axis of the ISR boost. Two additional approximate reference frames are defined relative to the \mathbf{S} frame according to:

$$\beta_V^S = \underset{\beta_V^S}{\operatorname{argmin}} \left(\Lambda_{\beta_V^S} \mathbf{p}_V^S \right)_0, \quad \beta_I^S = \underset{\beta_I^S}{\operatorname{argmin}} \left(\Lambda_{\beta_I^S} \mathbf{p}_I^S \right)_0, \quad (10)$$

where β_V^S and β_I^S are the velocities (restricted along the direction of the boost $\hat{\beta}_S^{\text{CM}}$) relating the \mathbf{S} frame to the respective reference frames. The \mathbf{V} and \mathbf{I} systems are at rest along the $\hat{\beta}_S^{\text{CM}}$ axis, and $\left(\Lambda_{\beta_V^S} \mathbf{p}_V^S \right)_0$ is the energy of the visible system in this frame after the Lorentz transformation $\Lambda_{\beta_V^S}$, which is minimized. As opposed to simply projecting the four-vectors $\mathbf{p}_{V_a/b}^S$ and $\mathbf{p}_{I_a/b}^S$

individually into the plane perpendicular to the $\hat{\beta}_S^{\text{CM}}$ boost direction, projecting the entire \mathbf{V} and \mathbf{I} groups maintains information along this axis and is insensitive to the previous inexact approximation.

From the “perpendicular” four-vectors in the two \mathbf{S} -adjacent frames, defined as

$$\mathbf{p}_{\mathbf{V}_{a/b},\perp}^S = \Lambda_{\beta_V^S} \mathbf{p}_{\mathbf{V}_{a/b}}^S, \quad \mathbf{p}_{\mathbf{I}_{a/b},\perp}^S = \Lambda_{\beta_I^S} \mathbf{p}_{\mathbf{I}_{a/b}}^S, \quad (11)$$

observables can be constructed:

$$\begin{aligned} M_{\mathbf{P}_{a/b},\perp}^2 &= \left(\mathbf{p}_{\mathbf{V}_{a/b},\perp}^S + \mathbf{p}_{\mathbf{I}_{a/b},\perp}^S \right)^2, \\ M_{\mathbf{S},\perp}^2 &= \left(\mathbf{p}_{\mathbf{V}_{a,\perp}}^S + \mathbf{p}_{\mathbf{V}_{b,\perp}}^S + \mathbf{p}_{\mathbf{I}_{a,\perp}}^S + \mathbf{p}_{\mathbf{I}_{b,\perp}}^S \right)^2. \end{aligned} \quad (12)$$

While representing some independent information, the masses $M_{\mathbf{P}_{a/b},\perp}$ and $M_{\mathbf{S},\perp}$ are not entirely uncorrelated. As the reconstruction in the \mathbf{S} frame is executed by choosing several unknowns by minimizing $M_{\mathbf{P}_a}^2 + M_{\mathbf{P}_b}^2$, a summary mass variable, M_{\perp} , is defined from a combination of these masses as

$$M_{\perp} = \sqrt{\frac{M_{\mathbf{P}_{a},\perp}^2 + M_{\mathbf{P}_{b},\perp}^2}{2}}, \quad (13)$$

such that it is related to the average (of squares) of the individual mass estimators for each sparticle parent.

The distribution of M_{\perp} is shown in Fig. 11 for compressed top squark signals and the SM backgrounds. As the individual invisible particle masses are set to zero in the reconstruction, their expected contribution to M_{\perp} is not accounted for, meaning that M_{\perp} is not sensitive to the masses $m_{\mathbf{P}_{a/b}}$ but rather to the mass splittings $m_{\mathbf{P}_{a/b}} - m_{\mathbf{I}_{a/b}}$. The resulting M_{\perp} distributions for signal events exhibit a kinematic endpoint at $m_{\mathbf{P}_{a/b}} - m_{\mathbf{I}_{a/b}}$ (modulo resolution effects), while backgrounds have falling distributions sensitive to the mass scale of particles appearing in the events.

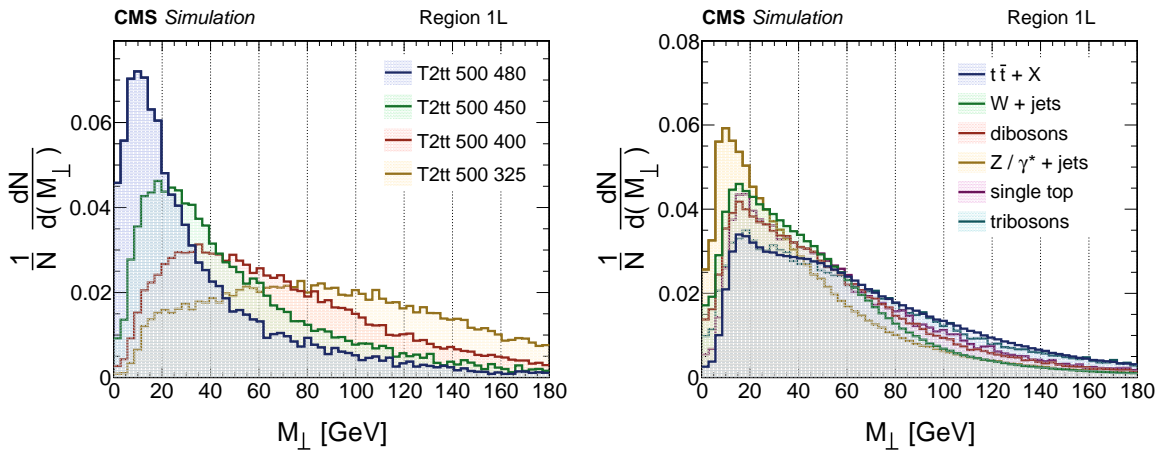


Figure 11: Distributions of M_{\perp} in one lepton final states for simulated events: compressed T2tt signal events with a parent top squark mass of 500 GeV and LSP masses ranging from 325 to 480 GeV (left) and the SM backgrounds (right).

The R_{ISR} and M_{\perp} variables are largely uncorrelated for both signal and backgrounds, as shown in Fig. 12. The practical result is that compressed SUSY signals appear as 2D “bumps” in the R_{ISR} vs. M_{\perp} plane, with the location dictated by the sparticle masses. Simultaneously,

backgrounds are dispersed over the larger R_{ISR} and M_{\perp} phase space, with larger values of R_{ISR} suppressed for increasingly large M_{\perp} .

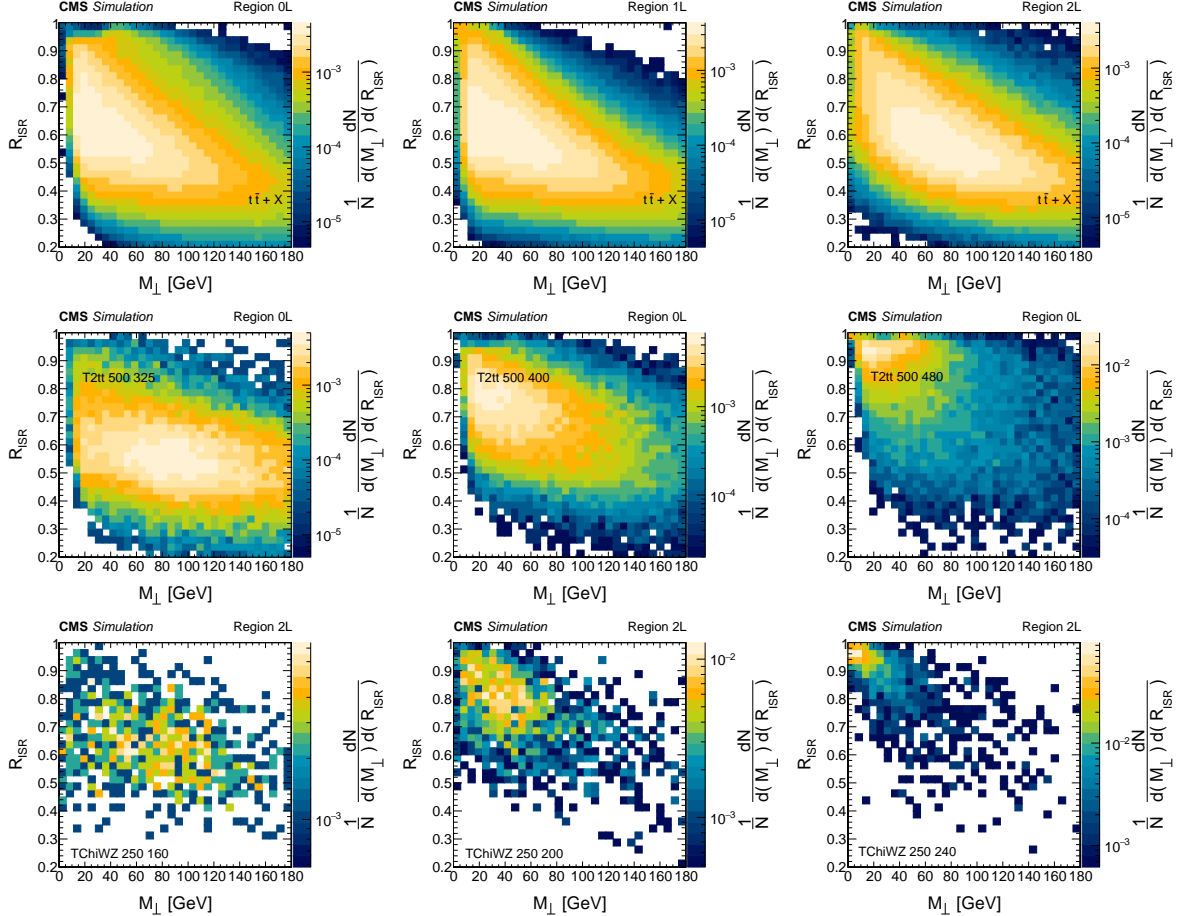


Figure 12: Distributions of R_{ISR} vs. M_{\perp} for simulated events in multiple final states. (Upper row) $t\bar{t} + \text{jets}$ background events in 0 lepton (0L), one lepton (1L), and two lepton (2L) final states. (Middle row) T2tt signals in 0L final states and (lower row) TChiWZ signals in 2L final states for various sparticle mass combinations.

An additional variable, complementary to M_{\perp} , is defined from a different combination of the “perpendicular” masses:

$$\gamma_{\perp} = \frac{2M_{\perp}}{M_{S,\perp}}. \quad (14)$$

The observable γ_{\perp} is sensitive to the asymmetry of the **S** system decay, taking larger values (closer to 1) when the event is maximally imbalanced (invisible particles recoiling together against visible). While the observable is not as powerful a discriminant as R_{ISR} or M_{\perp} , it tends to larger values for signals relative to backgrounds and is also used in the event categorization. It is particularly effective against certain, otherwise difficult backgrounds, such as nonresonant SM $WW \rightarrow 2\ell 2\nu$ production, where the decay topology mimics that of R -parity-conserving SUSY.

The analysis proceeds by counting objects (leptons, jets, b-tagged jets, and b-tagged SVs) that were assigned to either the sparticle **S** system or the **ISR** system with the RJR reconstruction. Any leptons reconstructed in the event are automatically assigned to the **S** system in the event interpretation, while jets and SVs can appear as either coming from sparticles or ISR. One of

the most important object counting observables is the multiplicity of jets assigned to the **S** system, $N_{\text{jet}}^{\text{S}}$. While the distribution of $N_{\text{jet}}^{\text{S}}$ exhibits large variations depending on the level of compression of the signal model, the distribution of $N_{\text{jet}}^{\text{ISR}}$, the number of jets assigned to the **ISR** system in each event, is more uniform between differing signal masses and, more relevantly, is more similar to backgrounds. Furthermore, $N_{\text{jet}}^{\text{S}}$ is a powerful discriminant when signals have mass splittings large enough to produce multiple above-threshold jets in sparticle decays. For this analysis, the only requirement on $N_{\text{jet}}^{\text{ISR}}$ is that there is at least one jet assigned to the **ISR** system. For both signal and background, larger R_{ISR} and smaller M_{\perp} are typically associated with lower $N_{\text{jet}}^{\text{S}}$, with much weaker correlations for signals than for SM backgrounds.

The analysis also categorizes events according to the number of jets that are tagged as coming from b quarks in each of the **S** and **ISR** systems, $N_{\text{b tag}}^{\text{S}}$ and $N_{\text{b tag}}^{\text{ISR}}$, respectively. The $t\bar{t} + \text{jets}$ background often leads to at least one b-tagged jet in the **ISR** system; this arises from cases where b-tagged jets from the top quark decays get assigned erroneously to the **ISR** system. This observation is used in the analysis by separating events with $N_{\text{b tag}}^{\text{ISR}} \geq 1$ from those with none in order to isolate $t\bar{t} + \text{jets}$ contributions. Also, requiring large $N_{\text{b tag}}^{\text{S}}$ and $N_{\text{b tag}}^{\text{ISR}} = 0$ selects a large fraction of top squark signal events, while rejecting most of the $Z/\gamma^* + \text{jets}$ and $t\bar{t} + \text{jets}$ backgrounds.

The final object multiplicity observable used in the analysis is the number of soft, stand-alone SVs assigned to the **S** system, N_{SV}^{S} . The SV multiplicity is nearly identical among the different background events, with top squark signals having a higher probability of observing $N_{\text{SV}}^{\text{S}} \geq 1$. In addition to categorizing based on the presence or absence of an SV in the **S** system, the $|\eta|$ distribution of identified SVs also serves as a useful discriminant. SVs associated with sparticle decays tend to be more central than those from background processes, especially backgrounds such as $W + \text{jets}$ where genuine bottom quarks usually arise from radiation or misidentification, as illustrated in Fig. 13. The analysis uses the observable $|\eta_{\text{SV}}^{\text{S}}|$, defined as the maximum absolute value of the η found for those SVs in the **S** system to categorize events with SVs into central ($|\eta_{\text{SV}}^{\text{S}}| < 1.5$) and forward regions, with the latter acting as a CR for constraining the SV reconstruction efficiencies and kinematics with data.

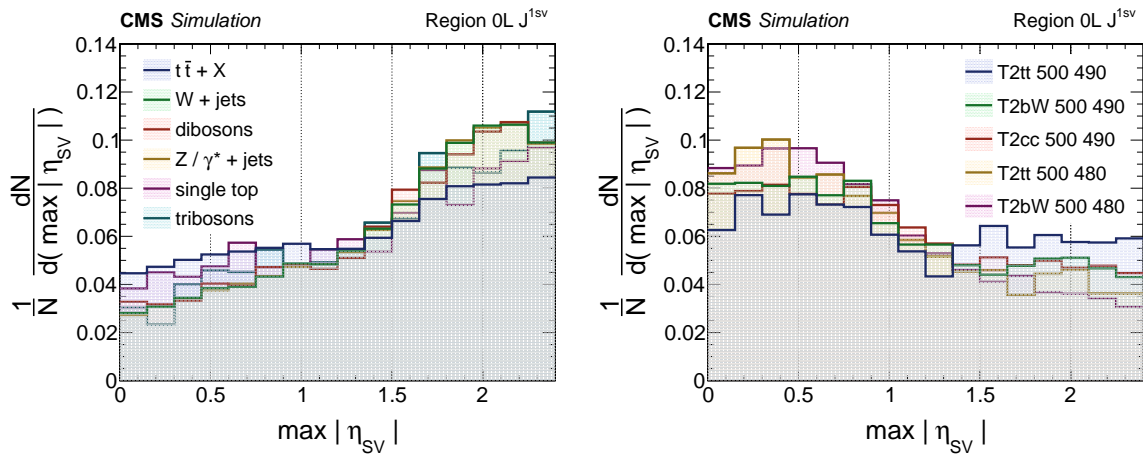


Figure 13: Distributions of $\max |\eta_{\text{SV}}^{\text{S}}|$ in final states with 0 leptons and ≥ 1 SVs associated with the **S** system, for simulated SM background events (left) and various top squark signal models (right).

6 Event selection and categorization

The analysis of data begins with preselection requirements that remove events that are not consistent with the compressed phase space of interest. Events are then categorized into mutually exclusive analysis regions that are defined according to a combination of object multiplicities assigned to the **S** and **ISR** systems as well as categorization based on kinematic variables. The events falling in each region are further binned in 2D in the primary sensitive variables, R_{ISR} and M_{\perp} , with bin boundaries common among regions with the same lepton and $N_{\text{jet}}^{\text{S}}$ multiplicities. This analysis implements a fitting approach based on control samples in data (described in Section 7) to model background, accounting for differences in lepton flavor and source in the rates of their contributions, while also considering potential kinematic data/simulation deviations associated with the leptons, jets, and SVs. Some of the categories effectively act as background-dominated CRs used to constrain both the normalization and shape of the R_{ISR} and M_{\perp} bin yields in signal-sensitive ones. A subset of these analysis bins (over many categories) are identified as having negligible expected signal yields (for all of the signal models considered in this analysis, through explicit evaluation) and are designated as control regions for use in blinded fits to data and model independent interpretations.

Events are selected from the $p_{\text{T}}^{\text{miss}}$ trigger data sets for each year by requiring that the offline $p_{\text{T}}^{\text{miss}} > 150 \text{ GeV}$ and applying the $p_{\text{T}}^{\text{miss}}$ related event filters [58]. These events must have at least one visible object assigned to the **S** system and at least one jet assigned to the **ISR** system. To provide a moderate ISR kick, only events with $p_{\text{T}}^{\text{ISR}} > 250 \text{ GeV}$ are retained and it is further required that $R_{\text{ISR}} > 0.5$ thus primarily targeting signals with LSP masses exceeding about half the parent sparticle mass. A $|\Delta\phi_{\vec{p}_{\text{T}}^{\text{miss}}, V}| < \pi/2$ requirement ensures that the visible and invisible systems associated with sparticle decays are pointing in the same transverse hemisphere. A further event filter requirement is used to remove events that are poorly modeled in simulation. The magnitude of the vector sum of the transverse momentum of the center of mass frame (p_{T}^{CM}) and the azimuthal angle between the center of mass system and the invisible system ($\Delta\phi_{\text{CM}, I}$) are defined. Larger values of p_{T}^{CM} tend to come from out-of-acceptance noise or misreconstruction of physics objects, including $p_{\text{T}}^{\text{miss}}$, while $\Delta\phi_{\text{CM}, I}$ will peak near 0 or π if there are misreconstructed events in data. Events are removed if $p_{\text{T}}^{\text{CM}} > 200 \text{ GeV}$ or $\Delta\phi_{\text{CM}, I}$ is near 0 or π (with a p_{T}^{CM} -dependent requirement). To account for inoperable HCAL endcap sectors during 2018 data taking, events are also discarded from the 2018 data set, if there are any leptons or jets passing the respective object selections and within the regions ($-3.2 < \eta < -1.2$, $-1.77 < \phi < -0.67$). Events with lepton pairs having invariant masses consistent with J/ ψ meson decays are rejected.

Categorization of events can be imagined with a hierarchical ordering using a notation, $\text{NL}_{\ell}^{\text{type}} \text{Nj}_{\text{NbS}}^{\text{NsS}} X_{\text{NbISR}}^{\text{kin}}$, that indicates the reconstruction category of the event, with NL corresponding to the number of reconstructed leptons; 0, 1, 2, and 3, with events containing more than three reconstructed leptons discarded. These categories are further subdivided by lepton flavor, charge, and reconstruction quality (gold, silver, bronze), appearing as superscripts and subscripts of NL, respectively. The next tier of categorization is by $N_{\text{jet}}^{\text{S}}$ (NJ), the multiplicity of reconstructed jets assigned to the **S** system in each event. Depending on the region, there are then further subdivisions according to the number of b-tagged jets observed in the **S** and **ISR** systems (NbS and NbISR), or the number of SVs assigned to **S** (NsS), which are further split into SV central and forward categories (svc and svf, respectively). Finally, some categories have additional subdivisions according to the kinematic variables $p_{\text{T}}^{\text{ISR}}$ and γ_{\perp} , with each variable being used to define a “low” signal-depleted region (denoted by p-, $\gamma-$ respectively) and a “high” signal-enriched region (denoted by p+, $\gamma+$ respectively), leading to potentially

four such separate subdivisions ($p-\gamma-$, $p-\gamma+$, $p+\gamma-$, and $p+\gamma+$). The cases where the four kinematic subdivisions are employed are denoted by “ $p \pm \gamma \pm$ ” in the category definition tables. In all cases, $\gamma-$ corresponds to $\gamma_\perp < 0.5$ and $\gamma+$ corresponds to $\gamma_\perp > 0.5$.

There are 84 exclusive zero lepton (0L) categories defined as outlined in Table 1. Within each of these categories, events are counted in bins of R_{ISR} and M_\perp , with the definition of the N_{jet}^S -dependent bin boundaries for all of the 0L regions listed in Table 2. In the limit of extreme mass spectrum compression it is still possible to reconstruct soft SVs, therefore, dedicated 0L categories that require the presence of soft SVs associated with the S system are introduced for regions with lower S jet multiplicities. For larger N_{jet}^S , there are regions ranging from 2 jets (2J) to 5 jets (5J) that target intermediate mass splittings in models such as T2tt and T2bW. The 0L categories with higher S object multiplicities and bins with lower R_{ISR} values are very good at providing constraints for QCD multijet and other backgrounds.

Table 1: Category definitions for 0L regions for each N_{jet}^S multiplicity. The highest (5J) is inclusive ($N_{\text{jet}}^S \geq 5$). There are 84 exclusive categories in total for the 0L regions.

N_{jet}^S	$N_{\text{b tag}}^S$	$N_{\text{b tag}}^{\text{ISR}}$	N_{SV}^S	kin	p_T^{ISR} [GeV]
0J			1 or ≥ 2	svc or svf	$[350, \infty)$
1J	0 or 1	0 or ≥ 1	≥ 1	svc or svf	$[400, \infty)$
			0	$p-$ or $p+$	$[400, 550]$ or $[550, \infty)$
2J	0 or 1	0 or ≥ 1		$p \pm \gamma \pm$	$[350, 500]$ or $[500, \infty)$
		≥ 2			
3J	0 or 1	0 or ≥ 1		$p \pm \gamma \pm$	$[350, 500]$ or $[500, \infty)$
		≥ 2			
4J	0 or 1	0 or ≥ 1		$p \pm \gamma \pm$	$[350, 500]$ or $[500, \infty)$
		≥ 2			
5J	0 or 1	0 or ≥ 1		$p \pm \gamma \pm$	$[350, 500]$ or $[500, \infty)$
		≥ 2			

The categorization of the one-lepton (1L) regions is the most expansive in the analysis with 178 exclusive regions, as they are applicable to a wide range of signals. Additional CRs are defined based on the lepton reconstruction quality, allowing for further background constraints among regions, particularly allowing for the shapes and normalization of various types of lepton contributions to be measured from data. Depending on N_{jet}^S , 1L events can be categorized by either the lepton flavor, or charge (to better control $W(\ell\nu) + \text{jets}$ backgrounds), or both. As in 0L, the 1L categories include dedicated regions requiring tagged SVs, which are most relevant for the most compressed signals also having soft heavy-flavor decays. The 1L category definitions are listed in Table 3. The $R_{\text{ISR}}-M_\perp$ bin definitions within each of these regions are shown in Table 4.

For the two lepton (2L) final-state categorization, the gold regions are defined as having two gold leptons. Similarly, silver categorization requires one gold and one silver or both silver, while bronze only includes the gold-bronze and silver-bronze cases. The 2L categories with gold leptons are signal rich, while the silver and bronze ones are important for constraining nonprompt- and misidentified-lepton backgrounds. Figure 14 shows an example $R_{\text{ISR}}-M_\perp$ distribution with the bin boundaries overlaid for the 2L, 0 S-jet category. The 2L category definitions are presented in Table 5. Depending on the N_{jet}^S multiplicity, different combinations of

Table 2: The R_{ISR} and M_{\perp} bin definitions for 0L regions for each N_{jet}^S multiplicity. The highest (5J) is inclusive ($N_{\text{jet}}^S \geq 5$). The lower R_{ISR} bins denoted as "CR" are used as control regions.

N_{jet}^S	R_{ISR}	M_{\perp} [GeV]	N_{bins}
0J	[0.95, 0.985] CR	[0, ∞)	4
	[0.985, 1]	[0, 5] or [5, 10] or [10, ∞)	
1J	[0.8, 0.9] CR	[0, ∞)	6
	[0.9, 0.93] CR	[0, ∞)	
	[0.93, 0.96]	[0, 20] or [20, ∞)	
	[0.96, 1]	[0, 15] or [15, ∞)	
2J	[0.65, 0.75] CR	[0, ∞)	6
	[0.75, 0.85] CR	[0, ∞)	
	[0.85, 0.9]	[0, ∞)	
	[0.9, 0.95]	[0, 20] or [20, ∞)	
3J	[0.95, 1]	[0, ∞)	6
	[0.55, 0.65] CR	[0, ∞)	
	[0.65, 0.75] CR	[0, ∞)	
	[0.75, 0.85]	[0, ∞)	
4J	[0.85, 0.9]	[0, 50] or [50, ∞)	5
	[0.9, 1]	[0, ∞)	
	[0.55, 0.65] CR	[0, ∞)	
	[0.65, 0.75] CR	[0, ∞)	
5J	[0.75, 0.85]	[0, 80] or [80, ∞)	5
	[0.85, 1]	[0, ∞)	
	[0.5, 0.6] CR	[0, ∞)	
	[0.6, 0.7] CR	[0, ∞)	
5J	[0.7, 0.8]	[0, 150] or [150, ∞)	5
	[0.8, 1]	[0, ∞)	

Table 3: Category definitions for 1L regions for each N_{jet}^S multiplicity. The highest (4J) is inclusive ($N_{\text{jet}}^S \geq 4$). There are a total of 178 categories for the 1L regions.

N_{jet}^S	lep qual	lep cat	$N_{\text{b tag}}^S$	$N_{\text{b tag}}^{\text{ISR}}$	N_{SV}^S	kin	p_T^{ISR} [GeV]
0J	gold silver or bronze	ℓ^+ or ℓ^- e or μ			≥ 1	svc or svf	$[350, \infty)$
	gold silver or bronze	e^+ or e^- or μ^+ or μ^- e or μ		0 or ≥ 1	0	$p-$ or $p+$	$[350, 500]$ or $[500, \infty)$
1J	gold silver or bronze	e or μ			≥ 1	svc or svf	$[350, \infty)$
	gold silver or bronze	ℓ^+ or ℓ^- e or μ	0 or 1	0 or ≥ 1	0	$p \pm \gamma \pm$	$[350, 500]$ or $[500, \infty)$
2J	gold		0 or 1	0 or ≥ 1			
	silver or bronze	e or μ	≥ 2			$p \pm \gamma \pm$	$[350, 500]$ or $[500, \infty)$
3J	gold		0 or 1	0 or ≥ 1			
	silver or bronze	e or μ	≥ 2			$p \pm \gamma \pm$	$[350, 500]$ or $[500, \infty)$
4J	gold		0 or 1	0 or ≥ 1			
	silver or bronze	e or μ	≥ 2			$p \pm \gamma \pm$	$[350, 500]$ or $[500, \infty)$

lepton charge and flavor are used to further split categories. In the 2L category with 0 S-jets, the gold category includes separate regions for each of the lepton flavor combinations, while the region requiring a soft SV tag integrates over lepton flavor and charge. There is also a same-sign (SS) lepton category, which is integrated over the lepton flavor.

Categories are established for cases where the dilepton pair is consistent with a “Z^{*}” candidate, specifically when there are one or two S jets present. Here, these Z^{*} candidates, have opposite-sign (OS) leptons with same flavor (SF) also in the same S-system hemisphere. The “noZ” categorization is for OS, different-flavor (DF) events, or OS-SF events with the leptons appearing in different hemispheres. These regions also have an SS dilepton category, with all three of these classes integrated over lepton flavor. For all of the 2L silver and bronze regions, leptons are separated by flavor (ee, $\mu\mu$, or e μ) in order to better serve as CRs capable of disentangling the contributions from different nonprompt-lepton sources and processes. Bin boundaries in R_{ISR} and M_{\perp} for all the 2L regions are summarized in Table 6.

For the three-lepton (3L) categories, the gold categories are defined such that all three leptons must have gold quality (GGG). The sub-splittings for these include events with 0 or ≥ 1 S-jet, the presence of a Z^{*} candidate, no Z boson, or three same-sign leptons. Throughout the 3L category there is no b-tagged jet counting and no other splitting of categories based on p_T^{ISR} , γ_{\perp} , or the presence of SVs. The 3L silver category includes GGS and GSS combinations for the individual lepton quality, while the 3L bronze category includes GGB and GS \bar{B} quality combinations. The sub-categorization for all lepton quality criteria in 3L is the same. The definitions of the 3L analysis regions are presented in Table 7. There are no M_{\perp} bins in the 3L

Table 4: The R_{ISR} and M_{\perp} bin definitions for 1L regions for each N_{jet}^S multiplicity. The highest (4J) is inclusive ($N_{\text{jet}}^S \geq 4$). The lower R_{ISR} bins denoted as "CR" are used as control regions.

N_{jet}^S	R_{ISR}	M_{\perp} [GeV]	N_{bins}
0J	[0.96, 0.98] CR	[0, 10] or $[10, \infty)$	5
	[0.98, 1]	[0, 5] or $[5, 10]$ or $[10, \infty)$	
1J	[0.85, 0.9] CR	[0, 30] or $[30, \infty)$	5
	[0.9, 0.95]	[0, 20] or $[20, \infty)$	
	[0.9, 0.95]	$[0, \infty)$	
2J	[0.8, 0.85] CR	[0, 70] or $[70, \infty)$	5
	[0.85, 0.9]	[0, 50] or $[50, \infty)$	
	[0.9, 1]	$[0, \infty)$	
3J	[0.65, 0.75] CR	[0, 100] or $[100, \infty)$	5
	[0.75, 0.85]	[0, 80] or $[80, \infty)$	
	[0.85, 1]	$[0, \infty)$	
4J	[0.6, 0.7] CR	[0, 180] or $[180, \infty)$	5
	[0.7, 0.8]	[0, 150] or $[150, \infty)$	
	[0.8, 1]	$[0, \infty)$	

categories (one integrated bin), only bins in R_{ISR} , with bin boundaries for 3L with 0 S jet and 3L with 1 S jet categories summarized in Table 8.

While the signal model-dependent results involve a simultaneous fit to all of the bins and categories included in this analysis, a subset of CR bins are identified in order to both study the fit model in data prior to the unblinding of signal-sensitive regions, and also to derive model-independent upper limits on a subset of bin/category combinations. To be included as a CR bin, there must be less than 1% signal contamination (relative to expected backgrounds) for any of the signals considered in the analysis. The CR bins account for 648 out of the total, 2443 bins, encompassing 62% of the expected SM background events. In general, the chosen CR bins are at lower values of R_{ISR} , where expected signal-to-background is significantly less favorable. A simultaneous fit of the CR bins is able to constrain all of the nuisance parameters with data.

To derive model-independent limits, combinations of the previously defined "signal" bins are combined into seven "superbins", defined in Table 9. Five of the superbins were derived by systematically examining the expected signal significance for clusters of bins from admixtures of signals corresponding to five groupings of top squark, electroweakino, and slepton pair models with low and intermediate Δm . To look for b-enriched signals similar to those from top squark pair decays, there are three superbins for low Δm and one for medium Δm . One of these low- Δm superbins was defined with only low-momentum SV candidates. One superbin is defined targeting signal models with sparticle decays to W or Z bosons, such as TChiWZ and TChiWW. For signals consistent with compressed slepton decays with $\Delta m < 10$ GeV, another superbin is similarly defined to feature two leptons with OS-SF. An additional superbin is defined for 3L final states.

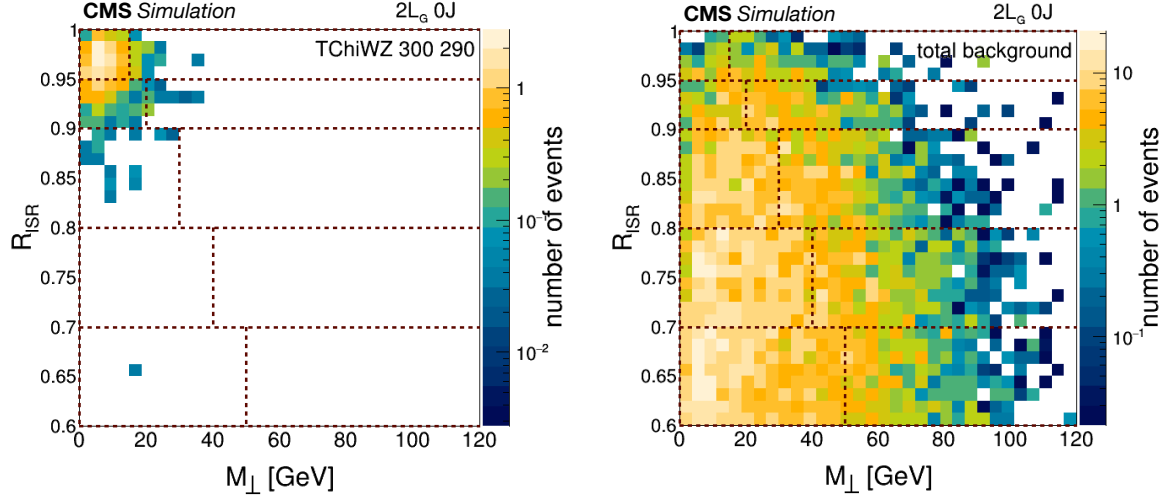


Figure 14: Distributions of R_{ISR} vs. M_{\perp} for a TChiWZ signal sample with a parent mass of 300 GeV and a LSP mass of 290 GeV (left) and the corresponding total SM background (right) for the 2L, 0 S-jet category. The dashed lines show the bin edges for this particular jet multiplicity.

Table 5: Category definitions for 2L regions for each N_{jet}^S multiplicity. The highest (2J) is inclusive ($N_{jet}^S \geq 2$). There is a total of 115 exclusive 2L categories.

N_{jet}^S	lep qual	lep cat	N_b^S tag	N_b^{ISR} tag	N_{SV}^S	kin	p_T^{ISR} [GeV]
0J	gold or silver or bronze				≥ 1	svc or svf	[250, ∞)
	gold	e^+e^- or $\mu^+\mu^-$ or $e^\pm\mu^\mp$		0 or ≥ 1	0	$p \pm \gamma \pm$	[250, 350] or [350, ∞)
	silver or bronze	ee or $\mu\mu$ or $e\mu$					[250, ∞)
1J	gold	Z* or noZ (OS)	0 or 1	0 or ≥ 1		$p \pm \gamma \pm$	[250, 350] or [350, ∞)
	silver or bronze	ee or $\mu\mu$ or $e\mu$					[350, ∞)
2J	gold	Z* or noZ (OS)	0 or ≥ 1	0 or ≥ 1		$p \pm \gamma \pm$	[250, 350] or [350, ∞)
	silver or bronze	ee or $\mu\mu$ or $e\mu$					[350, ∞)

7 Background and signal fit model

A maximum likelihood fit is performed simultaneously to all of the 2443 R_{ISR}/M_{\perp} bins in the 392 categories, as defined in the previous section. The fit model is implemented with the COMBINE statistical analysis tool [101] based on the ROOFIT [102] and ROOSTATS frameworks [103]. In the fit model, the likelihood is modeled as a product of Poisson probability distributions, one for each bin, with a rate parameter equal to the total expected event yield in that bin, calculated as the sum of contributions from different processes. The primary dependence on simulation in the background modeling is associated with the nominal initial values of these process-dependent bin yields (accounting for all previously described scale factors and corrections).

The modeling of different background contributions in the fit (e.g., $W + \text{jets}$, $t\bar{t}X + \text{jets}$) is fur-

Table 6: The R_{ISR} and M_{\perp} bin definitions for 2L regions for each N_{jet}^S multiplicity. The highest (2J) is inclusive ($N_{\text{jet}}^S \geq 2$). The lower R_{ISR} bins denoted as "CR" are used as control regions.

N_{jet}^S	R_{ISR}	M_{\perp} [GeV]	N_{bins}
0J	[0.6, 0.7] CR	[0, 50] or [50, ∞)	10
	[0.7, 0.8] CR	[0, 40] or [40, ∞)	
	[0.8, 0.9]	[0, 30] or [30, ∞)	
	[0.9, 0.95]	[0, 20] or [20, ∞)	
	[0.95, 1]	[0, 15] or [15, ∞)	
1J	[0.5, 0.6] CR	[0, 100] or [100, ∞)	10
	[0.6, 0.7] CR	[0, 80] or [80, ∞)	
	[0.7, 0.8]	[0, 60] or [60, ∞)	
	[0.8, 0.9]	[0, 40] or [40, ∞)	
	[0.9, 1]	[0, 30] or [30, ∞)	
2J	[0.5, 0.65] CR	[0, 100] or [100, ∞)	7
	[0.65, 0.75] CR	[0, 80] or [80, ∞)	
	[0.75, 0.85]	[0, 60] or [60, ∞)	
	[0.85, 1]	[0, ∞)	

Table 7: Category definitions for the 3L regions for each N_{jet}^S multiplicity. The highest (1J) is inclusive ($N_{\text{jet}}^S \geq 1$). There is a total of 15 exclusive 3L categories.

N_{jet}^S	lep qual	lep cat	p_T^{ISR} [GeV]
0J	gold or silver or bronze	Z^* or noZ or $\ell^{\pm}\ell^{\pm}\ell^{\pm}$	[250, ∞)
1J	gold or silver or bronze	Z^* or noZ or $\ell^{\pm}\ell^{\pm}\ell^{\pm}$	[250, ∞)

Table 8: The R_{ISR} and M_{\perp} bin definitions for 3L regions for each N_{jet}^S multiplicity. The highest (1J) is inclusive ($N_{\text{jet}}^S \geq 1$). The lower R_{ISR} bins denoted as "CR" are used as control regions. An additional control region with $0.5 \leq R_{\text{ISR}} < 0.6$ is also used with the 0 S-jet region.

N_{jet}^S	R_{ISR}	M_{\perp} [GeV]	N_{bins}
0J	[0.6, 0.7] CR	[0, ∞)	4
	[0.7, 0.8] CR	[0, ∞)	
	[0.8, 0.9]	[0, ∞)	
	[0.9, 1]	[0, ∞)	
1J	[0.55, 0.7] CR	[0, ∞)	3
	[0.7, 0.85]	[0, ∞)	
	[0.85, 1]	[0, ∞)	

Table 9: List of categories and M_{\perp}/R_{ISR} bins corresponding to each model-independent superbin.

Label	Lepton ID	N_{lep}	N_{jet}^S	$N_{\text{b/SV}}^S$	$p_{\text{T}}^{\text{ISR}}$	γ_{\perp}	$N_{\text{b tag}}^{\text{ISR}}$	$M_{\perp} [\text{GeV}]$	R_{ISR}
b jets low- Δm 1L	μ^-	1	0	0	high	incl	0	[0, 10]	[0.98, 1]
b jets low- Δm 2L	OS-DF	2	0	0	high	high	0	[0, 15]	[0.95, 1]
	OS-SF	2	0	0	high	high	0	[0, 15]	[0.95, 1]
	Z/noZ	2	1	0	high	high	0	[0, 30]	[0.85, 1]
	Z	2	≥ 2	0	high	high	0	$[0, \infty]$	[0.9, 1]
SV	-	0	0	≥ 2	low	low	≥ 1	$[5, \infty]$	[0.985, 1]
	ℓ^-	1	0	≥ 1	low	low	≥ 1	[0, 10]	[0.98, 1]
	ℓ^{\pm}	1	1	≥ 1	low	low	≥ 1	$[0, \infty]$	[0.95, 1]
	$\ell\ell$	2	0	≥ 1	low	low	≥ 1	[0, 15]	[0.95, 1]
b jets moderate- Δm	-	0	4	1	high	incl	0	$[0, \infty]$	[0.85, 1]
	-	0	4	2	high	incl	≥ 1	$[0, \infty]$	[0.85, 1]
	-	0	≥ 5	1	high	low	0	$[0, \infty]$	[0.8, 1]
	-	0	≥ 5	≥ 2	high	low	≥ 1	$[0, \infty]$	[0.8, 1]
	ℓ	1	2	1	high	high	0	$[0, \infty]$	[0.9, 1]
	ℓ	1	2	2	high	high	≥ 1	$[0, \infty]$	[0.9, 1]
	ℓ	1	3	1	high	high	0	$[0, \infty]$	[0.85, 1]
	ℓ	1	3	≥ 2	high	high	≥ 1	$[0, \infty]$	[0.85, 1]
	ℓ	1	≥ 4	1	high	high	0	$[0, \infty]$	[0.8, 1]
	ℓ	1	≥ 4	≥ 2	high	high	≥ 1	$[0, \infty]$	[0.8, 1]
	Z	2	1	≤ 1	high	high	0	$[0, \infty]$	[0.9, 1]
	Z	2	≥ 2	≤ 1	high	high	0	$[0, \infty]$	[0.85, 1]
	noZ	2	1	≤ 1	high	high	0	$[0, \infty]$	[0.9, 1]
	noZ	2	≥ 2	≤ 1	high	high	0	$[0, \infty]$	[0.85, 1]
Electroweak	OS-SF	2	0	0	high	high	0	[0, 15]	[0.95, 1]
	Z	2	1	0	high	incl	0	$[0, \infty]$	[0.9, 1]
	Z	2	≥ 2	0	high	incl	0	$[0, \infty]$	[0.85, 1]
	Z	3	0	0	low	incl	≥ 1	$[0, \infty]$	[0.9, 1]
	Z	3	≥ 1	0	low	incl	≥ 1	$[0, \infty]$	[0.85, 1]
2L OS-SF	OS-SF	2	0	0	high	incl	0	[0, 15]	[0.95, 1]
3L	Z	3	0	0	low	incl	≥ 1	$[0, \infty]$	[0.9, 1]
	Z	3	≥ 1	0	low	incl	≥ 1	$[0, \infty]$	[0.85, 1]
	noZ	3	0	0	low	incl	≥ 1	$[0, \infty]$	[0.9, 1]
	noZ	3	≥ 1	0	low	incl	≥ 1	$[0, \infty]$	[0.85, 1]
	SS	3	incl	0	low	incl	≥ 1	$[0, \infty]$	[0.9, 1]

ther subdivided by number and type of nonprompt leptons in defining the individual modeled processes. The nominal normalization for each process is modified by a collection of nuisance parameters, with each applied to one or (typically) more processes in a given category or bin, multiplying yields by a scale factor that is profiled in the maximum likelihood fit. This means that, for example, dibosons with one electron coming from a heavy-flavor decay and dibosons with two nonprompt muons are modeled as different processes with separate bin-dependent yields. This allows for a single nuisance parameter to modify the event yield of all diboson-associated processes or, independently, the yield of all events with nonprompt electrons from a single nonprompt source.

The nuisance parameters modeled in the fit are either *externally constrained* or *constrained with data*. Externally constrained parameters are associated with auxiliary measurements, performed using data sets independent of those considered in this analysis, from which prior uncertainties are correspondingly derived [54, 93]. These prior uncertainties, modeled as lognormal distributions, further multiply the likelihood such that externally constrained parameters are informed by both auxiliary measurements and the data set selected in this analysis. Alternatively, parameters are freely-floating in the fit, constrained instead using categorization and kinematic sidebands corresponding to CRs in data.

Data from all three years (2016–2018) are fit simultaneously in all categories and bins, with nuisances modeled as either common to all years or independent. There are numerous systematic uncertainties for which the parameters are determined in the fit. Each of the systematic uncertainty contributions, along with details of their number, year-by-year implementation, and size range, are summarized in Table 10.

7.1 Externally constrained systematic uncertainties

Uncertainties in the collected integrated luminosity are split by year, with correlations corresponding to common systematic uncertainty sources [104–106]. The uncertainty in the simulations of background processes resulting from missing higher-order corrections is estimated by varying the renormalization and factorization scales by a factor of two, with each of the two scales taken to be the same in each variation [107, 108]. Systematic uncertainties associated with the modeling of parton distribution functions are estimated using 100 variations provided with the NNPDF sets, while the effect of the uncertainty in the value of the strong coupling constant is estimated by varying the value $\alpha_s(m_Z) = 0.1180$ by ± 0.0015 [109]. Simulated events are reweighted such that the distribution of the number of additional pileup interactions matches that observed over the different data-taking periods, with associated systematic uncertainties evaluated by varying the total inelastic cross section within measured uncertainties [110]. The contribution from $t\bar{t}X + \text{jets}$ is normalized using the measured value of the cross section [111].

Differences between simulation and data in the efficiencies of lepton identification requirements for prompt leptons are evaluated using the tag-and-probe method applied to Z boson and J/ψ meson events, as described in Section 4. Independent scale factors and corresponding uncertainties are derived for electrons and muons, for each of the three data-taking years, and are separated by loose selection, identification, isolation, and impact parameter requirements. Uncertainties in the jet energy scale and resolution are modeled independently for each of the three data-taking periods [112, 113], with the effects of changes to the momentum of jets propagated to the p_T^{miss} . Similar year-independent nuisance parameters associated with the effects of unclustered energy on p_T^{miss} are included. The scale factors associated with differences for b jet tagging between simulation and data have corresponding nuisance parameters separated by source (heavy-flavor and light-flavor quark or gluon jets) and by year, with an additional

Table 10: Summary of systematic uncertainties for the full fit. The number of nuisance parameters is listed, with details as to how they are partitioned by data-taking period. The range of the parameter impact variation post-fit is given in the final column.

Source	Number of parameters	Uncertainty (%)
Externally constrained		
Integrated luminosity	1 / year (3)	1.5-2.5
Factorization/normalization scales, PDF, and Q^2	8	0-11
Pileup	1 / year (3)	1-7
p_T^{miss} trigger	2 / year (6)	1-3
Electron & muon efficiency	8 / year (24)	1
Jet energy scale and resolution	2 / year (6)	0-10
p_T^{miss} unclustered energy	1 / year (3)	0-6
p_T^{miss} trigger	2 / year (6)	1-3
b jet efficiency	2 + 2 / year (8)	0-3
Fast simulation corrections	7 / year (21)	1-10
Monte Carlo event count	1 / bin	1-15
Constrained with data		
W + jets normalization	9	1-12
t̄tX + jets normalization	9	2-20
QCD multijet normalization	9	5-30
Z/ γ^* + jets normalization	3	2-10
Diboson and Higgs boson normalization	3	2-10
Single top quark, triboson normalization	3	5-30
p_T^{ISR} and γ_{\perp}	28	1-10
Lepton category normalization	21	5-10
Misidentified and nonprompt leptons	36	3-12
b-tagged jet category normalization	68	1-10
SV tagging efficiency	3	1-10

parameter for each source accounting for correlations between years.

The efficiency as a function of p_T^{miss} to pass the trigger requirements has been measured with data collected using single-lepton reference triggers, and is compared to that found using background sample simulations to derive scale factors and corresponding uncertainties. These factors include variations depending on H_T (the scalar sum of the p_T of all jets with $p_T > 20 \text{ GeV}$ and $|\eta| < 5.0$ in the event), the number and flavor of leptons, as well as the S jet multiplicity.

Uncertainties arising from differences between the fast simulation used for signal processes and the full GEANT4-based simulation used for background processes are accounted for through a set of additional nuisance parameters. These uncertainties cover reconstructed leptons, b-tagged jets, SVs, and p_T^{miss} .

7.2 Systematic uncertainties determined from data

In order to account for data/simulation modeling differences that are not covered by the externally constrained systematic uncertainties included in the fit model, a collection of scale factor parameters obtained from control samples in data is included. Mismodeling can result from unaddressed topology-dependent effects in the derivation of prior constraints or from inherent shortcomings in the simulation. The large number and types of event categories included in the fit allows for these factors to be constrained directly from data, using a high-dimensional

collection of sidebands associated with kinematic, object quality, and multiplicity categorizations.

Background processes are separated into several groups that are treated with common systematic uncertainties: $W + \text{jets}$, $t\bar{t}X + \text{jets}$, $Z/\gamma^* + \text{jets}$, single top quark, dibosons (including Higgs to diboson final states), rare backgrounds, and QCD multijets. Each of these groups of processes is associated with a set of normalization parameters, which are determined directly from data, primarily using the effectively signal-free CR bins. The number of parameters for each group of processes depends on their relative importance to the analysis, and how well they can be constrained by CRs. The dominant backgrounds, $W + \text{jets}$ and $t\bar{t}X + \text{jets}$, have a separate scale factor for each lepton and S jet multiplicity category. The QCD background also has normalization factors, which are split by number of leptons and S jets. Intermediate backgrounds, such as diboson and $Z/\gamma^* + \text{jets}$, have one factor per lepton multiplicity. The single top quark and triboson/rare backgrounds have a single scale factor that maps to all subprocesses. The result is that major backgrounds have independent normalizations, constrained by data control regions, for each lepton and S jet multiplicity, allowing for data/simulation discrepancies specific to the modeling of that process to be evaluated from data without assumptions about how they could appear in different categories.

Kinematic requirements on p_T^{ISR} and γ_\perp are used to define categorizations expected to result in signal enriched and background dominated regions at higher and lower values, respectively. The analysis applies data-driven, kinematic category scale factors which are common to all background processes, with independent factors for p_T^{ISR} and γ_\perp categories that are also independently determined for different lepton and S jet multiplicities.

Lepton flavor, charge, quality, and configuration provide some of the most powerful types of categorization included in the analysis. There are scale factors modeled as common to all the processes in the analysis, which can account for data/simulation discrepancies in their relative rates that affect all processes in similar ways. This could follow from, for example, higher-order correlations between hadronic activity and lepton isolation, or mismodeling of event kinematics that modifies how leptons are clustered into hemispheres.

The analysis additionally measures scale factors for both electrons and muons that modify the rates of lepton candidates coming from either heavy-flavor decays or misidentified/non-prompt leptons from non-heavy-flavor decays, and also for changes in the M_\perp/R_{ISR} distributions for processes associated with these lepton sources. One set of factors scales all processes with an associated lepton, while two additional sets are specific to the lepton isolation and impact parameter requirements that define the various regions. In addition to normalization parameters, the fit also includes nuisance parameters that can change distribution shapes for nonprompt lepton backgrounds. Generic variations in R_{ISR} and M_\perp are parameterized in “up” and “down” templates calculated separately for R_{ISR} and M_\perp bins, where each bin is multiplied by a sliding fraction, which has the effect of skewing the kinematic distributions higher or lower. A nominal prior of 5% maximum variation is applied, leading to up to 10% relative variations in the highest and lowest M_\perp/R_{ISR} bins in a given category. These shape variations are implemented with separate factors for each lepton flavor and independently for each lepton and S jet multiplicity category. These constraints rely on the assumption that any such kinematic discrepancies in modeling of these background processes should be largely independent of the lepton quality, such that the bronze regions are used to predominantly constrain shape parameters common with gold for a given process.

To take into account uncertainties appearing due to the assignment of b-tagged jets to the S or the ISR system, there are scale factors to specifically account for data/simulation differences

in relative categorization frequencies, in addition to the constrained efficiency scale factors previously described. Top quark and non-top-quark backgrounds are modeled with separate scale factors. For the SVs, signal events will tend to have more central ($|\eta| \leq 1.5$) SV candidates resulting from real bottom or charm quarks, so scale factors are defined independently for central and forward SV categories.

The background fit model was studied using a full CR fit (also split by data-taking period), a fit also including all bronze lepton categories, and finally in a fit to all of the bins and categories included in the analysis over the entire data set. The quality of these background-only fits was primarily assessed by considering the distribution of data/fit-model residuals in each bin in the analysis. Each fit is observed to give a reasonably consistent description of event yields in data.

The fit quality for the full fit to the entire dataset is assessed more quantitatively by considering the distribution of the post-fit tail probability computed for each fit bin. The significance of an excess or deficit per bin is evaluated using the one-sided upper-tail Poisson probability. This probability is corrected³ for bias associated with double-counting $n = n_{\text{obs}}$ such that the average expected probability for background-only is 0.5 and the corresponding one-sided upper- and lower-tail probabilities sum to unity. The pseudo-data based evaluation integrates the upper-tail probability over the post-fit uncertainty in the background event yield per bin using a Gaussian posterior model; the method is closely related to the Z_N procedure of Ref. [114]. The resulting background-averaged probability (pseudo p -value) for consistency with the background-only hypothesis is then expressed in signed Gaussian quantiles as a z-score.

For the considered data set, under the simplifying assumptions of independent bins and neglecting the small expected reduction in variance associated with the fit to data, this post-fit z-score distribution is expected to be approximately Gaussian with a mean of zero and a standard deviation of 1.0. The distribution of the observed post-fit z-scores per bin is shown in Fig. 15 and is compared with the Gaussian distribution inferred from the sample mean and standard deviation. The observed distribution is consistent with a Gaussian having a mean of zero and a standard deviation 12% larger than unity. The characteristics of the ten most outlying bins have been examined; it is found that all but one is a CR bin.

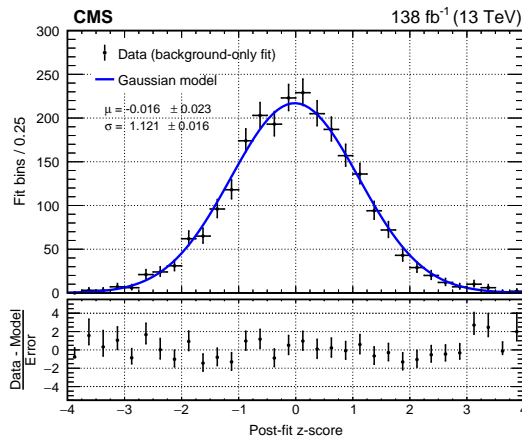


Figure 15: Distribution of post-fit z-scores for the full data set background-only fit. The superimposed Gaussian model uses the observed mean and standard deviation.

³The corrected upper-tail probability sum reads as $p(n_{\text{obs}}; \mu_b) = \sum_{n=n_{\text{obs}}}^{\infty} \text{Po}(n; \mu_b) - \frac{1}{2}\text{Po}(n_{\text{obs}}; \mu_b)$, where n_{obs} events are observed, μ_b is the expected number of background events, and Po represents the Poisson distribution.

8 Results

The maximum likelihood fit over 2443 bins in 392 categories is performed using the full data set. Event yields in data are observed to be in statistically good agreement with the background-only fit model within the uncertainties included in the fit model. Summaries of these data yields, integrated over categories and bins of M_{\perp} , are shown in Figs. 16 and 17 for the 0L, 1L, 2L, and 3L regions.

Event yields in data are compared to the background-only fit model for 0L and 1L final states in Fig. 18 for categories with higher S jet multiplicities and also separated by b-tagged jet categorization. These categories are designed to be particularly sensitive to signal models with larger numbers of jets following from sparticle decays, including heavy-flavor quarks following from intermediate top quark decays, as is the case for sparticle production of top squarks and gluinos. Such signals would appear as excesses in the high- R_{ISR} bins; no such excesses are observed in this data set.

Similarly, comparisons of data and background-only fit model event yields for regions with two gold leptons and no S jets and categories containing one or more central SV candidates are shown in Fig. 19. Overall, no significant deviations between the background model and data are observed, particularly those consistent with patterns expected from the presence of signals with electroweakinos, sleptons, or top squarks.

Event yields in data are also compared to the background-only fit model for all 0L, 1L, and 2L categories for the most compressed bin (the one with the highest R_{ISR} and lower M_{\perp}) for the gold regions in Fig. 20 (0L), Fig. 21 (0L & 1L), Fig. 22 (1L) and Figs. 23 and 24 (2L) amounting to 294 independent bins. Each panel also shows the observed post-fit z-score for the bin. Again, the data and the background-only fit model are generally in reasonable agreement and with no significant excess over the background-only fit model that could be an indication for a compressed signal.

We proceed to interpret results as constraints on potential signals using both model-dependent and model-independent interpretations. In order to constrain signal models outside of the collection considered in this analysis, aggregations of signal-sensitive bins in different final state categories, or superbins (defined in Section 6) are considered. Upper limits at 95% confidence level (CL) for the signal strength ($S_{\text{UL}}^{95\%}$) are calculated for each of these superbins using the modified frequentist CL_s method [115, 116]. The distribution of the expected number of events in each superbin is evaluated from the generation of pseudo-experiments from the background-only fit model, taking into account the posterior covariance of all nuisance parameters. From these distributions, the mean expected background, $N_{\text{bkg}}^{\text{pred}}$, standard deviation, $\sigma(N_{\text{bkg}}^{\text{pred}})$, and signal event number upper limits, $S_{\text{UL}}^{95\%}$, are calculated, as summarized in Table 11 for each of the eight superbins.

Model-dependent interpretations are calculated by performing signal-plus-background model fits for each considered scenario, independently for each simulated combination of sparticle masses. Using these signal-plus-background fits, along with the background-only fit to data, a profile likelihood ratio test statistic is used to evaluate upper limits on each of these model points. These are then interpolated among model points to fill in the complete sparticle mass plane. The model-dependent results represent upper exclusion limits at 95% CL on the product of the cross section and branching fractions for top squark, neutralino/chargino, and slepton processes. The asymptotic approximation of the modified frequentist approach is used to calculate these confidence levels with the profile likelihood ratio test statistic [115–117].

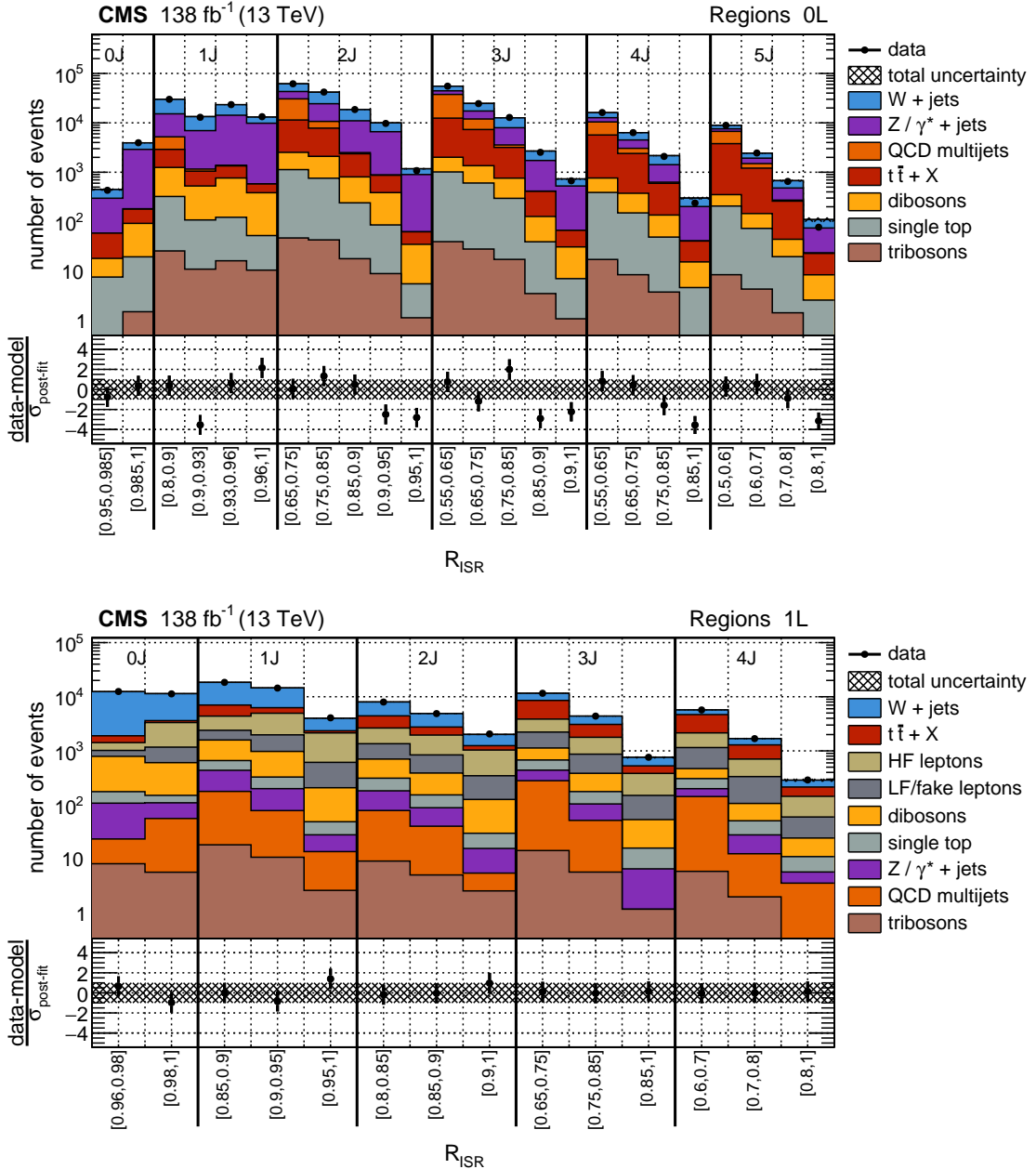


Figure 16: Post-fit distributions of data with the background-only fit model for the full data set in the 0L region (upper) and 1L region (lower). Bins are split by R_{ISR} along with N_{jet}^S . Yields are integrated over all other sub-categorizations and M_\perp . The sub-panels below the panels show the data minus fit model scaled by the post-fit model uncertainty.

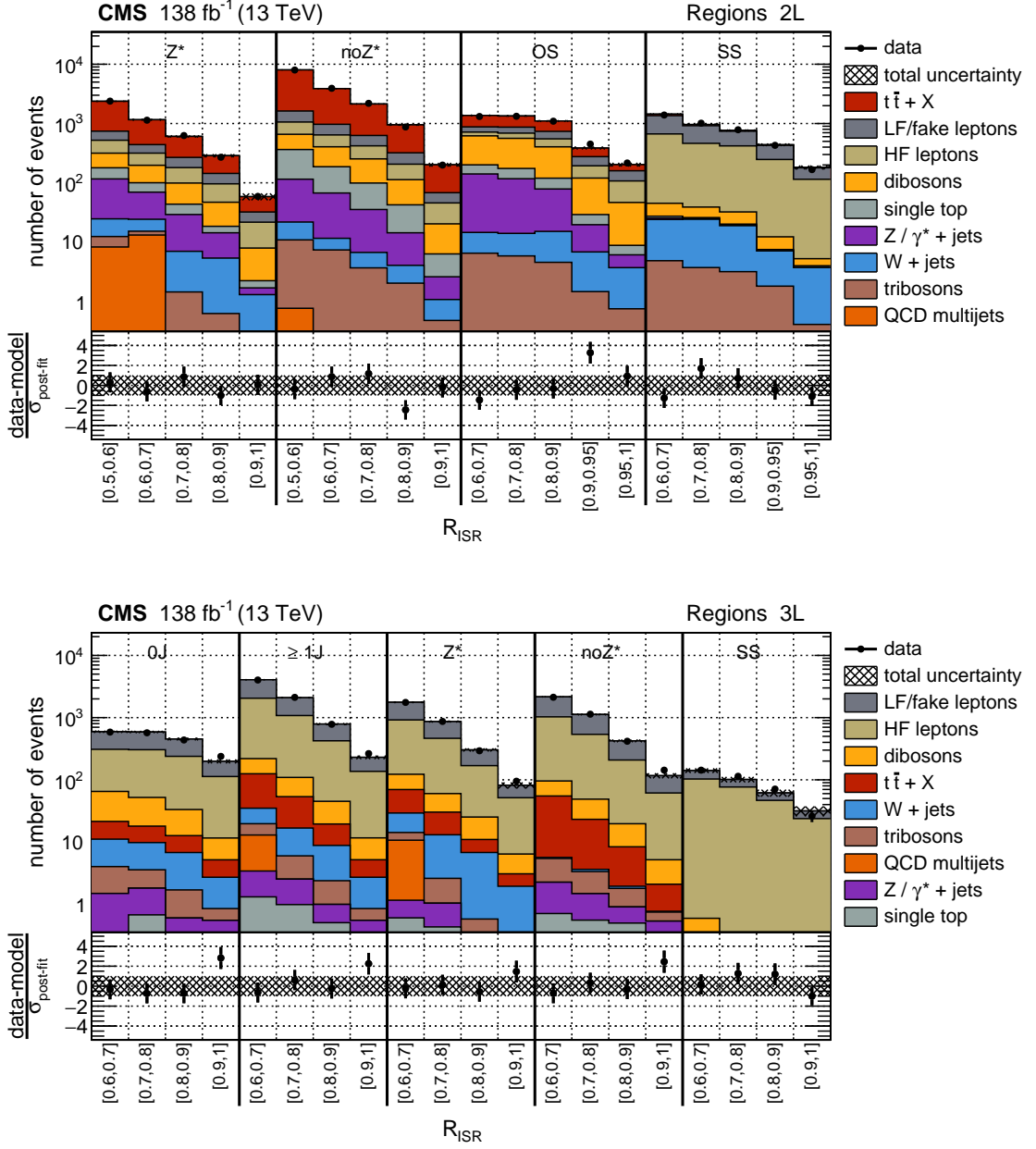


Figure 17: Post-fit distributions of data with the background-only fit model for the full data set in the 2L region (upper) and 3L region (lower). Bins are split by R_{ISR} along with lepton categorization. Yields are integrated over all other sub-categorizations and M_{\perp} . The sub-panels below the panels show the data minus fit model scaled by the post-fit model uncertainty.

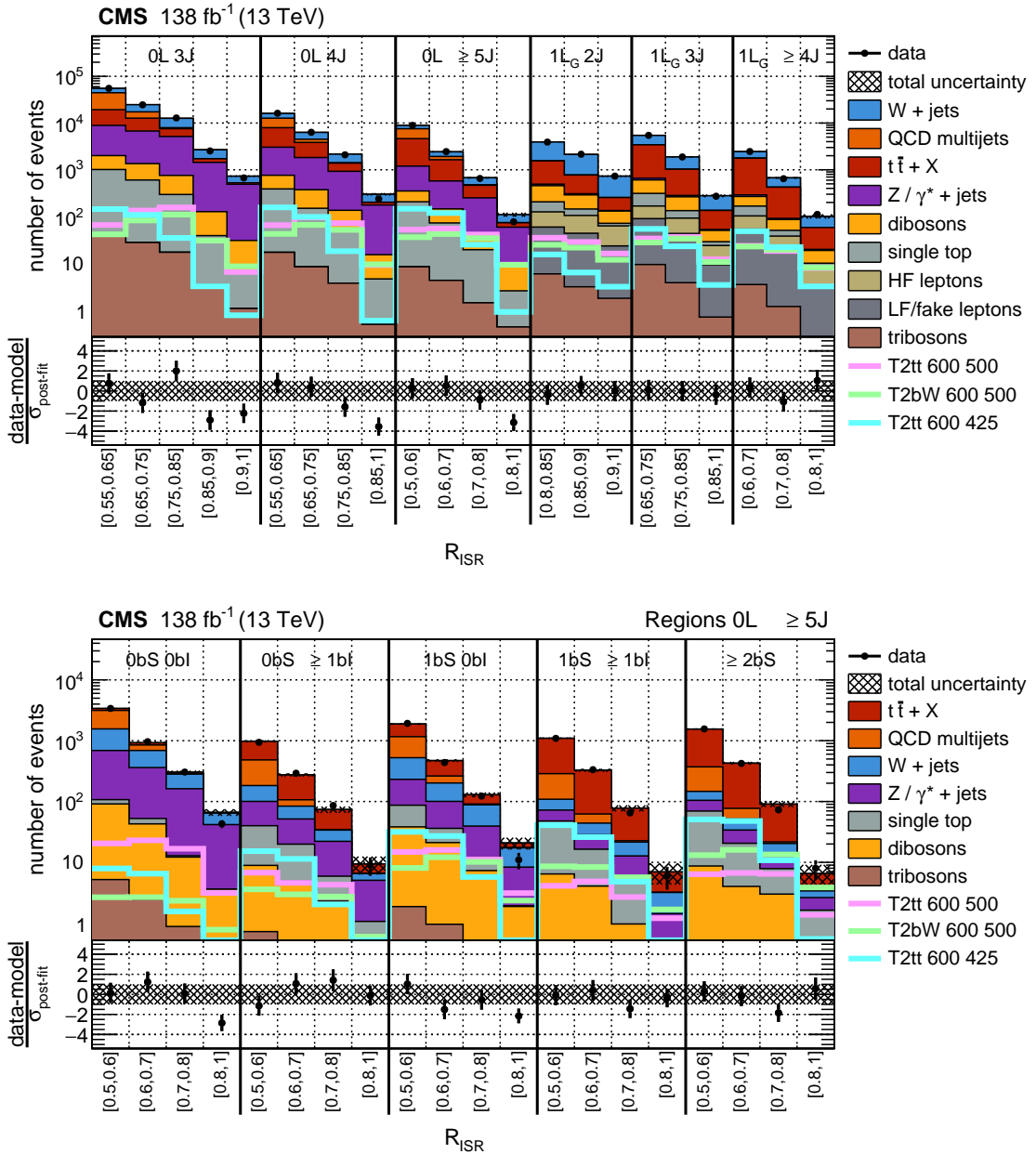


Figure 18: Post-fit distributions of data with the background-only fit model for the full data set. (Upper) 0L and 1L gold regions with larger jet multiplicities. (Lower) 0L 5J regions separated by b -tagged jet multiplicities in the S and ISR systems. Bins are split by R_{ISR} with yields integrated over all other sub-categorizations and M_{\perp} . The sub-panels below the panels show the data minus fit model scaled by the post-fit model uncertainty. Expected yields for example signal models are superimposed.

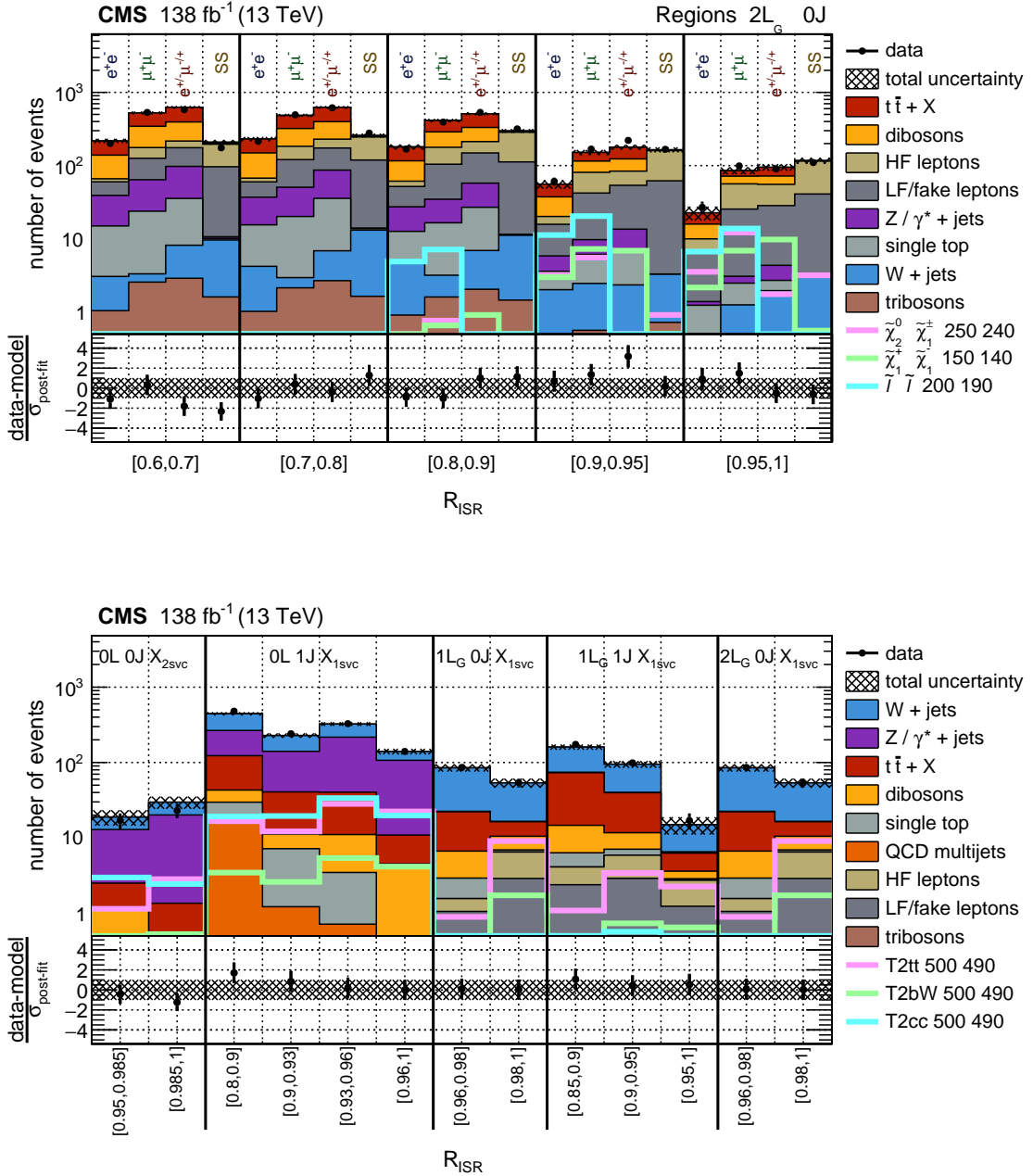


Figure 19: Post-fit distributions of data with the background-only model for the full data set. (Upper) 2L 0J gold regions separated by lepton flavor and charge. (Lower) Central b-tagged SV regions in 0L, 1L, and 2L final states. Bins are split by R_{ISR} with yields integrated over all other sub-categorizations and M_{\perp} . The sub-panels below the panels show the data minus fit model scaled by the post-fit model uncertainty. Expected yields for example signal models are superimposed.

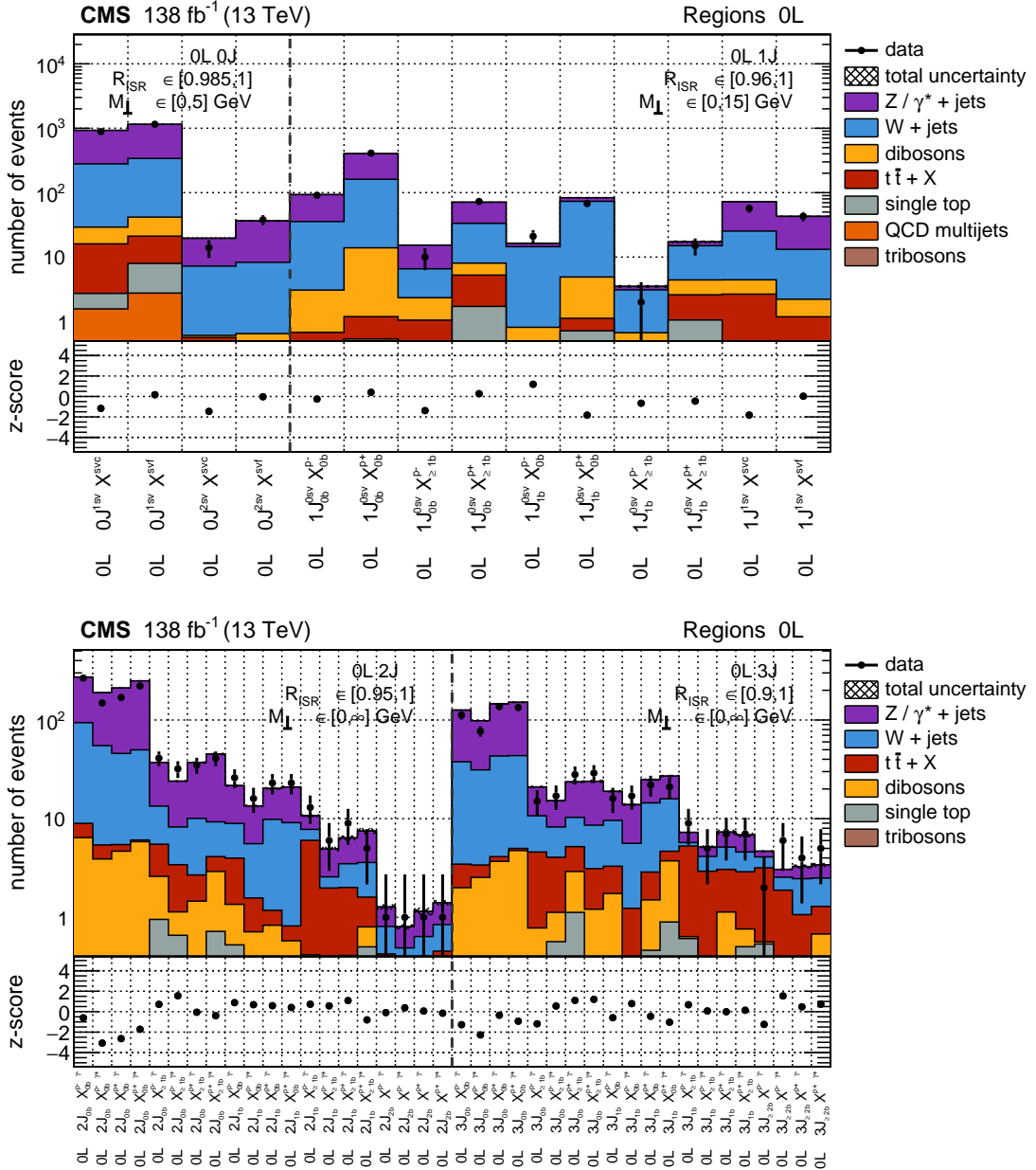


Figure 20: Post-fit distributions of data with the background-only model for the full data set for the highest R_{ISR} bin in each analysis category. (Upper) 0L 0J and 1J regions. (Lower) 0L 2J and 3J regions. The sub-panels below the panels indicate the post-fit z-score for each bin.

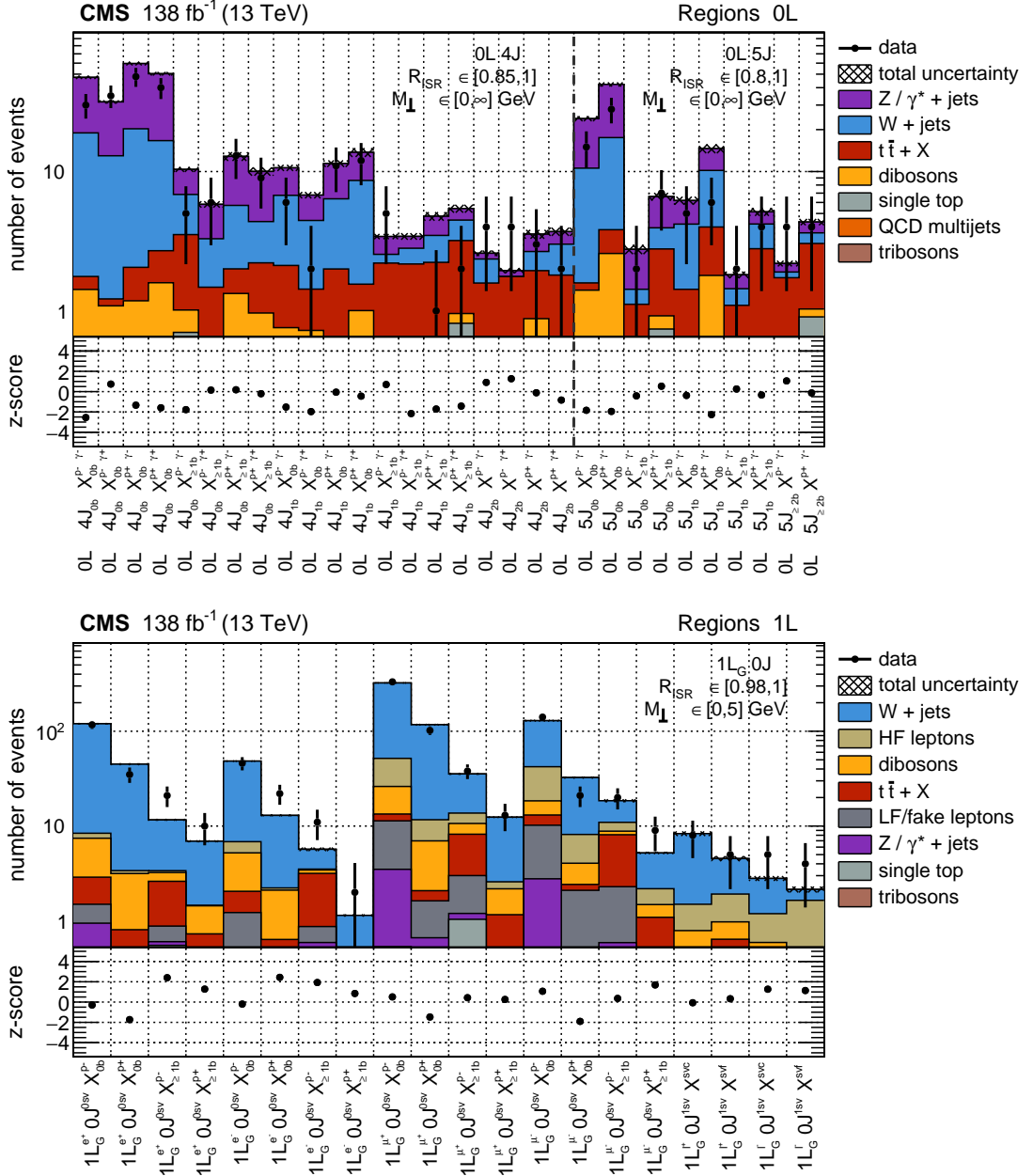


Figure 21: Post-fit distributions of data with the background-only model for the full data set for the highest R_{ISR} bin in each analysis category. (Upper) 0L 4J and $\geq 5\text{J}$ regions. (Lower) 1L 0J regions with a gold lepton. The sub-panels below the panels indicate the post-fit z-score for each bin.

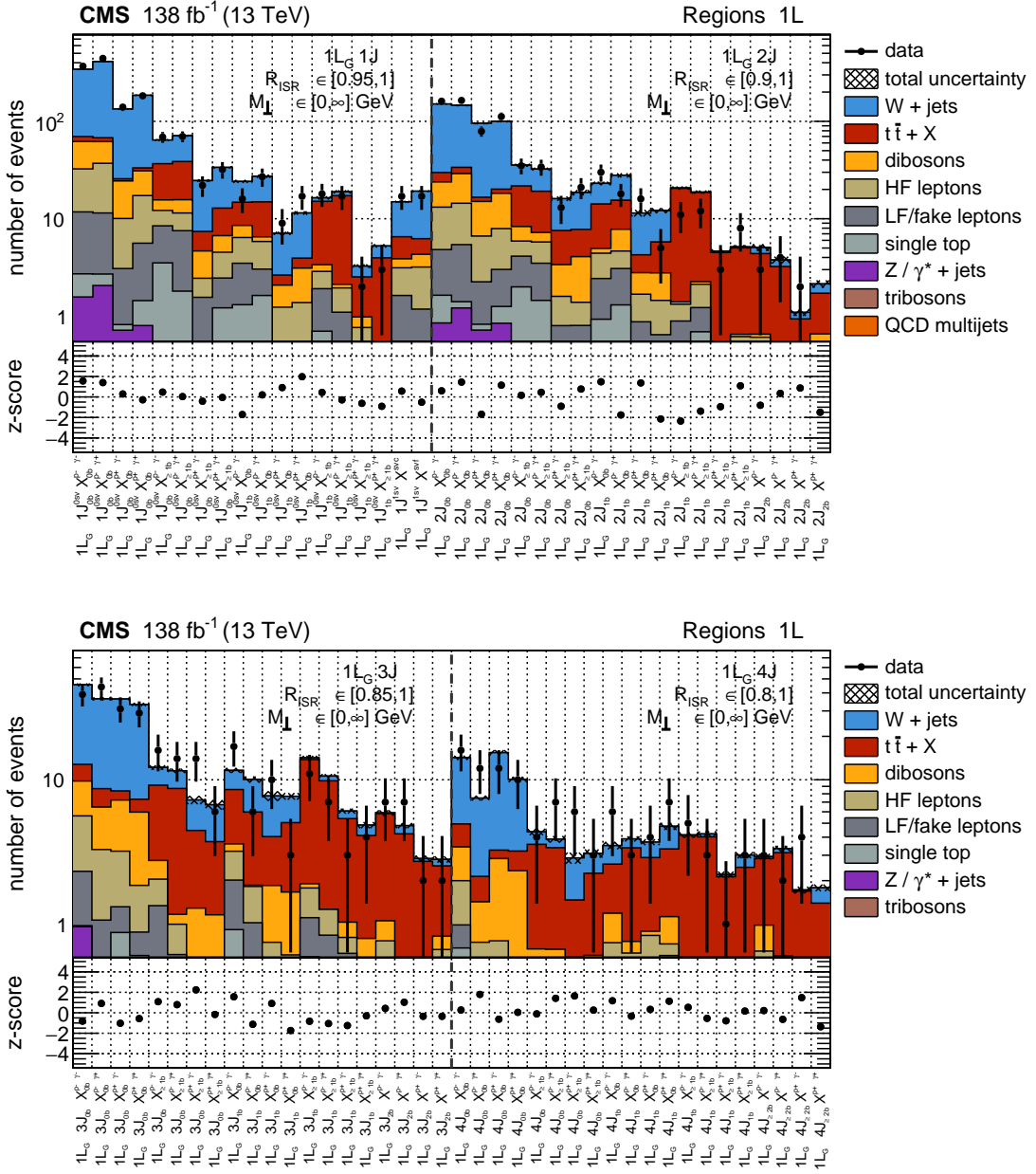


Figure 22: Post-fit distributions of data with the background-only model for the full data set for the highest R_{ISR} bin in each analysis category. (Upper) 1L 1J and 2J regions with a gold lepton. (Lower) 1L 3J and ≥ 4 J regions with a gold lepton. The sub-panels below the panels indicate the post-fit z-score for each bin.

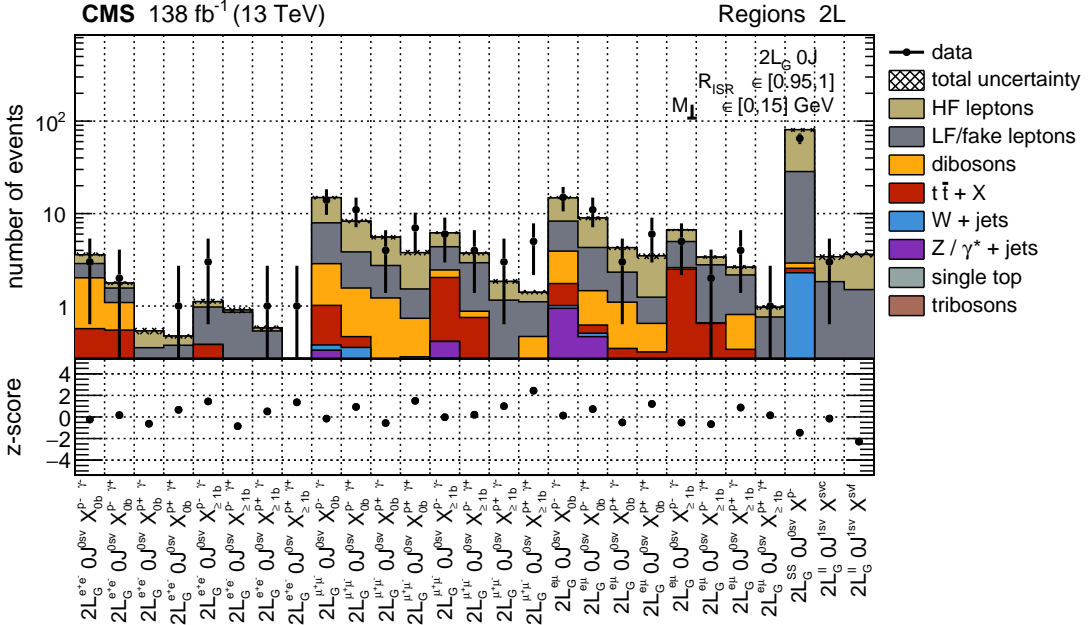


Figure 23: Post-fit distributions of data with the background-only model for the full data set for the highest R_{ISR} bin in each analysis category of the 2L 0J regions with gold leptons. The sub-panels below the panels indicate the post-fit z-score for each bin.

Table 11: Event counts observed in data, N_{obs} , in each of the model-independent bins, compared with predictions from the CR fit, $N_{\text{bkg}}^{\text{pred}}$, their corresponding uncertainties, $\sigma(N_{\text{bkg}}^{\text{pred}})$, and the upper limits at 95% CL on the signal strength ($S_{\text{UL}}^{95\%}$) in event counts. All superbins are mutually exclusive except the b jets low- Δm case which aggregates the b jets low- Δm 1L, b jets low- Δm 2L, and SV superbins.

Region	N_{obs}	$N_{\text{bkg}}^{\text{pred}}$	$\sigma(N_{\text{bkg}}^{\text{pred}})$	$S_{\text{UL}}^{95\%}$
b jets low- Δm 1L	50	65.8	21.4	9.5
b jets low- Δm 2L	16	10.3	3.9	14.6
SV	38	37.2	8.5	17.8
b jets low- Δm	104	115.5	22.3	16.2
b jets moderate- Δm	83	108.1	18.2	9.9
Electroweak	26	30.2	5.5	9.6
2L OSSF	12	10.2	4.5	9.9
3L	21	25.2	5.0	9.0

Figure 25 shows the limits found for top squark pair production with the decay $\tilde{t} \rightarrow t\tilde{\chi}_1^0$ (the T2tt model) in the left panel and for $\tilde{t} \rightarrow b\tilde{\chi}_1^+$ with $\tilde{\chi}_1^+ \rightarrow W^+\tilde{\chi}_1^0$ decay (the T2bW model) in the right panel. Figure 26 shows the limits found for top squark pair production with the decay $\tilde{t} \rightarrow c\tilde{\chi}_1^0$ (the T2cc model). The T2tt limits are generally stronger than the previous limits from CMS and ATLAS for these compressed models with $\Delta m < 200 \text{ GeV}$ [13, 17–20].

Limits on the TChiWZ model are presented in Fig. 27, using both wino-like and higgsino-like cross sections. These limits are generally stronger than the previous limits from CMS and ATLAS for these compressed models with $\Delta m < 80 \text{ GeV}$ [8, 10, 11, 21, 35]. For $3 < \Delta m < 50 \text{ GeV}$, the observed 95% CL lower mass limit on higgsino-like chargino-neutralino production

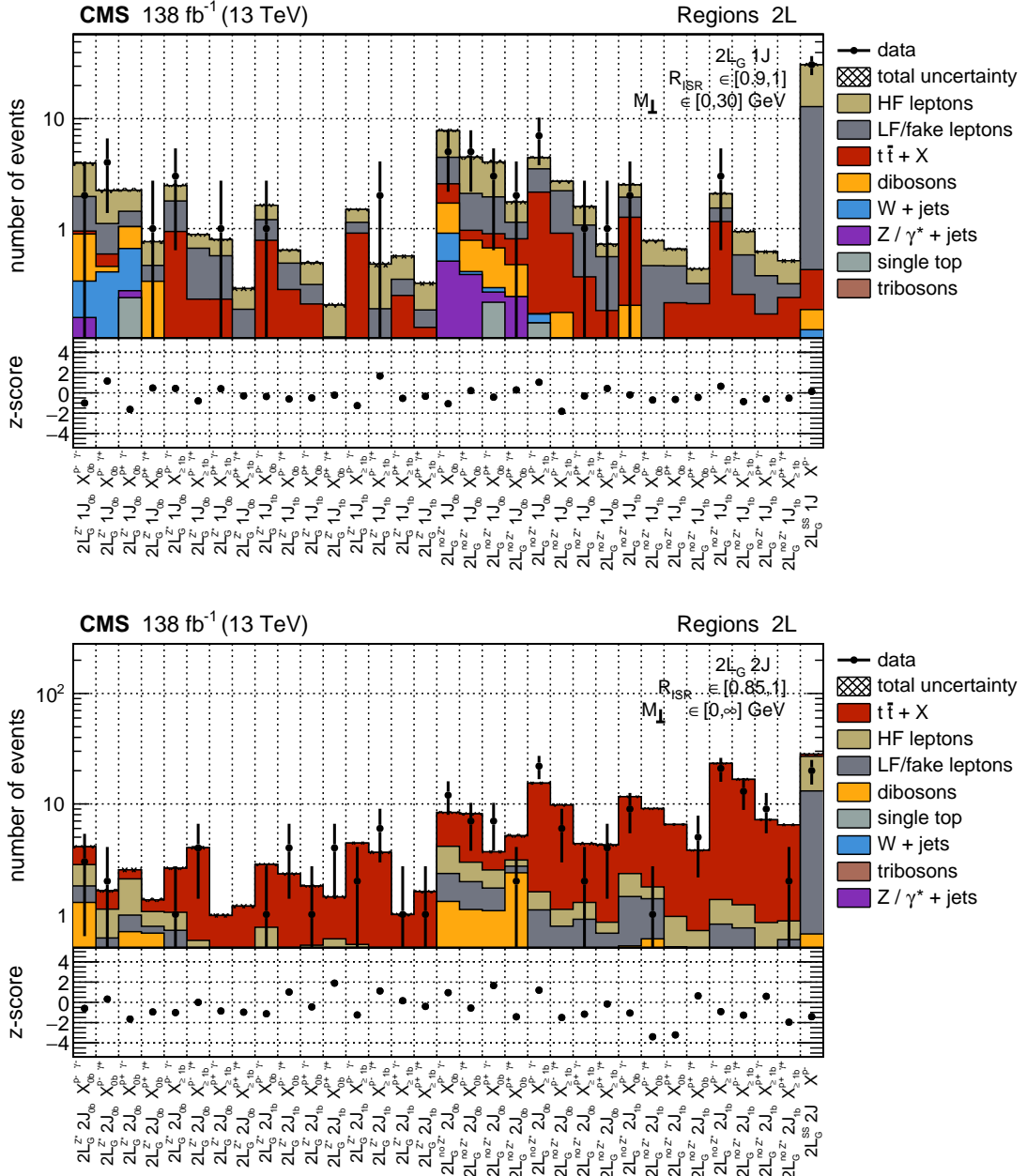


Figure 24: Post-fit distributions of data with the background-only model for the full data set for the highest R_{ISR} bin in each analysis category. (Upper) 2L 1J regions with gold leptons. (Lower) 2L \geq 2J regions with gold leptons. The sub-panels below the panels indicate the post-fit z-score for each bin.

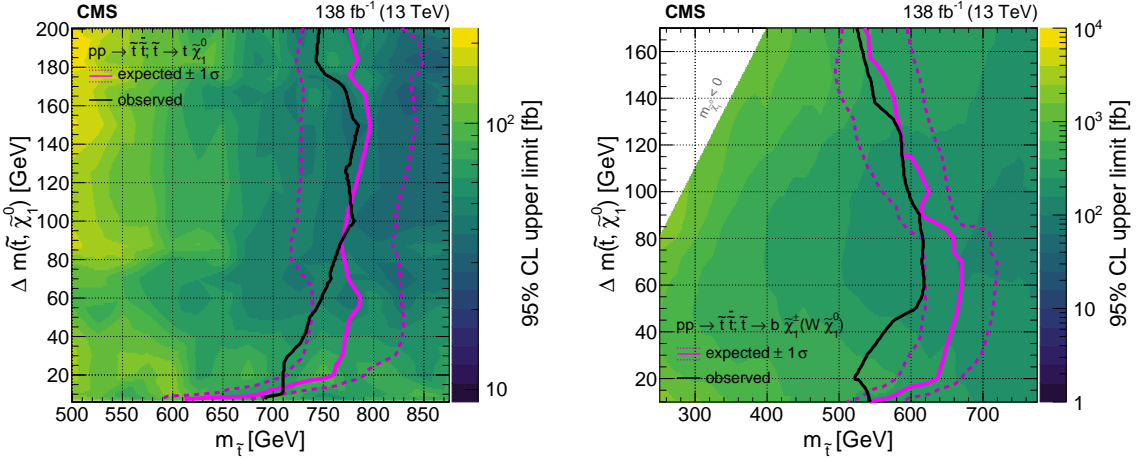


Figure 25: Top squark pair production. Observed upper limits at 95% CL on the product of the cross section and relevant branching fractions are shown using the color scale where the \tilde{t} mass is on the x -axis and the mass difference between the \tilde{t} and the LSP is on the y -axis. The expected lower mass limits (magenta line) together with their $\pm 1\sigma$ uncertainties (magenta dashed lines) and the observed lower mass limits (black line) are indicated for 100% branching fractions. The left panel shows the results for the T2tt model with limits on $\sigma(\tilde{t}\tilde{t}) \mathcal{B}^2(\tilde{t} \rightarrow t\tilde{\chi}_1^0)$. The right panel shows the results for the T2bW model with limits on $\sigma(\tilde{t}\tilde{t}) \mathcal{B}^2(\tilde{t} \rightarrow b\tilde{\chi}_1^+ \mathcal{B}^2(\tilde{\chi}_1^+ \rightarrow W^+\tilde{\chi}_1^0))$.

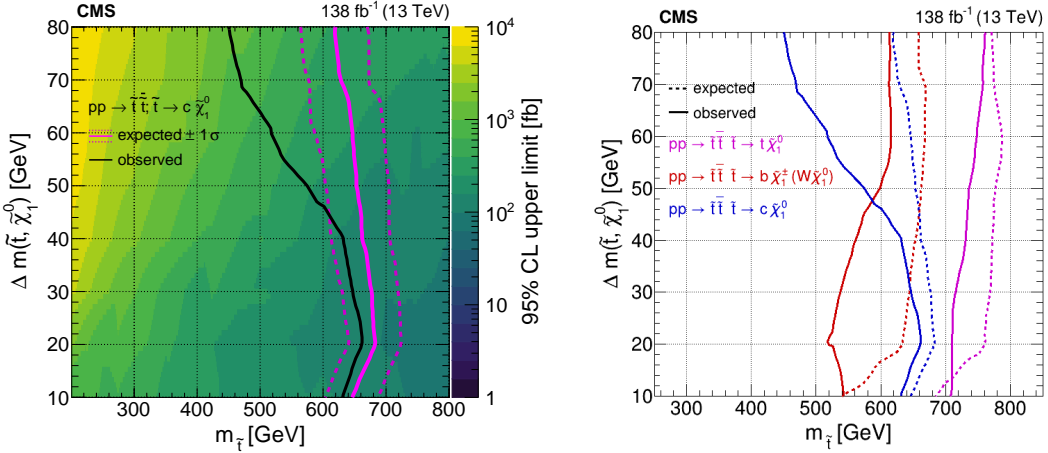


Figure 26: Top squark pair production. Observed upper limits at 95% CL on the product of the cross section and branching fraction squared, $\sigma(\tilde{t}\tilde{t}) \mathcal{B}^2(\tilde{t} \rightarrow c\tilde{\chi}_1^0)$ (left), are shown using the color scale where the \tilde{t} mass is on the x -axis and the mass difference between the \tilde{t} and the LSP is on the y -axis. The expected lower mass limits (magenta line) together with their $\pm 1\sigma$ uncertainties (magenta dashed lines) and the observed lower mass limits (black line) are indicated for 100% branching fractions. Observed and median expected limits for top squark pair production at 95% CL (right) for the three decay modes investigated.

exceeds 163 GeV. For $8 < \Delta m < 65$ GeV, the observed 95% CL lower mass limit on wino-like chargino-neutralino production exceeds 300 GeV; this can be compared with the combined lower mass limit exceeding 200 GeV in this Δm range in [35], and a similar combined lower mass limit exceeding 215 GeV in [24].

Figure 28 shows the experimental upper limits on chargino pair production for the decays associated with the TChiWW model and the TChiSlepSnu model. The TChiWW results exclude

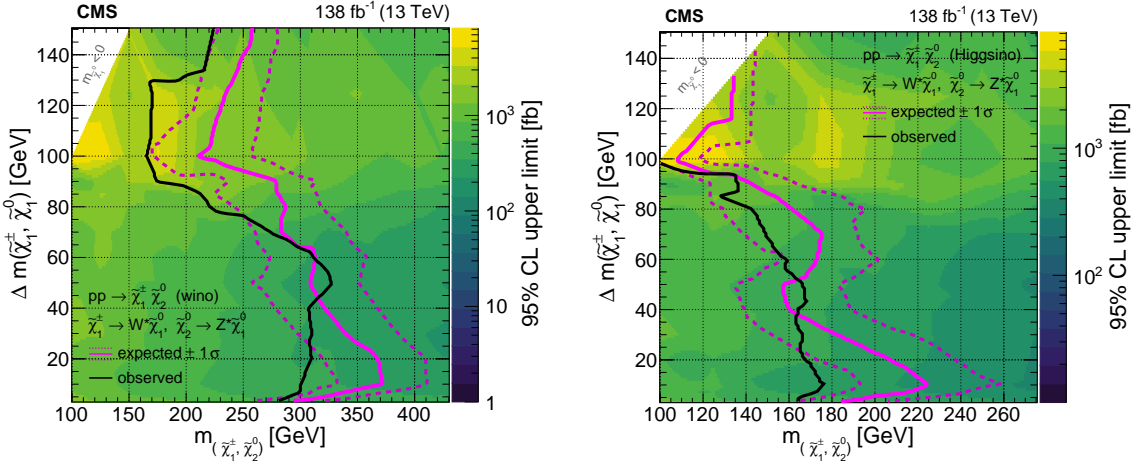


Figure 27: Chargino-neutralino production. Observed upper limits at 95% CL on the product of the cross section and the two branching fractions, $\sigma(\tilde{\chi}_1^\pm \tilde{\chi}_2^0) \mathcal{B}(\tilde{\chi}_1^\pm \rightarrow W^\pm \tilde{\chi}_1^0) \mathcal{B}(\tilde{\chi}_2^0 \rightarrow Z \tilde{\chi}_1^0)$, are shown using the color scale where the $\tilde{\chi}_1^\pm / \tilde{\chi}_2^0$ mass is on the x -axis and the mass difference between the $\tilde{\chi}_1^\pm / \tilde{\chi}_2^0$ and the LSP is on the y -axis. For these results, based on the TChiWW simplified model, the $\tilde{\chi}_1^\pm$ and $\tilde{\chi}_2^0$ masses are set equal. The expected lower mass limits (magenta line) together with their $\pm 1\sigma$ uncertainties (magenta dashed lines) and the observed lower mass limits (black line) are indicated for 100% branching fractions for wino-like cross-sections (left) and for higgsino-like cross-sections (right).

charginos with masses less than 120 GeV and mass differences exceeding 5 GeV at 95% CL for wino cross sections and $\mathcal{B}(\tilde{\chi}_1^\pm \rightarrow W^\pm \tilde{\chi}_1^0) = 1$. These TChiWW results on direct chargino pair production extend beyond the mass scales probed by the CERN LEP experiments that established 95% CL chargino lower mass limits around 100 GeV generally also for wino-like couplings and mass differences exceeding 5 GeV [118–121]. The generally applicable combined lower limit on the chargino mass from LEP is derived as 103.5 GeV [3]. The TChiSlepSnu results are very competitive in the compressed mass regime reaching masses as high as 490 GeV using wino cross sections for this model that features favorable leptonic branching fractions. This complements other direct chargino pair results with the same decay assumptions such as [122] that probes to higher chargino masses but only for large mass splittings.

The model exclusion results for chargino-neutralino production and chargino pair production are summarized in Fig. 29.

Figures 30 and 31 show the experimental upper limits on the product of the cross section and branching fraction squared for direct slepton pair production in the (mass, mass-difference) plane using a color scale. A particular focus is given to compressed mass spectra, where this analysis contributes substantially with respect to previous LHC analyses with $\sqrt{s} = 13$ TeV datasets performed by ATLAS and CMS [8, 10, 11, 36], and generally extends the regions probed by prior results from the LEP experiments [119, 123–125]. Figure 30 illustrates the results for selectron and smuon channels combined assuming degenerate selectron and smuon masses, while Fig. 31 has the results separately for selectrons and smuons. Additionally, in both figures the three different model exclusion lines for 100% branching fraction show the 95% CL exclusion regions for pair production of only the superpartners of the left-handed leptons, only the superpartners of the right-handed leptons, and for both superpartners (where the two chirality partners are assumed mass degenerate). Figures 32 and 33 show the 95% CL mass exclusion regions for each of the three production possibilities under the 100% branching fraction assumption. Each figure shows separate model exclusion lines for the three possible

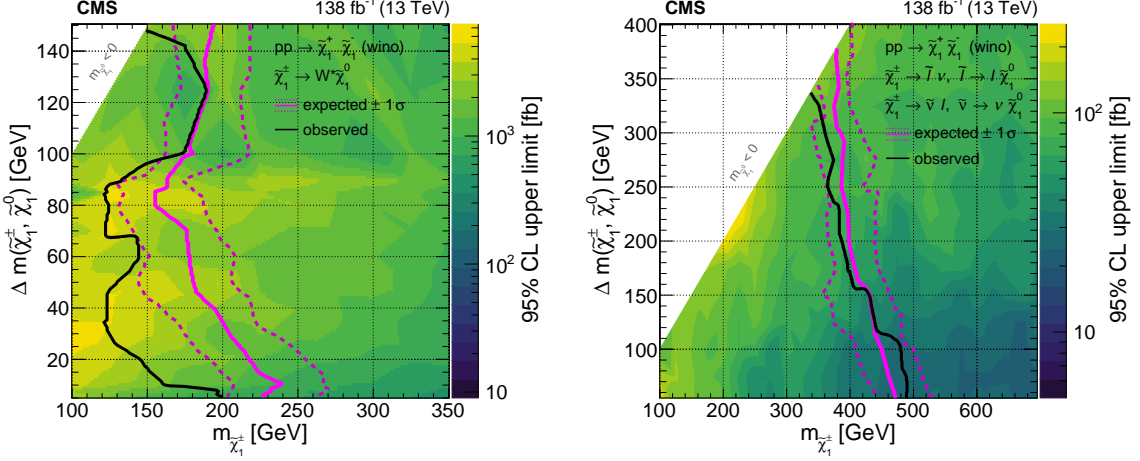


Figure 28: Chargino pair production. The left panel shows the observed upper limits at 95% CL on the product of the cross section and the branching fraction squared, $\sigma(\tilde{\chi}_1^\pm \tilde{\chi}_1^0) \mathcal{B}^2(\tilde{\chi}_1^\pm \rightarrow W^\pm \tilde{\chi}_1^0)$ are shown using the color scale where the $\tilde{\chi}_1^\pm$ mass is on the x -axis and the mass difference between the $\tilde{\chi}_1^\pm$ and the LSP is on the y -axis. The expected lower mass limits (magenta line) together with their $\pm 1\sigma$ uncertainties (magenta dashed lines) and the observed lower mass limits (black line) are indicated for 100% branching fractions for wino-like cross-sections. The right panel shows the results for chargino pair production with decays as in the TChiSlep-Snu model with democratic decay via an intermediate sneutrino or charged slepton ($\tilde{\ell}_L^\pm$) with mass halfway between the chargino and the lightest neutralino. These model predictions also assume wino-like cross sections.

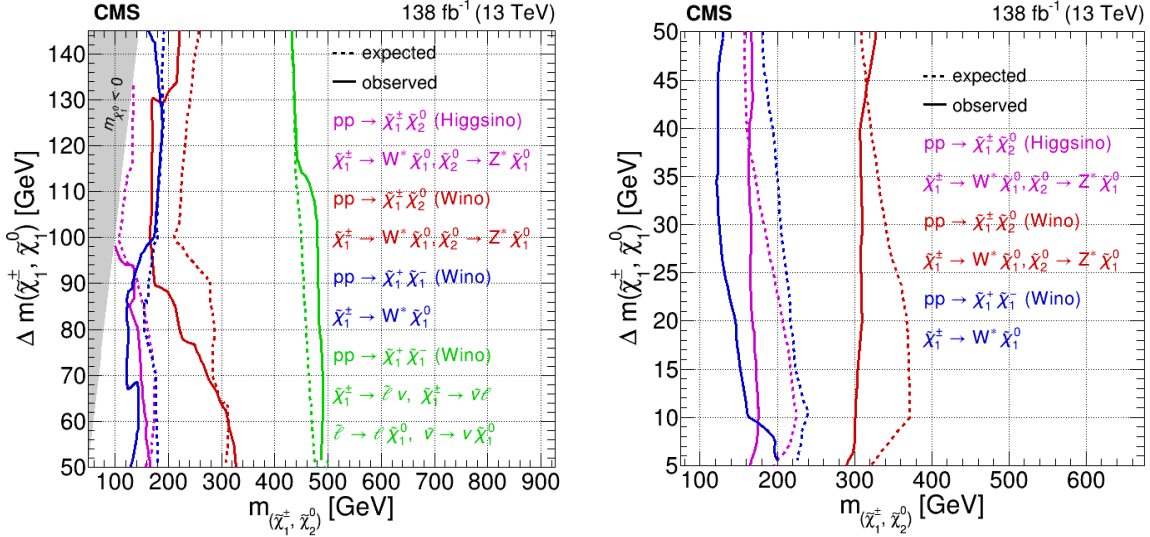


Figure 29: Summary of the model exclusion results on chargino-neutralino production and chargino pair production. Solid lines are 95% CL observed limits and dashed lines are the corresponding median expected limits. The left panel shows the results for mass differences exceeding 50 GeV and the right panel for mass differences below 50 GeV.

slepton flavor combinations (selectrons only, smuons only, and both light-flavor sleptons).

These results are stronger and more comprehensive than previously reported by the LHC experiments for compressed masses; they include separate results for selectrons and smuons, and separate and combined results for the supersymmetric partners of the left- and right-handed

charged leptons.

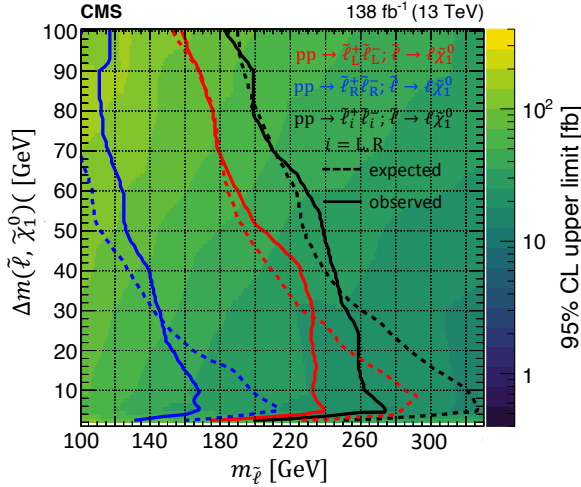


Figure 30: Slepton pair production. Observed 95% CL upper limits on the product of the cross section and branching fraction squared for direct slepton pair production followed by decay of both sleptons to the corresponding lepton and neutralino (color scale). Slepton $\tilde{\ell}_{L/R}$ indicates the scalar supersymmetric partner of left- and right-handed electrons and muons. The limit is shown as a function of the slepton mass and the mass difference between the slepton and the lightest neutralino. The regions to the left of the lines denote the regions excluded for a branching fraction of 100%. The median expected exclusion regions for 100% branching fraction are delimited by the dashed lines.

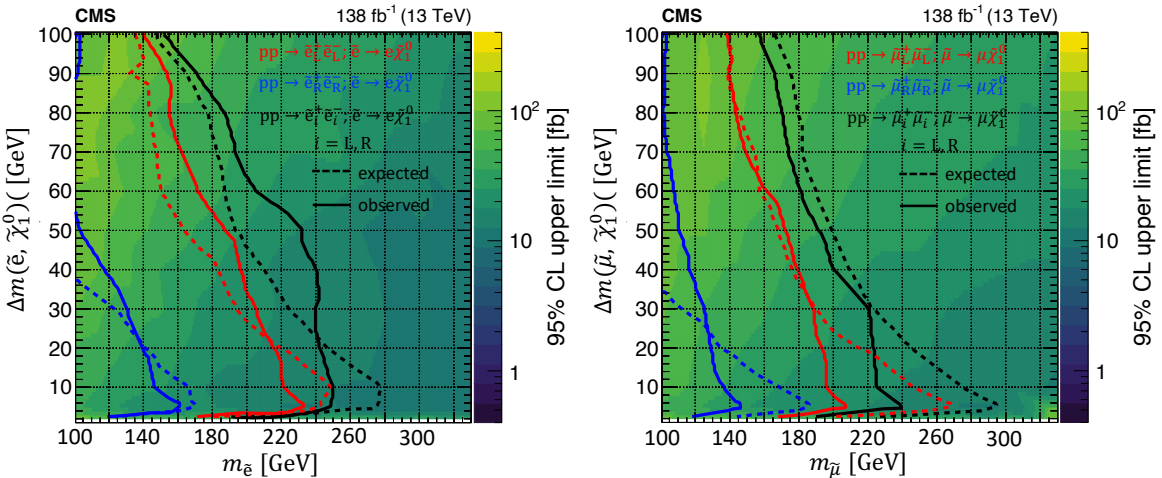


Figure 31: Slepton pair production. Observed 95% CL upper limits on the cross section times branching fraction squared for direct selectron pair production (left) and smuon pair production (right) followed by decay of both sleptons to the corresponding lepton and neutralino (color scale). The limits are shown as a function of the slepton mass and the mass difference between the slepton and the lightest neutralino for the three different simplified possibilities of only RR, only LL, and both RR and LL where it is assumed that the R and L masses are identical. The regions to the left of the lines denote the regions excluded for a branching fraction of 100%. Median expected limits for 100% branching fraction are delimited by the dashed lines.

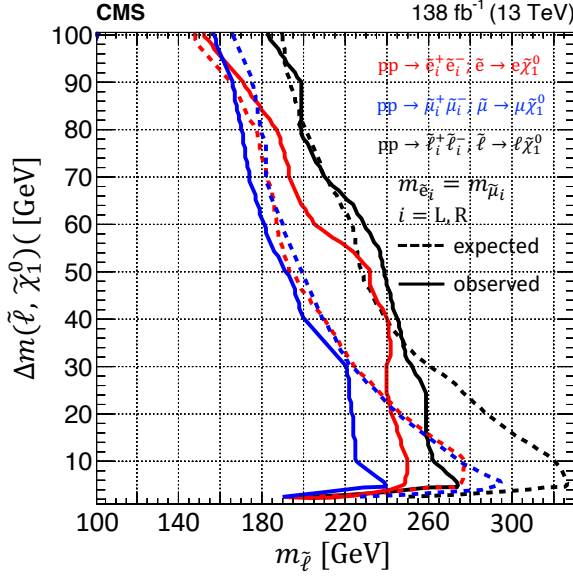


Figure 32: Slepton pair production. Observed and median expected limits for direct slepton pair production at 95% CL. Slepton $\tilde{\ell}_{L/R}$ indicates the scalar supersymmetric partner of left- and right-handed electrons and muons. The limit is shown as a function of the slepton mass and the mass difference between the slepton and the lightest neutralino. The corresponding selectron only and smuon only results of Fig. 31 are shown too assuming a 100% branching fraction.

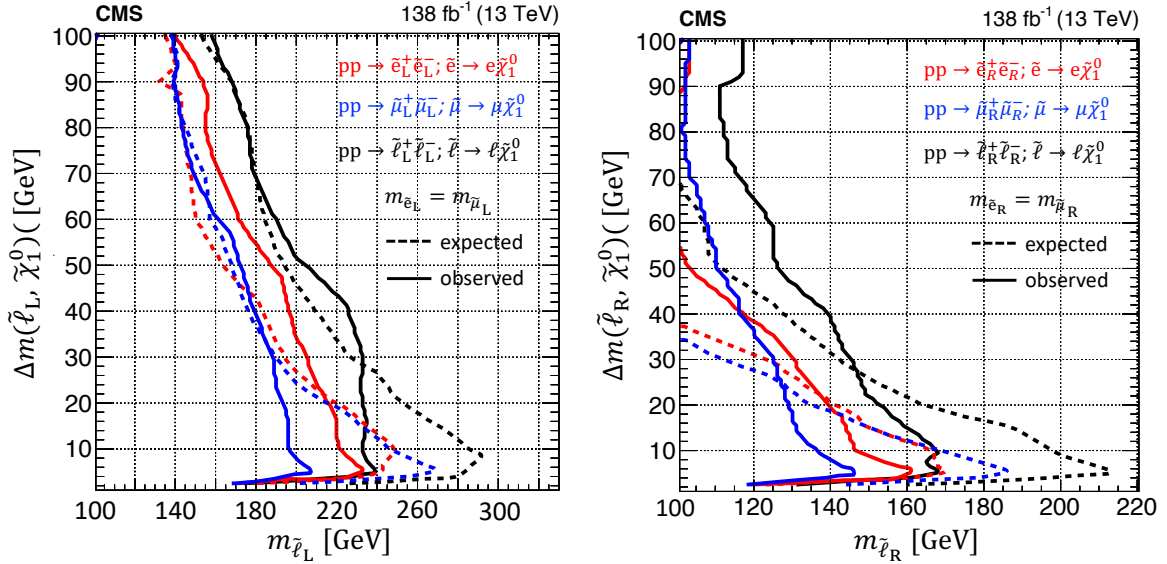


Figure 33: Slepton pair production. Observed 95% CL exclusion regions for direct pair production of the superpartners of the left-handed leptons (left) and direct pair production of the superpartners of the right-handed leptons (right) followed by decay of both sleptons to the corresponding lepton and neutralino with 100% branching fraction. The limits are shown as a function of the slepton mass and the mass difference between the slepton and the lightest neutralino. The regions to the left of the lines denote the excluded regions. Median expected limits are displayed with dashed lines.

9 Summary

A general search has been presented for supersymmetric particles (sparticles) in proton-proton collisions at a center-of-mass energy of 13 TeV with the CMS detector at the LHC using a data sample corresponding to an integrated luminosity of 138 fb^{-1} . A wide range of potential sparticle signatures are targeted including production of pairs of electroweakinos, sleptons, and top squarks. The search is focused on events with a high transverse momentum system from initial-state-radiation jets recoiling against a potential sparticle system with significant missing transverse momentum. Events are categorized based on their lepton multiplicity, jet multiplicity, b tags, and kinematic variables sensitive to the sparticle masses and mass splittings. The sensitivity extends to higher parent sparticle masses than previously probed at the LHC for production of pairs of electroweakinos, sleptons, and top squarks for compressed mass spectra. The results on pair production of charginos and sleptons in the compressed mass regime extend well beyond the canonical 100 GeV sparticle mass scale previously explored at LEP. The observed results demonstrate reasonable agreement with the predictions of the background-only model and model-independent event count upper limits for seven mutually exclusive event selections are reported. Competitive 95% confidence level (CL) lower mass limits are set on sparticle pair production, especially in the compressed mass regime, with mass differences between the lightest and parent sparticle as low as 3 GeV being tested.

Top squark mass limits for three decay models are presented in the plane of the top squark mass and the mass difference. Limits on the decay via a top quark extend to 780 GeV with a mass of 750 GeV excluded at 95% CL or higher for mass differences between 60 and 175 GeV; the most stringent exclusion is at a mass difference of 150 GeV. Limits on the decay via a bottom quark and an intermediate chargino extend to 620 GeV with a mass of 550 GeV excluded at 95% CL or higher for mass differences between 35 and 140 GeV; the most stringent exclusion is at mass differences of between 50 and 90 GeV. Limits on the decay via a charm quark extend to 660 GeV with a mass of 520 GeV excluded at 95% CL or higher for mass differences between 10 and 60 GeV; the most stringent exclusion is at a mass difference of 20 GeV.

The 95% CL lower mass limits on chargino-neutralino production assuming heavy sleptons extend to 325 (175) GeV for wino (higgsino) cross sections, where the most stringent mass limits are set for mass differences of 50 (10) GeV. The limits with wino cross sections exceed 300 GeV for the broad range of mass differences between 8 and 65 GeV, while the limits with the higgsino cross section assumption exceed 163 GeV for mass differences between 3 and 50 GeV. For chargino pair production, 95% CL lower mass limits are obtained for wino cross sections and decay via a W boson. These extend to 200 GeV with the most stringent mass limit set for a mass difference of 5 GeV while masses exceeding 120 GeV are excluded for all mass differences above 5 GeV. Related chargino pair production limits for the case of decays via sleptons and sneutrinos and with wino cross sections extend to 490 GeV for a mass difference of 55 GeV.

The 95% CL lower mass limits on pair production of charged sleptons extend to 168 GeV (slepton partner of right-handed lepton only), 240 GeV (slepton partner of left-handed lepton only), and 270 GeV (both sleptons mass degenerate) for the most favorable mass splitting of around 5 GeV for the case of mass-degenerate first- and second-generation sleptons. Slepton masses exceeding 110, 175, and 200 GeV for all mass splittings ranging from 3 to 80 GeV are excluded at 95% CL or higher for the same three cases respectively. Similar results are also presented separately for selectrons and smuons assuming that the other slepton is not produced. For selectrons (smuons), the most stringent 95% CL lower mass limits are set at 160, 230, 250 GeV (145, 195, 240 GeV) for mass differences around 5 GeV for the three cases and with sensitivity to a broad range of mass differences from 3 to 100 GeV.

Acknowledgments

We congratulate our colleagues in the CERN accelerator departments for the excellent performance of the LHC and thank the technical and administrative staffs at CERN and at other CMS institutes for their contributions to the success of the CMS effort. In addition, we gratefully acknowledge the computing centers and personnel of the Worldwide LHC Computing Grid and other centers for delivering so effectively the computing infrastructure essential to our analyses. Finally, we acknowledge the enduring support for the construction and operation of the LHC, the CMS detector, and the supporting computing infrastructure provided by the following funding agencies: SC (Armenia), BMBWF and FWF (Austria); FNRS and FWO (Belgium); CNPq, CAPES, FAPERJ, FAPERGS, and FAPESP (Brazil); MES and BNSF (Bulgaria); CERN; CAS, MoST, and NSFC (China); MINCIENCIAS (Colombia); MSES and CSF (Croatia); RIF (Cyprus); SENESCYT (Ecuador); ERC PRG, TARISTU24-TK10 and MoER TK202 (Estonia); Academy of Finland, MEC, and HIP (Finland); CEA and CNRS/IN2P3 (France); SRNSF (Georgia); BMBF, DFG, and HGF (Germany); GSRI (Greece); NKFH (Hungary); DAE and DST (India); IPM (Iran); SFI (Ireland); INFN (Italy); MSIT and NRF (Republic of Korea); MES (Latvia); LMELT (Lithuania); MOE and UM (Malaysia); BUAP, CINVESTAV, CONACYT, LNS, SEP, and UASLP-FAI (Mexico); MOS (Montenegro); MBIE (New Zealand); PAEC (Pakistan); MES, NSC, and NAWA (Poland); FCT (Portugal); MESTD (Serbia); MICIU/AEI and PCTI (Spain); MOSTR (Sri Lanka); Swiss Funding Agencies (Switzerland); MST (Taipei); MHESI and NSTDA (Thailand); TUBITAK and TENMAK (Türkiye); NASU (Ukraine); STFC (United Kingdom); DOE and NSF (USA).

Individuals have received support from the Marie-Curie program and the European Research Council and Horizon 2020 Grant, contract Nos. 675440, 724704, 752730, 758316, 765710, 824093, 101115353, 101002207, 101001205, and COST Action CA16108 (European Union); the Leventis Foundation; the Alfred P. Sloan Foundation; the Alexander von Humboldt Foundation; the Science Committee, project no. 22rl-037 (Armenia); the Fonds pour la Formation à la Recherche dans l'Industrie et dans l'Agriculture (FRIA-Belgium); the Beijing Municipal Science & Technology Commission, No. Z191100007219010, the Fundamental Research Funds for the Central Universities, the Ministry of Science and Technology of China under Grant No. 2023YFA1605804, and the Natural Science Foundation of China under Grant No. 12061141002 (China); the Ministry of Education, Youth and Sports (MEYS) of the Czech Republic; the Shota Rustaveli National Science Foundation, grant FR-22-985 (Georgia); the Deutsche Forschungsgemeinschaft (DFG), among others, under Germany's Excellence Strategy – EXC 2121 "Quantum Universe" – 390833306, and under project number 400140256 - GRK2497; the Hellenic Foundation for Research and Innovation (HFRI), Project Number 2288 (Greece); the Hungarian Academy of Sciences, the New National Excellence Program - ÚNKP, the NKFH research grants K 131991, K 133046, K 138136, K 143460, K 143477, K 146913, K 146914, K 147048, 2020-2.2.1-ED-2021-00181, TKP2021-NKTA-64, and 2021-4.1.2-NEMZ-KI-2024-00036 (Hungary); the Council of Science and Industrial Research, India; ICSC – National Research Center for High Performance Computing, Big Data and Quantum Computing, FAIR – Future Artificial Intelligence Research, and CUP I53D23001070006 (Mission 4 Component 1), funded by the NextGenerationEU program (Italy); the Latvian Council of Science; the Ministry of Education and Science, project no. 2022/WK/14, and the National Science Center, contracts Opus 2021/41/B/ST2/01369, 2021/43/B/ST2/01552, 2023/49/B/ST2/03273, and the NAWA contract BPN/PPO/2021/1/00011 (Poland); the Fundação para a Ciência e a Tecnologia, grant CEECIND/01334/2018 (Portugal); the National Priorities Research Program by Qatar National Research Fund; MICIU/AEI/10.13039/501100011033, ERDF/EU, "European Union NextGenerationEU/PRTR", and Programa Severo Ochoa del Principado de Asturias (Spain); the Chu-

lalongkorn Academic into Its 2nd Century Project Advancement Project, and the National Science, Research and Innovation Fund via the Program Management Unit for Human Resources & Institutional Development, Research and Innovation, grant B39G680009 (Thailand); the Kavli Foundation; the Nvidia Corporation; the SuperMicro Corporation; the Welch Foundation, contract C-1845; and the Weston Havens Foundation (USA).

References

- [1] ATLAS Collaboration, “Observation of a new particle in the search for the standard model Higgs boson with the ATLAS detector at the LHC”, *Phys. Lett. B* **716** (2012) 1, doi:[10.1016/j.physletb.2012.08.020](https://doi.org/10.1016/j.physletb.2012.08.020), arXiv:[1207.7214](https://arxiv.org/abs/1207.7214).
- [2] CMS Collaboration, “Observation of a new boson at a mass of 125 GeV with the CMS experiment at the LHC”, *Phys. Lett. B* **716** (2012) 30, doi:[10.1016/j.physletb.2012.08.021](https://doi.org/10.1016/j.physletb.2012.08.021), arXiv:[1207.7235](https://arxiv.org/abs/1207.7235).
- [3] Particle Data Group and Navas, S. and others Collaboration, “Review of particle physics”, *Phys. Rev. D* **110** (2024) 030001, doi:[10.1103/PhysRevD.110.030001](https://doi.org/10.1103/PhysRevD.110.030001).
- [4] G. Jungman, M. Kamionkowski, and K. Griest, “Supersymmetric dark matter”, *Phys. Rept.* **267** (1996) 195, doi:[10.1016/0370-1573\(95\)00058-5](https://doi.org/10.1016/0370-1573(95)00058-5), arXiv:[hep-ph/9506380](https://arxiv.org/abs/hep-ph/9506380).
- [5] M. Drees, R. Godbole, and P. Roy, “Theory and phenomenology of sparticles: An account of four-dimensional N = 1 supersymmetry in high energy physics”. World Scientific Publishing, 2004.
- [6] H. Baer and X. Tata, “Weak scale supersymmetry: From superfields to scattering events”. Cambridge University Press, 2006.
- [7] S. P. Martin, “A supersymmetry primer”, *Adv. Ser. Direct. High Energy Phys.* **21** (2010) 1, doi:[10.1142/9789812839657_0001](https://doi.org/10.1142/9789812839657_0001), arXiv:[hep-ph/9709356](https://arxiv.org/abs/hep-ph/9709356).
- [8] ATLAS Collaboration, “Search for electroweak production of supersymmetric states in scenarios with compressed mass spectra at $\sqrt{s} = 13$ TeV with the ATLAS detector”, *Phys. Rev. D* **97** (2018) 052010, doi:[10.1103/PhysRevD.97.052010](https://doi.org/10.1103/PhysRevD.97.052010), arXiv:[1712.08119](https://arxiv.org/abs/1712.08119).
- [9] CMS Collaboration, “Search for supersymmetry with a compressed mass spectrum in events with a soft τ lepton, a highly energetic jet, and large missing transverse momentum in proton-proton collisions at $\sqrt{s} = 13$ TeV”, *Phys. Rev. Lett.* **124** (2020) 041803, doi:[10.1103/PhysRevLett.124.041803](https://doi.org/10.1103/PhysRevLett.124.041803), arXiv:[1910.01185](https://arxiv.org/abs/1910.01185).
- [10] CMS Collaboration, “Search for supersymmetry with a compressed mass spectrum in the vector boson fusion topology with 1-lepton and 0-lepton final states in proton-proton collisions at $\sqrt{s} = 13$ TeV”, *JHEP* **08** (2019) 150, doi:[10.1007/JHEP08\(2019\)150](https://doi.org/10.1007/JHEP08(2019)150), arXiv:[1905.13059](https://arxiv.org/abs/1905.13059).
- [11] ATLAS Collaboration, “Searches for electroweak production of supersymmetric particles with compressed mass spectra in $\sqrt{s} = 13$ TeV pp collisions with the ATLAS detector”, *Phys. Rev. D* **101** (2020) 052005, doi:[10.1103/PhysRevD.101.052005](https://doi.org/10.1103/PhysRevD.101.052005), arXiv:[1911.12606](https://arxiv.org/abs/1911.12606).

- [12] CMS Collaboration, “Search for supersymmetry in final states with two oppositely charged same-flavor leptons and missing transverse momentum in proton-proton collisions at $\sqrt{s} = 13 \text{ TeV}$ ”, *JHEP* **04** (2021) 123, doi:10.1007/JHEP04(2021)123, arXiv:2012.08600.
- [13] CMS Collaboration, “Search for top squark pair production using dilepton final states in pp collision data collected at $\sqrt{s} = 13 \text{ TeV}$ ”, *Eur. Phys. J. C* **81** (2021) 3, doi:10.1140/epjc/s10052-020-08701-5, arXiv:2008.05936.
- [14] ATLAS Collaboration, “Search for direct production of electroweakinos in final states with one lepton, missing transverse momentum and a Higgs boson decaying into two b-jets in pp collisions at $\sqrt{s} = 13 \text{ TeV}$ with the ATLAS detector”, *Eur. Phys. J. C* **80** (2020) 691, doi:10.1140/epjc/s10052-020-8050-3, arXiv:1909.09226.
- [15] ATLAS Collaboration, “Search for chargino-neutralino production with mass splittings near the electroweak scale in three-lepton final states in $\sqrt{s} = 13 \text{ TeV}$ pp collisions with the ATLAS detector”, *Phys. Rev. D* **101** (2020) 072001, doi:10.1103/PhysRevD.101.072001, arXiv:1912.08479.
- [16] ATLAS Collaboration, “Search for squarks and gluinos in final states with one isolated lepton, jets, and missing transverse momentum at $\sqrt{s} = 13 \text{ TeV}$ with the ATLAS detector”, *Eur. Phys. J. C* **81** (2021) 600, doi:10.48550/arXiv.2101.01629, arXiv:2101.01629.
- [17] CMS Collaboration, “Search for supersymmetry in final states with two or three soft leptons and missing transverse momentum in proton-proton collisions at $\sqrt{s} = 13 \text{ TeV}$ ”, *JHEP* **04** (2022) 091, doi:10.1007/JHEP04(2022)091, arXiv:2111.06296.
- [18] CMS Collaboration, “Search for top squark production in fully hadronic final states in proton-proton collisions at $\sqrt{s} = 13 \text{ TeV}$ ”, *Phys. Rev. D* **104** (2021) 052001, doi:10.1103/PhysRevD.104.052001, arXiv:2103.01290.
- [19] ATLAS Collaboration, “Search for a scalar partner of the top quark in the all-hadronic $t\bar{t}$ plus missing transverse momentum final state at $\sqrt{s} = 13 \text{ TeV}$ with the ATLAS detector”, *Eur. Phys. J. C* **80** (2020) 737, doi:10.1140/epjc/s10052-020-8102-8, arXiv:2004.14060.
- [20] ATLAS Collaboration, “Search for new phenomena with top quark pairs in final states with one lepton, jets, and missing transverse momentum in pp collisions at $\sqrt{s} = 13 \text{ TeV}$ with the ATLAS detector”, *JHEP* **04** (2021) 174, doi:10.1007/JHEP04(2021)174, arXiv:2012.103799.
- [21] ATLAS Collaboration, “Search for new phenomena in events with an energetic jet and missing transverse momentum in pp collisions at $\sqrt{s} = 13 \text{ TeV}$ with the ATLAS detector”, *Phys. Rev. D* **103** (2021) 112006, doi:10.1103/PhysRevD.103.112006, arXiv:2102.10874.
- [22] ATLAS Collaboration, “The quest to discover supersymmetry at the ATLAS experiment”, *Phys. Rept.* **1116** (2025) 261, doi:10.1016/j.physrep.2024.09.010, arXiv:2403.02455.
- [23] ATLAS Collaboration, “Search for electroweak production of charginos and sleptons decaying into final states with two leptons and missing transverse momentum in

- $\sqrt{s} = 13 \text{ TeV}$ pp collisions using the ATLAS detector”, *Eur. Phys. J. C* **80** (2020) 123, doi:10.1140/epjc/s10052-019-7594-6, arXiv:1908.08215.
- [24] ATLAS Collaboration, “Search for chargino–neutralino pair production in final states with three leptons and missing transverse momentum in $\sqrt{s} = 13 \text{ TeV}$ pp collisions with the ATLAS detector”, *Eur. Phys. J. C* **81** (2021) 1118, doi:10.1140/epjc/s10052-021-09749-7, arXiv:2106.01676.
- [25] ATLAS Collaboration, “Search for charginos and neutralinos in final states with two boosted hadronically decaying bosons and missing transverse momentum in pp collisions at $\sqrt{s} = 13 \text{ TeV}$ with the ATLAS detector”, *Phys. Rev. D* **104** (2021) 112010, doi:10.1103/PhysRevD.104.112010, arXiv:2108.07586.
- [26] ATLAS Collaboration, “Searches for new phenomena in events with two leptons, jets, and missing transverse momentum in 139 fb^{-1} of $\sqrt{s} = 13 \text{ TeV}$ pp collisions with the ATLAS detector”, *Eur. Phys. J. C* **83** (2023) 515, doi:10.1140/epjc/s10052-023-11434-w, arXiv:2204.13072.
- [27] ATLAS Collaboration, “Search for direct pair production of sleptons and charginos decaying to two leptons and neutralinos with mass splittings near the W-boson mass in $\sqrt{s} = 13 \text{ TeV}$ pp collisions with the ATLAS detector”, *JHEP* **06** (2023) 031, doi:10.1007/JHEP06(2023)031, arXiv:2209.13935.
- [28] ATLAS Collaboration, “Search for direct production of electroweakinos in final states with one lepton, jets and missing transverse momentum in pp collisions at $\sqrt{s} = 13 \text{ TeV}$ with the ATLAS detector”, *JHEP* **12** (2023) 167, doi:10.1007/JHEP12(2023)167, arXiv:2310.08171.
- [29] ATLAS Collaboration, “Search for electroweak production of supersymmetric particles in final states with two τ -leptons in $\sqrt{s} = 13 \text{ TeV}$ pp collisions with the ATLAS detector”, *JHEP* **05** (2024) 150, doi:10.1007/JHEP05(2024)150, arXiv:2402.00603.
- [30] ATLAS Collaboration, “Statistical combination of ATLAS Run 2 searches for charginos and neutralinos at the LHC”, *Phys. Rev. Lett.* **133** (2024) 031802, doi:10.1103/PhysRevLett.133.031802, arXiv:2402.08347.
- [31] CMS Collaboration, “Search for electroweak production of charginos and neutralinos in proton-proton collisions at $\sqrt{s} = 13 \text{ TeV}$ ”, *JHEP* **04** (2022) 147, doi:10.1007/JHEP04(2022)147, arXiv:2106.14246.
- [32] CMS Collaboration, “Search for chargino-neutralino production in events with Higgs and W bosons using 137 fb^{-1} of proton-proton collisions at $\sqrt{s} = 13 \text{ TeV}$ ”, *JHEP* **10** (2021) 045, doi:10.1007/JHEP10(2021)045, arXiv:2107.12553.
- [33] CMS Collaboration, “Search for higgsinos decaying to two Higgs bosons and missing transverse momentum in proton-proton collisions at $\sqrt{s} = 13 \text{ TeV}$ ”, *JHEP* **05** (2022) 014, doi:10.1007/JHEP05(2022)014, arXiv:2201.04206.
- [34] CMS Collaboration, “Search for electroweak production of charginos and neutralinos at $\sqrt{s} = 13 \text{ TeV}$ in final states containing hadronic decays of WW, WZ, or WH and missing transverse momentum”, *Phys. Lett. B* **842** (2023) 137460, doi:10.1016/j.physletb.2022.137460, arXiv:2205.09597.

- [35] CMS Collaboration, “Combined search for electroweak production of winos, binos, higgsinos, and sleptons in proton-proton collisions at $\sqrt{s} = 13 \text{ TeV}$ ”, *Phys. Rev. D* **109** (2024) 112001, doi:[10.1103/PhysRevD.109.112001](https://doi.org/10.1103/PhysRevD.109.112001), arXiv:[2402.01888](https://arxiv.org/abs/2402.01888).
- [36] ATLAS Collaboration, “Searches for direct slepton production in the compressed-mass corridor in $\sqrt{s} = 13 \text{ TeV}$ pp collisions with the ATLAS detector”, 2025. arXiv:[2503.17186](https://arxiv.org/abs/2503.17186). Submitted to *JHEP*.
- [37] ATLAS Collaboration, “Search for cascade decays of charged sleptons and sneutrinos in final states with three leptons and missing transverse momentum in pp collisions at $\sqrt{s} = 13 \text{ TeV}$ with the ATLAS detector”, *Phys. Rev. D* **112** (2025) 012005, doi:[10.1103/PhysRevD.112.012005](https://doi.org/10.1103/PhysRevD.112.012005), arXiv:[2503.13135](https://arxiv.org/abs/2503.13135).
- [38] Z. Han, G. D. Kribs, A. Martin, and A. Menon, “Hunting quasidegenerate higgsinos”, *Phys. Rev. D* **89** (2014) 075007, doi:[10.1103/PhysRevD.89.075007](https://doi.org/10.1103/PhysRevD.89.075007), arXiv:[1401.1235](https://arxiv.org/abs/1401.1235).
- [39] A. Canepa, T. Han, and X. Wang, “The search for electroweakinos”, *Ann. Rev. Nucl. Part. Sci.* **70** (2020) 425, doi:[10.1146/annurev-nucl-031020-121031](https://doi.org/10.1146/annurev-nucl-031020-121031), arXiv:[2003.05450](https://arxiv.org/abs/2003.05450).
- [40] H. Baer et al., “The LHC higgsino discovery plane for present and future SUSY searches”, *Phys. Lett. B* **810** (2020) 135777, doi:[10.1016/j.physletb.2020.135777](https://doi.org/10.1016/j.physletb.2020.135777), arXiv:[2007.09252](https://arxiv.org/abs/2007.09252).
- [41] Muon g-2 Collaboration, “Final report of the E821 muon anomalous magnetic moment measurement at BNL”, *Phys. Rev. D* **73** (2006) 072003, doi:[10.1103/PhysRevD.73.072003](https://doi.org/10.1103/PhysRevD.73.072003), arXiv:[hep-ex/0602035](https://arxiv.org/abs/hep-ex/0602035).
- [42] Muon g-2 Collaboration, “Measurement of the positive muon anomalous magnetic moment to 0.20 ppm”, *Phys. Rev. Lett.* **131** (2023) 161802, doi:[10.1103/PhysRevLett.131.161802](https://doi.org/10.1103/PhysRevLett.131.161802), arXiv:[2308.06230](https://arxiv.org/abs/2308.06230).
- [43] Muon g-2 Collaboration, “Measurement of the positive muon anomalous magnetic moment to 127 ppb”, 2025. arXiv:[2506.03069](https://arxiv.org/abs/2506.03069). Submitted to *Phys. Rev. Lett.*
- [44] T. Moroi, “The muon anomalous magnetic dipole moment in the minimal supersymmetric standard model”, *Phys. Rev. D* **53** (1996) 6565, doi:[10.1103/PhysRevD.53.6565](https://doi.org/10.1103/PhysRevD.53.6565), arXiv:[hep-ph/9512396](https://arxiv.org/abs/hep-ph/9512396). [Erratum: *Phys. Rev. D* **56**, 4424 (1997)].
- [45] S. P. Martin and J. D. Wells, “Muon anomalous magnetic dipole moment in supersymmetric theories”, *Phys. Rev. D* **64** (2001) 035003, doi:[10.1103/PhysRevD.64.035003](https://doi.org/10.1103/PhysRevD.64.035003), arXiv:[hep-ph/0103067](https://arxiv.org/abs/hep-ph/0103067).
- [46] D. Stockinger, “The muon magnetic moment and supersymmetry”, *J. Phys. G* **34** (2007) R45, doi:[10.1088/0954-3899/34/2/R01](https://doi.org/10.1088/0954-3899/34/2/R01), arXiv:[hep-ph/0609168](https://arxiv.org/abs/hep-ph/0609168).
- [47] G. R. Farrar and P. Fayet, “Phenomenology of the production, decay, and detection of new hadronic states associated with supersymmetry”, *Phys. Lett. B* **76** (1978) 575, doi:[10.1016/0370-2693\(78\)90858-4](https://doi.org/10.1016/0370-2693(78)90858-4).
- [48] HEPData record for this analysis, 2025. doi:[10.17182/hepdata.156121](https://doi.org/10.17182/hepdata.156121).

- [49] CMS Collaboration, "The CMS experiment at the CERN LHC", *JINST* **3** (2008) S08004, doi:[10.1088/1748-0221/3/08/S08004](https://doi.org/10.1088/1748-0221/3/08/S08004).
- [50] CMS Collaboration, "Development of the CMS detector for the CERN LHC Run 3", *JINST* **19** (2024) P05064, doi:[10.1088/1748-0221/19/05/P05064](https://doi.org/10.1088/1748-0221/19/05/P05064), arXiv:[2309.05466](https://arxiv.org/abs/2309.05466).
- [51] CMS Collaboration, "Particle-flow reconstruction and global event description with the CMS detector", *JINST* **12** (2017) P10003, doi:[10.1088/1748-0221/12/10/P10003](https://doi.org/10.1088/1748-0221/12/10/P10003), arXiv:[1706.04965](https://arxiv.org/abs/1706.04965).
- [52] M. Cacciari, G. P. Salam, and G. Soyez, "The anti- k_T jet clustering algorithm", *JHEP* **04** (2008) 063, doi:[10.1088/1126-6708/2008/04/063](https://doi.org/10.1088/1126-6708/2008/04/063), arXiv:[0802.1189](https://arxiv.org/abs/0802.1189).
- [53] M. Cacciari, G. P. Salam, and G. Soyez, "FastJet user manual", *Eur. Phys. J. C* **72** (2012) 1896, doi:[10.1140/epjc/s10052-012-1896-2](https://doi.org/10.1140/epjc/s10052-012-1896-2), arXiv:[1111.6097](https://arxiv.org/abs/1111.6097).
- [54] CMS Collaboration, "Jet energy scale and resolution in the CMS experiment in pp collisions at 8 TeV", *JINST* **12** (2017) P02014, doi:[10.1088/1748-0221/12/02/P02014](https://doi.org/10.1088/1748-0221/12/02/P02014), arXiv:[1607.03663](https://arxiv.org/abs/1607.03663).
- [55] CMS Collaboration, "Performance of electron reconstruction and selection with the CMS detector in proton-proton collisions at $\sqrt{s} = 8$ TeV", *JINST* **10** (2015) P06005, doi:[10.1088/1748-0221/10/6/P06005](https://doi.org/10.1088/1748-0221/10/6/P06005), arXiv:[1502.02701](https://arxiv.org/abs/1502.02701).
- [56] CMS Collaboration, "Electron and photon reconstruction and identification with the CMS experiment at the CERN LHC", *JINST* **16** (2021) P05014, doi:[10.1088/1748-0221/16/05/P05014](https://doi.org/10.1088/1748-0221/16/05/P05014), arXiv:[2012.06888](https://arxiv.org/abs/2012.06888).
- [57] CMS Collaboration, "Performance of CMS muon reconstruction in pp collision events at $\sqrt{s} = 7$ TeV", *JINST* **7** (2012) P10002, doi:[10.1088/1748-0221/7/10/P10002](https://doi.org/10.1088/1748-0221/7/10/P10002), arXiv:[1206.4071](https://arxiv.org/abs/1206.4071).
- [58] CMS Collaboration, "Performance of missing transverse momentum reconstruction in proton-proton collisions at $\sqrt{s} = 13$ TeV using the CMS detector", *JINST* **14** (2019) P07004, doi:[10.1088/1748-0221/14/07/P07004](https://doi.org/10.1088/1748-0221/14/07/P07004), arXiv:[1903.06078](https://arxiv.org/abs/1903.06078).
- [59] E. Chabanat and N. Estre, "Deterministic annealing for vertex finding at CMS", *Proc. Int. Conf. on Computing in High Energy Physics and Nuclear Physics 2004* (2005) 287, doi:[10.5170/CERN-2005-002.287](https://doi.org/10.5170/CERN-2005-002.287).
- [60] CMS Collaboration, "Technical proposal for the Phase-II upgrade of the Compact Muon Solenoid", CMS Technical Proposal CERN-LHCC-2015-010, CMS-TDR-15-02, 2015.
- [61] CMS Collaboration, "The CMS trigger system", *JINST* **12** (2017) P01020, doi:[10.1088/1748-0221/12/01/P01020](https://doi.org/10.1088/1748-0221/12/01/P01020), arXiv:[1609.02366](https://arxiv.org/abs/1609.02366).
- [62] CMS Collaboration, "Performance of the CMS high-level trigger during LHC Run 2", *JINST* **19** (2024) P11021, doi:[10.1088/1748-0221/19/11/P11021](https://doi.org/10.1088/1748-0221/19/11/P11021), arXiv:[2410.17038](https://arxiv.org/abs/2410.17038).
- [63] J. Alwall, P. Schuster, and N. Toro, "Simplified models for a first characterization of new physics at the LHC", *Phys. Rev. D* **79** (2009) 075020, doi:[10.1103/PhysRevD.79.075020](https://doi.org/10.1103/PhysRevD.79.075020), arXiv:[0810.3921](https://arxiv.org/abs/0810.3921).

- [64] J. Alwall, M.-P. Le, M. Lisanti, and J. G. Wacker, “Model-independent jets plus missing energy searches”, *Phys. Rev. D* **79** (2009) 015005, doi:10.1103/PhysRevD.79.015005, arXiv:0809.3264.
- [65] LHC New Physics Working Group Collaboration, “Simplified models for LHC new physics searches”, *J. Phys. G* **39** (2012) 105005, doi:10.1088/0954-3899/39/10/105005, arXiv:1105.2838.
- [66] NNPDF Collaboration, “Parton distributions for the LHC Run II”, *JHEP* **04** (2015) 040, doi:10.1007/JHEP04(2015)040, arXiv:1410.8849.
- [67] NNPDF Collaboration, “Parton distributions from high-precision collider data”, *Eur. Phys. J. C* **77** (2017) 663, doi:10.1140/epjc/s10052-017-5199-5, arXiv:1706.00428.
- [68] T. Sjöstrand et al., “An introduction to PYTHIA 8.2”, *Comput. Phys. Commun.* **191** (2015) 159, doi:10.1016/j.cpc.2015.01.024, arXiv:1410.3012.
- [69] CMS Collaboration, “Extraction and validation of a new set of CMS PYTHIA8 tunes from underlying-event measurements”, *Eur. Phys. J. C* **80** (2020) 4, doi:10.1140/epjc/s10052-019-7499-4, arXiv:1903.12179.
- [70] GEANT4 Collaboration, “GEANT4—a simulation toolkit”, *Nucl. Instrum. Meth. A* **506** (2003) 250, doi:10.1016/S0168-9002(03)01368-8.
- [71] S. Abdullin et al., “The fast simulation of the CMS detector at LHC”, *J. Phys. Conf. Ser.* **331** (2011) 032049, doi:10.1088/1742-6596/331/3/032049.
- [72] A. Giannanco, “The fast simulation of the CMS experiment”, *J. Phys. Conf. Ser.* **513** (2014) 022012, doi:10.1088/1742-6596/513/2/022012.
- [73] J. Alwall et al., “The automated computation of tree-level and next-to-leading order differential cross sections, and their matching to parton shower simulations”, *JHEP* **07** (2014) 079, doi:10.1007/JHEP07(2014)079, arXiv:1405.0301.
- [74] B. Fuks, M. Klasen, D. R. Lamprea, and M. Rothering, “Gaugino production in proton-proton collisions at a center-of-mass energy of 8 TeV”, *JHEP* **10** (2012) 081, doi:10.1007/JHEP10(2012)081, arXiv:1207.2159.
- [75] B. Fuks, M. Klasen, D. R. Lamprea, and M. Rothering, “Precision predictions for electroweak superpartner production at hadron colliders with RESUMMINO”, *Eur. Phys. J. C* **10** (2013) 2480, doi:10.1140/epjc/s10052-013-2480-0, arXiv:1304.0790.
- [76] W. Beenakker, R. Höpker, and M. Spira, “PROSPINO: A program for the production of supersymmetric particles in next-to-leading order QCD”, 1996. arXiv:hep-ph/9611232.
- [77] C. Borschensky et al., “Squark and gluino production cross sections in pp collisions at $\sqrt{s} = 13, 14, 33$ and 100 TeV”, *Eur. Phys. J. C* **74** (2014) 3174, doi:10.1140/epjc/s10052-014-3174-y, arXiv:1407.5066.
- [78] W. Beenakker et al., “Production of charginos, neutralinos, and sleptons at hadron colliders”, *Phys. Rev. Lett.* **83** (1999) 3780, doi:10.1103/PhysRevLett.83.3780, arXiv:hep-ph/9906298.

- [79] W. Beenakker et al., “Stop production at hadron colliders”, *Nucl. Phys. B* **515** (1998) 3, doi:10.1016/S0550-3213(98)00014-5, arXiv:hep-ph/9710451.
- [80] W. Beenakker et al., “Supersymmetric top and bottom squark production at hadron colliders”, *JHEP* **08** (2010) 098, doi:10.1007/JHEP08(2010)098, arXiv:1006.4771.
- [81] W. Beenakker et al., “NNLL resummation for stop pair-production at the LHC”, *JHEP* **05** (2016) 153, doi:10.1007/JHEP05(2016)153, arXiv:1601.02954.
- [82] S. Alioli, P. Nason, C. Oleari, and E. Re, “A general framework for implementing NLO calculations in shower Monte Carlo programs: the POWHEG BOX”, *JHEP* **06** (2010) 043, doi:10.1007/JHEP06(2010)043, arXiv:1002.2581.
- [83] E. Re, “Single-top Wt-channel production matched with parton showers using the POWHEG method”, *Eur. Phys. J. C* **71** (2011) 1547, doi:10.1140/epjc/s10052-011-1547-z, arXiv:1009.2450.
- [84] P. Nason, “A new method for combining NLO QCD with shower Monte Carlo algorithms”, *JHEP* **11** (2004) 040, doi:10.1088/1126-6708/2004/11/040, arXiv:hep-ph/0409146.
- [85] S. Frixione, P. Nason, and C. Oleari, “Matching NLO QCD computations with parton shower simulations: the POWHEG method”, *JHEP* **11** (2007) 070, doi:10.1088/1126-6708/2007/11/070, arXiv:0709.2092.
- [86] R. Frederix and S. Frixione, “Merging meets matching in MC@NLO”, *JHEP* **12** (2012) 061, doi:10.1007/JHEP12(2012)061, arXiv:1209.6215.
- [87] T. Melia, P. Nason, R. Röntsch, and G. Zanderighi, “ W^+W^- , WZ , and ZZ production in the POWHEG-BOX”, *JHEP* **11** (2011) 078, doi:10.1007/JHEP11(2011)078, arXiv:1107.5051.
- [88] P. Nason and G. Zanderighi, “ W^+W^- , WZ , and ZZ production in the POWHEG-BOX-V2”, *Eur. Phys. J. C* **74** (2014) 2702, doi:10.1140/epjc/s10052-013-2702-5, arXiv:1311.1365.
- [89] CMS Collaboration, “Performance of the CMS muon detector and muon reconstruction with proton-proton collisions at $\sqrt{s} = 13$ TeV”, *JINST* **13** (2018) P06015, doi:10.1088/1748-0221/13/06/P06015, arXiv:1804.04528.
- [90] M. Cacciari, G. P. Salam, and G. Soyez, “The catchment area of jets”, *JHEP* **04** (2008) 005, doi:10.1088/1126-6708/2008/04/005, arXiv:0802.1188.
- [91] CMS Collaboration, “Jet algorithms performance in 13 TeV data”, CMS Physics Analysis Summary CMS-PAS-JME-16-003, 2017.
- [92] E. Bols et al., “Jet Flavour Classification Using DeepJet”, *JINST* **15** (2020) P12012, doi:10.1088/1748-0221/15/12/P12012, arXiv:2008.10519.
- [93] CMS Collaboration, “Performance of the DEEPJET b tagging algorithm using 41.9 fb^{-1} of data from proton-proton collisions at 13 TeV with Phase 1 CMS detector”, CMS Detector Performance Note CMS-DP-2018-058, 2018.

- [94] CMS Collaboration, “Measurement of $B\bar{B}$ angular correlations based on secondary vertex reconstruction at $\sqrt{s} = 7 \text{ TeV}$ ”, *JHEP* **03** (2011) 136,
doi:10.1007/jhep03(2011)136, arXiv:1102.3194.
- [95] S. S. Mehta, “DeepJet: a portable ML environment for HEP”, in *2nd IML Machine Learning Workshop*. apr, 2018.
- [96] J. Kieseler et al., “DeepJetCore (2.0)”, *Zenodo* (2020) doi:10.5281/zenodo.3670882.
- [97] CMS Collaboration, “Identification of heavy-flavour jets with the CMS detector in pp collisions at 13 TeV”, *JINST* **13** (2018) P05011,
doi:10.1088/1748-0221/13/05/P05011, arXiv:1712.07158.
- [98] M. R. Buckley, J. D. Lykken, C. Rogan, and M. Spiropulu, “Super-razor and searches for sleptons and charginos at the LHC”, *Phys. Rev. D* **89** (2014) 055020,
doi:10.1103/PhysRevD.89.055020, arXiv:1310.4827.
- [99] P. Jackson, C. Rogan, and M. Santoni, “Sparticles in motion: Analyzing compressed SUSY scenarios with a new method of event reconstruction”, *Phys. Rev. D* **95** (2017) 035031, doi:10.1103/PhysRevD.95.035031, arXiv:1607.08307.
- [100] P. Jackson and C. Rogan, “Recursive jigsaw reconstruction: HEP event analysis in the presence of kinematic and combinatoric ambiguities”, *Phys. Rev. D* **96** (2017) 112007,
doi:10.1103/PhysRevD.96.112007, arXiv:1705.10733.
- [101] CMS Collaboration, “The CMS statistical analysis and combination tool: COMBINE”, *Comput. Softw. Big Sci.* **8** (2024) 19, doi:10.1007/s41781-024-00121-4,
arXiv:2404.06614.
- [102] W. Verkerke and D. P. Kirkby, “The RooFit toolkit for data modeling”, in *Proceedings of the 13th International Conference for Computing in High-Energy and Nuclear Physics (CHEP03)*. 2003. arXiv:physics/0306116. [eConf C0303241, MOLT007].
- [103] L. Moneta et al., “The RooStats Project”, in *PoS*, T. Speer et al., eds., volume ACAT2010, p. 057. 2010. arXiv:1009.1003. doi:10.22323/1.093.0057.
- [104] CMS Collaboration, “Precision luminosity measurement in proton-proton collisions at $\sqrt{s} = 13 \text{ TeV}$ in 2015 and 2016 at CMS”, *Eur. Phys. J. C* **81** (2021) 800,
doi:10.1140/epjc/s10052-021-09538-2, arXiv:2104.01927.
- [105] CMS Collaboration, “CMS luminosity measurement for the 2017 data-taking period at $\sqrt{s} = 13 \text{ TeV}$ ”, CMS Physics Analysis Summary CMS-PAS-LUM-17-004, 2018.
- [106] CMS Collaboration, “CMS luminosity measurement for the 2018 data-taking period at $\sqrt{s} = 13 \text{ TeV}$ ”, CMS Physics Analysis Summary CMS-PAS-LUM-18-002, 2019.
- [107] S. Catani, D. de Florian, M. Grazzini, and P. Nason, “Soft-gluon resummation for Higgs boson production at hadron colliders”, *JHEP* **07** (2003) 028,
doi:10.1088/1126-6708/2003/07/028, arXiv:hep-ph/0306211.
- [108] M. Cacciari et al., “The $t\bar{t}$ cross-section at 1.8 and 1.96 TeV: a study of the systematics due to parton densities and scale dependence”, *JHEP* **04** (2004) 068,
doi:10.1088/1126-6708/2004/04/068, arXiv:hep-ph/0303085.

- [109] J. Butterworth et al., “PDF4LHC recommendations for LHC Run II”, *J. Phys. G* **43** (2016) 023001, doi:10.1088/0954-3899/43/2/023001, arXiv:1510.03865.
- [110] CMS Collaboration, “Measurement of the inelastic proton-proton cross section at $\sqrt{s} = 13 \text{ TeV}$ ”, *JHEP* **07** (2018) 161, doi:10.1007/JHEP07(2018)161, arXiv:1802.02613.
- [111] CMS Collaboration, “Measurement of the cross section for top quark pair production in association with a W or Z boson in proton-proton collisions at $\sqrt{s} = 13 \text{ TeV}$ ”, *JHEP* **08** (2018) 011, doi:10.1007/jhep08(2018)011, arXiv:1711.02547.
- [112] W. S. Cleveland, “Robust locally weighted regression and smoothing scatterplots”, *J. Am. Stat. Assoc.* **74** (1979) 829, doi:10.1080/01621459.1979.10481038.
- [113] W. S. Cleveland, “Locally weighted regression: An approach to regression analysis by local fitting”, *J. Am. Stat. Assoc.* **83** (1988) 596, doi:10.1080/01621459.1988.10478639.
- [114] R. D. Cousins, J. T. Linnemann, and J. Tucker, “Evaluation of three methods for calculating statistical significance when incorporating a systematic uncertainty into a test of the background-only hypothesis for a Poisson process”, *Nucl. Instrum. Meth. A* **595** (2008) 480, doi:10.1016/j.nima.2008.07.086, arXiv:physics/0702156.
- [115] T. Junk, “Confidence level computation for combining searches with small statistics”, *Nucl. Instrum. Meth. A* **434** (1999) 435, doi:10.1016/S0168-9002(99)00498-2, arXiv:hep-ex/9902006.
- [116] A. L. Read, “Presentation of search results: The CL_s technique”, *J. Phys. G* **28** (2002) 2693, doi:10.1088/0954-3899/28/10/313.
- [117] G. Cowan, K. Cranmer, E. Gross, and O. Vitells, “Asymptotic formulae for likelihood-based tests of new physics”, *Eur. Phys. J. C* **71** (2011) 1554, doi:10.1016/epjc/s10052-011-1554-0, arXiv:1007.1727. [Erratum: *Eur. Phys. J. C* **73** (2013) 2501].
- [118] ALEPH Collaboration, “Absolute mass lower limit for the lightest neutralino of the MSSM from e^+e^- data at \sqrt{s} up to 209 GeV”, *Phys. Lett. B* **583** (2004) 247, doi:10.1016/j.physletb.2003.12.066.
- [119] DELPHI Collaboration, “Searches for supersymmetric particles in e^+e^- collisions up to 208 GeV and interpretation of the results within the MSSM”, *Eur. Phys. J. C* **31** (2003) 421, doi:10.1140/epjc/s2003-01355-5, arXiv:hep-ex/0311019.
- [120] L3 Collaboration, “Search for charginos and neutralinos in e^+e^- collisions at $\sqrt{s} = 189 \text{ GeV}$ ”, *Phys. Lett. B* **472** (2000) 420, doi:10.1016/S0370-2693(99)01388-X, arXiv:hep-ex/9910007.
- [121] OPAL Collaboration, “Search for chargino and neutralino production at $\sqrt{s} = 192$ to 209 GeV at LEP”, *Eur. Phys. J. C* **35** (2004) 1, doi:10.1140/epjc/s2004-01758-8, arXiv:hep-ex/0401026.
- [122] CMS Collaboration, “Searches for pair production of charginos and top squarks in final states with two oppositely charged leptons in proton-proton collisions at $\sqrt{s} = 13 \text{ TeV}$ ”, *JHEP* **11** (2018) 079, doi:10.1007/JHEP11(2018)079, arXiv:1807.07799.

- [123] ALEPH Collaboration, “Search for scalar leptons in e^+e^- collisions at center-of-mass energies up to 209 GeV”, *Phys. Lett. B* **526** (2002) 206,
doi:[10.1016/S0370-2693\(01\)01494-0](https://doi.org/10.1016/S0370-2693(01)01494-0), arXiv:[hep-ex/0112011](https://arxiv.org/abs/hep-ex/0112011).
- [124] L3 Collaboration, “Search for scalar leptons and scalar quarks at LEP”, *Phys. Lett. B* **580** (2004) 37, doi:[10.1016/j.physletb.2003.10.010](https://doi.org/10.1016/j.physletb.2003.10.010), arXiv:[hep-ex/0310007](https://arxiv.org/abs/hep-ex/0310007).
- [125] OPAL Collaboration, “Search for anomalous production of dilepton events with missing transverse momentum in e^+e^- collisions at $\sqrt{s} = 183 - 209$ GeV”, *Eur. Phys. J. C* **32** (2004) 453, doi:[10.1140/epjc/s2003-01466-y](https://doi.org/10.1140/epjc/s2003-01466-y), arXiv:[hep-ex/0309014](https://arxiv.org/abs/hep-ex/0309014).

A The CMS Collaboration

Yerevan Physics Institute, Yerevan, Armenia

V. Chekhovsky, A. Hayrapetyan, V. Makarenko , A. Tumasyan¹ 

Institut für Hochenergiephysik, Vienna, Austria

W. Adam , J.W. Andrejkovic, L. Benato , T. Bergauer , K. Damanakis , M. Dragicevic , C. Giordano, P.S. Hussain , M. Jeitler² , N. Krammer , A. Li , D. Liko , I. Mikulec , J. Schieck² , R. Schöfbeck² , D. Schwarz , M. Sonawane , W. Waltenberger , C.-E. Wulz² 

Universiteit Antwerpen, Antwerpen, Belgium

T. Janssen , H. Kwon , T. Van Laer , P. Van Mechelen 

Vrije Universiteit Brussel, Brussel, Belgium

N. Breugelmans, J. D'Hondt , S. Dansana , A. De Moor , M. Delcourt , F. Heyen, Y. Hong , S. Lowette , I. Makarenko , D. Müller , S. Tavernier , M. Tytgat³ , G.P. Van Onsem , S. Van Putte , D. Vannerom 

Université Libre de Bruxelles, Bruxelles, Belgium

B. Bilin , B. Clerbaux , A.K. Das, I. De Bruyn , G. De Lentdecker , H. Evard , L. Favart , P. Gianneios , A. Khalilzadeh, F.A. Khan , A. Malara , M.A. Shahzad, L. Thomas , M. Vanden Bemden , C. Vander Velde , P. Vanlaer , F. Zhang 

Ghent University, Ghent, Belgium

M. De Coen , D. Dobur , G. Gokbulut , J. Knolle , L. Lambrecht , D. Marckx , K. Skovpen , N. Van Den Bossche , J. van der Linden , J. Vandebroeck , L. Wezenbeek 

Université Catholique de Louvain, Louvain-la-Neuve, Belgium

S. Bein , A. Benecke , A. Bethani , G. Bruno , A. Cappati , J. De Favereau De Jeneret , C. Delaere , A. Giammanco , A.O. Guzel , Sa. Jain , V. Lemaitre, J. Lidrych , P. Mastrapasqua , S. Turkcapar 

Centro Brasileiro de Pesquisas Fisicas, Rio de Janeiro, Brazil

G.A. Alves , E. Coelho , G. Correia Silva , C. Hensel , T. Menezes De Oliveira , C. Mora Herrera⁴ , P. Rebello Teles , M. Soeiro , E.J. Tonelli Manganote⁵ , A. Vilela Pereira⁴ 

Universidade do Estado do Rio de Janeiro, Rio de Janeiro, Brazil

W.L. Aldá Júnior , M. Barroso Ferreira Filho , H. Brandao Malbouisson , W. Carvalho , J. Chinellato⁶ , E.M. Da Costa , G.G. Da Silveira⁷ , D. De Jesus Damiao , S. Fonseca De Souza , R. Gomes De Souza , S. S. Jesus , T. Laux Kuhn⁷ , M. Macedo , K. Mota Amarilo , L. Mundim , H. Nogima , J.P. Pinheiro , A. Santoro , A. Sznajder , M. Thiel 

Universidade Estadual Paulista, Universidade Federal do ABC, São Paulo, Brazil

C.A. Bernardes⁷ , L. Calligaris , T.R. Fernandez Perez Tomei , E.M. Gregores , I. Maietto Silverio , P.G. Mercadante , S.F. Novaes , B. Orzari , Sandra S. Padula , V. Scheurer

Institute for Nuclear Research and Nuclear Energy, Bulgarian Academy of Sciences, Sofia, Bulgaria

A. Aleksandrov , G. Antchev , R. Hadjiiska , P. Iaydjiev , M. Misheva , M. Shopova , G. Sultanov 

University of Sofia, Sofia, Bulgaria

A. Dimitrov , L. Litov , B. Pavlov , P. Petkov , A. Petrov , E. Shumka 

Instituto De Alta Investigación, Universidad de Tarapacá, Casilla 7 D, Arica, Chile

S. Keshri , D. Laroze , S. Thakur 

Beihang University, Beijing, China

T. Cheng , T. Javaid , L. Yuan 

Department of Physics, Tsinghua University, Beijing, China

Z. Hu , Z. Liang, J. Liu

Institute of High Energy Physics, Beijing, China

G.M. Chen⁸ , H.S. Chen⁸ , M. Chen⁸ , Q. Hou , F. Iemmi , C.H. Jiang, A. Kapoor⁹ , H. Liao , Z.-A. Liu¹⁰ , R. Sharma¹¹ , J.N. Song¹⁰, J. Tao , C. Wang⁸, J. Wang , H. Zhang , J. Zhao 

State Key Laboratory of Nuclear Physics and Technology, Peking University, Beijing, China

A. Agapitos , Y. Ban , A. Carvalho Antunes De Oliveira , S. Deng , B. Guo, C. Jiang , A. Levin , C. Li , Q. Li , Y. Mao, S. Qian, S.J. Qian , X. Qin, X. Sun , D. Wang , H. Yang, Y. Zhao, C. Zhou 

State Key Laboratory of Nuclear Physics and Technology, Institute of Quantum Matter, South China Normal University, Guangzhou, China

S. Yang 

Sun Yat-Sen University, Guangzhou, China

Z. You 

University of Science and Technology of China, Hefei, China

K. Jaffel , N. Lu 

Nanjing Normal University, Nanjing, China

G. Bauer¹², B. Li¹³, H. Wang , K. Yi¹⁴ , J. Zhang 

Institute of Modern Physics and Key Laboratory of Nuclear Physics and Ion-beam Application (MOE) - Fudan University, Shanghai, China

Y. Li

Zhejiang University, Hangzhou, Zhejiang, China

Z. Lin , C. Lu , M. Xiao 

Universidad de Los Andes, Bogota, Colombia

C. Avila , D.A. Barbosa Trujillo , A. Cabrera , C. Florez , J. Fraga , J.A. Reyes Vega

Universidad de Antioquia, Medellin, Colombia

J. Jaramillo , C. Rendón , M. Rodriguez , A.A. Ruales Barbosa , J.D. Ruiz Alvarez 

University of Split, Faculty of Electrical Engineering, Mechanical Engineering and Naval Architecture, Split, Croatia

D. Giljanovic , N. Godinovic , D. Lelas , A. Sculac 

University of Split, Faculty of Science, Split, Croatia

M. Kovac , A. Petkovic , T. Sculac 

Institute Rudjer Boskovic, Zagreb, Croatia

P. Bargassa , V. Brigljevic , B.K. Chitroda , D. Ferencek , K. Jakovcic, A. Starodumov 

T. Susa 

University of Cyprus, Nicosia, Cyprus

A. Attikis , K. Christoforou , A. Hadjiagapiou, C. Leonidou , J. Mousa , C. Nicolaou, L. Paizanatos , F. Ptochos , P.A. Razis , H. Rykaczewski, H. Saka , A. Stepennov 

Charles University, Prague, Czech Republic

M. Finger , M. Finger Jr. , A. Kveton 

Escuela Politecnica Nacional, Quito, Ecuador

E. Ayala 

Universidad San Francisco de Quito, Quito, Ecuador

E. Carrera Jarrin 

Academy of Scientific Research and Technology of the Arab Republic of Egypt, Egyptian Network of High Energy Physics, Cairo, Egypt

H. Abdalla¹⁵ , R. Aly^{16,17} , Y. Assran^{18,16}

Center for High Energy Physics (CHEP-FU), Fayoum University, El-Fayoum, Egypt

M. Abdullah Al-Mashad , M.A. Mahmoud 

National Institute of Chemical Physics and Biophysics, Tallinn, Estonia

K. Ehataht , M. Kadastik, T. Lange , C. Nielsen , J. Pata , M. Raidal , L. Tani , C. Veelken 

Department of Physics, University of Helsinki, Helsinki, Finland

K. Osterberg , M. Voutilainen 

Helsinki Institute of Physics, Helsinki, Finland

N. Bin Norjoharuddeen , E. Brücke , F. Garcia , P. Inkaew , K.T.S. Kallonen , T. Lampén , K. Lassila-Perini , S. Lehti , T. Lindén , M. Myllymäki , M.m. Rantanen , S. Saariokari , J. Tuominiemi 

Lappeenranta-Lahti University of Technology, Lappeenranta, Finland

H. Kirschenmann , P. Luukka , H. Petrow 

IRFU, CEA, Université Paris-Saclay, Gif-sur-Yvette, France

M. Besancon , F. Couderc , M. Dejardin , D. Denegri, J.L. Faure , F. Ferri , S. Ganjour , P. Gras , G. Hamel de Monchenault , M. Kumar , V. Lohezic , J. Malcles , F. Orlandi , L. Portales , A. Rosowsky , M.Ö. Sahin , A. Savoy-Navarro¹⁹ , P. Simkina , M. Titov , M. Tornago 

Laboratoire Leprince-Ringuet, CNRS/IN2P3, Ecole Polytechnique, Institut Polytechnique de Paris, Palaiseau, France

F. Beaudette , G. Boldrini , P. Busson , C. Charlot , M. Chiusi , T.D. Cuisset , F. Damas , O. Davignon , A. De Wit , I.T. Ehle , B.A. Fontana Santos Alves , S. Ghosh , A. Gilbert , R. Granier de Cassagnac , B. Harikrishnan , L. Kalipoliti , G. Liu , M. Manoni , M. Nguyen , S. Obraztsov , C. Ochando , R. Salerno , J.B. Sauvan , Y. Sirois , G. Sokmen, L. Urda Gómez , E. Vernazza , A. Zabi , A. Zghiche 

Université de Strasbourg, CNRS, IPHC UMR 7178, Strasbourg, France

J.-L. Agram²⁰ , J. Andrea , D. Bloch , J.-M. Brom , E.C. Chabert , C. Collard , S. Falke , U. Goerlach , R. Haeberle , A.-C. Le Bihan , M. Meena , O. Poncet , G. Saha , M.A. Sessini , P. Van Hove , P. Vaucelle 

**Centre de Calcul de l’Institut National de Physique Nucléaire et de Physique des Particules,
CNRS/IN2P3, Villeurbanne, France**

A. Di Florio 

Institut de Physique des 2 Infinis de Lyon (IP2I), Villeurbanne, France

D. Amram, S. Beauceron , B. Blançon , G. Boudoul , N. Chanon , D. Contardo , P. Depasse , C. Dozen²¹ , H. El Mamouni, J. Fay , S. Gascon , M. Gouzevitch , C. Greenberg , G. Grenier , B. Ille , E. Jourd’huiy, I.B. Laktineh, M. Lethuillier , L. Mirabito, S. Perries, A. Purohit , M. Vander Donckt , P. Verdier , J. Xiao

Georgian Technical University, Tbilisi, Georgia

A. Khvedelidze²² , I. Lomidze , Z. Tsamalaidze²² 

RWTH Aachen University, I. Physikalisches Institut, Aachen, Germany

V. Botta , S. Consuegra Rodríguez , L. Feld , K. Klein , M. Lipinski , D. Meuser , A. Pauls , D. Pérez Adán , N. Röwert , M. Teroerde 

RWTH Aachen University, III. Physikalisches Institut A, Aachen, Germany

S. Diekmann , A. Dodonova , N. Eich , D. Eliseev , F. Engelke , J. Erdmann , M. Erdmann , B. Fischer , T. Hebbeker , K. Hoepfner , F. Ivone , A. Jung , N. Kumar , M.y. Lee , F. Mausolf , M. Merschmeyer , A. Meyer , F. Nowotny, A. Pozdnyakov , Y. Rath, W. Redjeb , F. Rehm, H. Reithler , V. Sarkisovi , A. Schmidt , C. Seth, A. Sharma , J.L. Spah , F. Torres Da Silva De Araujo²³ , S. Wiedenbeck , S. Zaleski

RWTH Aachen University, III. Physikalisches Institut B, Aachen, Germany

C. Dziwok , G. Flügge , T. Kress , A. Nowack , O. Pooth , A. Stahl , T. Ziemons , A. Zottz 

Deutsches Elektronen-Synchrotron, Hamburg, Germany

H. Aarup Petersen , M. Aldaya Martin , J. Alimena , S. Amoroso, Y. An , J. Bach , S. Baxter , M. Bayatmakou , H. Becerril Gonzalez , O. Behnke , A. Belvedere , F. Blekman²⁴ , K. Borras²⁵ , A. Campbell , A. Cardini , S. Chatterjee , F. Colombina , M. De Silva , G. Eckerlin, D. Eckstein , E. Gallo²⁴ , A. Geiser , V. Guglielmi , M. Guthoff , A. Hinzmann , L. Jeppe , B. Kaech , M. Kasemann , C. Kleinwort , R. Kogler , M. Komm , D. Krücker , W. Lange, D. Leyva Pernia , K. Lipka²⁶ , W. Lohmann²⁷ , F. Lorkowski , R. Mankel , I.-A. Melzer-Pellmann , M. Mendizabal Morentin , A.B. Meyer , G. Milella , K. Moral Figueroa , A. Mussgiller , L.P. Nair , J. Niedziela , A. Nürnberg , J. Park , E. Ranken , A. Raspereza , D. Rastorguev , J. Rübenach, L. Rygaard, M. Scham^{28,25} , S. Schnake²⁵ , P. Schütze , C. Schwanenberger²⁴ , D. Selivanova , K. Sharko , M. Shchedrolosiev , D. Stafford , F. Vazzoler , A. Ventura Barroso , R. Walsh , D. Wang , Q. Wang , K. Wichmann, L. Wiens²⁵ , C. Wissing , Y. Yang , S. Zakharov, A. Zimermanne Castro Santos

University of Hamburg, Hamburg, Germany

A. Albrecht , S. Albrecht , M. Antonello , S. Bollweg, M. Bonanomi , P. Connor , K. El Morabit , Y. Fischer , E. Garutti , A. Grohsjean , J. Haller , D. Hundhausen, H.R. Jabusch , G. Kasieczka , P. Keicher , R. Klanner , W. Korcari , T. Kramer , C.c. Kuo, V. Kutzner , F. Labe , J. Lange , A. Lobanov , C. Matthies , L. Moureux , M. Mrowietz, A. Nigamova , K. Nikolopoulos , Y. Nissan, A. Paasch , K.J. Pena Rodriguez , T. Quadfasel , B. Raciti , M. Rieger , D. Savoiu , J. Schindler , P. Schleper , M. Schröder , J. Schwandt , M. Sommerhalder , H. Stadie , G. Steinbrück , A. Tews, B. Wiederspan, M. Wolf

Karlsruher Institut fuer Technologie, Karlsruhe, Germany

S. Brommer , E. Butz , Y.M. Chen , T. Chwalek , A. Dierlamm , G.G. Dincer , U. Elicabuk, N. Faltermann , M. Giffels , A. Gottmann , F. Hartmann²⁹ , R. Hofsaess , M. Horzela , U. Husemann , J. Kieseler , M. Klute , O. Lavoryk , J.M. Lawhorn , M. Link, A. Lintuluoto , S. Maier , M. Mormile , Th. Müller , M. Neukum, M. Oh , E. Pfeffer , M. Presilla , G. Quast , K. Rabbertz , B. Regnery , R. Schmieder, N. Shadskiy , I. Shvetsov , H.J. Simonis , L. Sowa , L. Stockmeier, K. Tauqueer, M. Toms , B. Topko , N. Trevisani , T. Voigtländer , R.F. Von Cube , J. Von Den Driesch, M. Wassmer , S. Wieland , F. Wittig, R. Wolf , X. Zuo

Institute of Nuclear and Particle Physics (INPP), NCSR Demokritos, Aghia Paraskevi, Greece

G. Anagnostou , G. Daskalakis , A. Kyriakis , A. Papadopoulos²⁹ , A. Stakia 

National and Kapodistrian University of Athens, Athens, Greece

G. Melachroinos, Z. Painesis , I. Paraskevas , N. Saoulidou , K. Theofilatos , E. Tziaferi , K. Vellidis , I. Zisopoulos 

National Technical University of Athens, Athens, Greece

T. Chatzistavrou, G. Karapostoli , K. Kousouris , E. Siamarkou, G. Tsipolitis 

University of Ioánnina, Ioánnina, Greece

I. Bestintzanos, I. Evangelou , C. Foudas, C. Kamtsikis, P. Katsoulis, P. Kokkas , P.G. Kosmoglou Kiouseoglou , N. Manthos , I. Papadopoulos , J. Strologas 

HUN-REN Wigner Research Centre for Physics, Budapest, Hungary

C. Hajdu , D. Horvath^{30,31} , K. Márton, A.J. Rádl³² , F. Sikler , V. Veszpremi 

MTA-ELTE Lendület CMS Particle and Nuclear Physics Group, Eötvös Loránd University, Budapest, Hungary

M. Csand , K. Farkas , A. Fehrkuti³³ , M.M.A. Gadallah³⁴ , . Kadlecsik , G. Psztor , G.I. Veres 

Faculty of Informatics, University of Debrecen, Debrecen, Hungary

B. Ujvari , G. Zilizi 

HUN-REN ATOMKI - Institute of Nuclear Research, Debrecen, Hungary

G. Bencze, S. Czellar, J. Molnar, Z. Szillasi

Karoly Robert Campus, MATE Institute of Technology, Gyongyos, Hungary

T. Csorgo³³ , F. Nemes³³ , T. Novak 

Panjab University, Chandigarh, India

S. Bansal , S.B. Beri, V. Bhatnagar , G. Chaudhary , S. Chauhan , N. Dhingra³⁵ , A. Kaur , A. Kaur , H. Kaur , M. Kaur , S. Kumar , T. Sheokand, J.B. Singh , A. Singla 

University of Delhi, Delhi, India

A. Bhardwaj , A. Chhetri , B.C. Choudhary , A. Kumar , A. Kumar , M. Naimuddin , K. Ranjan , M.K. Saini, S. Saumya 

Indian Institute of Technology Kanpur, Kanpur, India

S. Mukherjee 

Saha Institute of Nuclear Physics, HBNI, Kolkata, India

S. Baradia , S. Barman³⁶ , S. Bhattacharya , S. Das Gupta, S. Dutta , S. Dutta, S. Sarkar

Indian Institute of Technology Madras, Madras, India

M.M. Ameen , P.K. Behera , S.C. Behera , S. Chatterjee , G. Dash , A. Dattamunsi, P. Jana , P. Kalbhor , S. Kamble , J.R. Komaragiri³⁷ , D. Kumar³⁷ , T. Mishra , B. Parida³⁸ , P.R. Pujahari , N.R. Saha , A.K. Sikdar , R.K. Singh , P. Verma , S. Verma , A. Vijay 

Tata Institute of Fundamental Research-A, Mumbai, India

S. Dugad , G.B. Mohanty , M. Shelake , P. Suryadevara

Tata Institute of Fundamental Research-B, Mumbai, India

A. Bala , S. Banerjee , S. Bhowmik³⁹ , R.M. Chatterjee, M. Guchait , Sh. Jain , A. Jaiswal, B.M. Joshi , S. Kumar , G. Majumder , K. Mazumdar , S. Parolia , A. Thachayath 

National Institute of Science Education and Research, An OCC of Homi Bhabha National Institute, Bhubaneswar, Odisha, India

S. Bahinipati⁴⁰ , C. Kar , D. Maity⁴¹ , P. Mal , K. Naskar⁴¹ , A. Nayak⁴¹ , S. Nayak, K. Pal , R. Raturi, P. Sadangi, S.K. Swain , S. Varghese⁴¹ , D. Vats⁴¹ 

Indian Institute of Science Education and Research (IISER), Pune, India

S. Acharya⁴² , A. Alpana , S. Dube , B. Gomber⁴² , P. Hazarika , B. Kansal , A. Laha , B. Sahu⁴² , S. Sharma , K.Y. Vaish 

Isfahan University of Technology, Isfahan, Iran

H. Bakhshiansohi⁴³ , A. Jafari⁴⁴ , M. Zeinali⁴⁵ 

Institute for Research in Fundamental Sciences (IPM), Tehran, Iran

S. Bashiri , S. Chenarani⁴⁶ , S.M. Etesami , Y. Hosseini , M. Khakzad , E. Khazaie , M. Mohammadi Najafabadi , S. Tizchang⁴⁷ 

University College Dublin, Dublin, Ireland

M. Felcini , M. Grunewald 

INFN Sezione di Bari^a, Università di Bari^b, Politecnico di Bari^c, Bari, Italy

M. Abbrescia^{a,b} , M. Buonsante^{a,b} , A. Colaleo^{a,b} , D. Creanza^{a,c} , B. D'Anzi^{a,b} , N. De Filippis^{a,c} , M. De Palma^{a,b} , W. Elmetenawee^{a,b,17} , N. Ferrara^{a,b} , L. Fiore^a , G. Iaselli^{a,c} , L. Longo^a , M. Louka^{a,b} , G. Maggi^{a,c} , M. Maggi^a , I. Margjeka^a , V. Mastrapasqua^{a,b} , S. My^{a,b} , S. Nuzzo^{a,b} , A. Pellecchia^{a,b} , A. Pompili^{a,b} , G. Pugliese^{a,c} , R. Radogna^{a,b} , D. Ramos^a , A. Ranieri^a , L. Silvestris^a , F.M. Simone^{a,c} , Ü. Sözbilir^a , A. Stamerra^{a,b} , D. Troiano^{a,b} , R. Venditti^{a,b} , P. Verwilligen^a , A. Zaza^{a,b} 

INFN Sezione di Bologna^a, Università di Bologna^b, Bologna, Italy

G. Abbiendi^a , C. Battilana^{a,b} , D. Bonacorsi^{a,b} , P. Capiluppi^{a,b} , A. Castro^{+a,b} , F.R. Cavallo^a , M. Cuffiani^{a,b} , G.M. Dallavalle^a , T. Diotalevi^{a,b} , F. Fabbri^a , A. Fanfani^{a,b} , D. Fasanella^a , P. Giacomelli^a , L. Giommi^{a,b} , C. Grandi^a , L. Guiducci^{a,b} , S. Lo Meo^{a,48} , M. Lorusso^{a,b} , L. Lunerti^a , S. Marcellini^a , G. Masetti^a , F.L. Navarria^{a,b} , G. Paggi^{a,b} , A. Perrotta^a , F. Primavera^{a,b} , A.M. Rossi^{a,b} , S. Rossi Tisbeni^{a,b} , T. Rovelli^{a,b} , G.P. Siroli^{a,b} 

INFN Sezione di Catania^a, Università di Catania^b, Catania, Italy

S. Costa^{a,b,49} , A. Di Mattia^a , A. Lapertosa^a , R. Potenza^{a,b} , A. Tricomi^{a,b,49} 

INFN Sezione di Firenze^a, Università di Firenze^b, Firenze, Italy

P. Assiouras^a , G. Barbagli^a , G. Bardelli^{a,b} , M. Bartolini^{a,b} , B. Camaiani^{a,b} 

A. Cassese^a , R. Ceccarelli^a , V. Ciulli^{a,b} , C. Civinini^a , R. D'Alessandro^{a,b} , L. Damenti^{a,b}, E. Focardi^{a,b} , T. Kello^a , G. Latino^{a,b} , P. Lenzi^{a,b} , M. Lizzo^a , M. Meschini^a , S. Paoletti^a , A. Papanastassiou^{a,b}, G. Sguazzoni^a , L. Viliani^a

INFN Laboratori Nazionali di Frascati, Frascati, Italy

L. Benussi , S. Bianco , S. Meola⁵⁰ , D. Piccolo 

INFN Sezione di Genova^a, Università di Genova^b, Genova, Italy

M. Alves Gallo Pereira^a , F. Ferro^a , E. Robutti^a , S. Tosi^{a,b} 

INFN Sezione di Milano-Bicocca^a, Università di Milano-Bicocca^b, Milano, Italy

A. Benaglia^a , F. Brivio^a , F. Cetorelli^{a,b} , F. De Guio^{a,b} , M.E. Dinardo^{a,b} , P. Dini^a , S. Gennai^a , R. Gerosa^{a,b} , A. Ghezzi^{a,b} , P. Govoni^{a,b} , L. Guzzi^a , G. Lavizzari^{a,b}, M.T. Lucchini^{a,b} , M. Malberti^a , S. Malvezzi^a , A. Massironi^a , D. Menasce^a , L. Moroni^a , M. Paganoni^{a,b} , S. Palluotto^{a,b} , D. Pedrini^a , A. Perego^{a,b} , B.S. Pinolini^a, G. Pizzati^{a,b} , S. Ragazzi^{a,b} , T. Tabarelli de Fatis^{a,b}

INFN Sezione di Napoli^a, Università di Napoli 'Federico II'^b, Napoli, Italy; Università della Basilicata^c, Potenza, Italy; Scuola Superiore Meridionale (SSM)^d, Napoli, Italy

S. Buontempo^a , A. Cagnotta^{a,b} , F. Carnevali^{a,b} , N. Cavallo^{a,c} , C. Di Fraia^a , F. Fabozzi^{a,c} , A.O.M. Iorio^{a,b} , L. Lista^{a,b,51} , P. Paolucci^{a,29} , B. Rossi^a

INFN Sezione di Padova^a, Università di Padova^b, Padova, Italy; Universita degli Studi di Cagliari^c, Cagliari, Italy

R. Ardino^a , P. Azzi^a , N. Bacchetta^{a,52} , D. Bisello^{a,b} , P. Bortignon^a , G. Bortolato^{a,b}, A.C.M. Bulla^a , R. Carlin^{a,b} , P. Checchia^a , T. Dorigo^{a,53} , F. Gasparini^{a,b} , U. Gasparini^{a,b} , S. Giorgetti^a , A. Gozzelino^a , E. Lusiani^a , M. Margoni^{a,b} , J. Pazzini^{a,b} , P. Ronchese^{a,b} , R. Rossin^{a,b} , F. Simonetto^{a,b} , M. Tosi^{a,b} , A. Triossi^{a,b} , S. Ventura^a , M. Zanetti^{a,b} , P. Zotto^{a,b} , A. Zucchetta^{a,b} , G. Zumerle^{a,b}

INFN Sezione di Pavia^a, Università di Pavia^b, Pavia, Italy

A. Braghieri^a , S. Calzaferri^a , D. Fiorina^a , P. Montagna^{a,b} , M. Pelliccioni^a , V. Re^a , C. Riccardi^{a,b} , P. Salvini^a , I. Vai^{a,b} , P. Vitulo^{a,b}

INFN Sezione di Perugia^a, Università di Perugia^b, Perugia, Italy

S. Ajmal^{a,b} , M.E. Ascoli^{a,b}, G.M. Bilei^a , C. Carrivale^{a,b}, D. Ciangottini^{a,b} , L. Fanò^{a,b} , V. Mariani^{a,b} , M. Menichelli^a , F. Moscatelli^{a,54} , A. Rossi^{a,b} , A. Santocchia^{a,b} , D. Spiga^a , T. Tedeschi^{a,b}

INFN Sezione di Pisa^a, Università di Pisa^b, Scuola Normale Superiore di Pisa^c, Pisa, Italy; Università di Siena^d, Siena, Italy

C. Aimè^{a,b} , C.A. Alexe^{a,c} , P. Asenov^{a,b} , P. Azzurri^a , G. Bagliesi^a , R. Bhattacharya^a , L. Bianchini^{a,b} , T. Boccali^a , E. Bossini^a , D. Bruschini^{a,c} , R. Castaldi^a , F. Cattafesta^{a,c} , M.A. Ciocci^{a,b} , M. Cipriani^{a,b} , V. D'Amante^{a,d} , R. Dell'Orso^a , S. Donato^{a,b} , A. Giassi^a , F. Ligabue^{a,c} , A.C. Marini^{a,b} , D. Matos Figueiredo^a , A. Messineo^{a,b} , S. Mishra^a , V.K. Muraleedharan Nair Bindhu^{a,b,41} , M. Musich^{a,b} , S. Nandan^a , F. Palla^a , A. Rizzi^{a,b} , G. Rolandi^{a,c} , S. Roy Chowdhury^{a,39} , T. Sarkar^a , A. Scribano^a , P. Spagnolo^a , F. Tenchini^{a,b} , R. Tenchini^a , G. Tonelli^{a,b} , N. Turini^{a,d} , F. Vaselli^{a,c} , A. Venturi^a , P.G. Verdini^a

INFN Sezione di Roma^a, Sapienza Università di Roma^b, Roma, Italy

P. Akrap^{a,b} , C. Basile^{a,b} , F. Cavallari^a , L. Cunqueiro Mendez^{a,b} , F. De Riggi^{a,b} 

D. Del Re^{a,b} , E. Di Marco^{a,b} , M. Diemoz^a , F. Errico^{a,b} , R. Gargiulo^{a,b} , F. Lombardi^{a,b} , E. Longo^{a,b} , L. Martikainen^{a,b} , J. Mijuskovic^{a,b} , G. Organtini^{a,b} , N. Palmeri^{a,b} , F. Pandolfi^a , R. Paramatti^{a,b} , C. Quaranta^{a,b} , S. Rahatlou^{a,b} , C. Rovelli^a , F. Santanastasio^{a,b} , L. Soffi^a , V. Vladimirov^{a,b}

INFN Sezione di Torino^a, Università di Torino^b, Torino, Italy; Università del Piemonte Orientale^c, Novara, Italy

N. Amapane^{a,b} , R. Arcidiacono^{a,c} , S. Argiro^{a,b} , M. Arneodo^{a,c} , N. Bartosik^{a,c} , R. Bellan^{a,b} , C. Biino^a , C. Borca^{a,b} , N. Cartiglia^a , M. Costa^{a,b} , G. Cotto^{a,b} , R. Covarelli^{a,b} , N. Demaria^a , L. Finco^a , M. Grippo^{a,b} , B. Kiani^{a,b} , F. Legger^a , F. Luongo^{a,b} , C. Mariotti^a , L. Markovic^{a,b} , S. Maselli^a , A. Mecca^{a,b} , L. Menzio^{a,b} , P. Meridiani^a , E. Migliore^{a,b} , M. Monteno^a , R. Mulargia^a , M.M. Obertino^{a,b} , G. Ortona^a , L. Pacher^{a,b} , N. Pastrone^a , M. Ruspa^{a,c} , F. Siviero^{a,b} , V. Sola^{a,b} , A. Solano^{a,b} , C. Tarricone^{a,b} , D. Trocino^a , G. Umoret^{a,b} , R. White^{a,b}

INFN Sezione di Trieste^a, Università di Trieste^b, Trieste, Italy

J. Babbar^{a,b} , S. Belforte^a , V. Candelise^{a,b} , M. Casarsa^a , F. Cossutti^a , K. De Leo^a , G. Della Ricca^{a,b} 

Kyungpook National University, Daegu, Korea

S. Dogra , J. Hong , J. Kim, D. Lee, H. Lee , J. Lee, S.W. Lee , C.S. Moon , Y.D. Oh , M.S. Ryu , S. Sekmen , B. Tae, Y.C. Yang

Department of Mathematics and Physics - GWNU, Gangneung, Korea

M.S. Kim 

Chonnam National University, Institute for Universe and Elementary Particles, Kwangju, Korea

G. Bak , P. Gwak , H. Kim , D.H. Moon 

Hanyang University, Seoul, Korea

E. Asilar , J. Choi⁵⁵ , D. Kim , T.J. Kim , J.A. Merlin, Y. Ryou

Korea University, Seoul, Korea

S. Choi , S. Han, B. Hong , K. Lee, K.S. Lee , S. Lee , J. Yoo 

Kyung Hee University, Department of Physics, Seoul, Korea

J. Goh , S. Yang 

Sejong University, Seoul, Korea

Y. Kang , H. S. Kim , Y. Kim , S. Lee

Seoul National University, Seoul, Korea

J. Almond, J.H. Bhyun, J. Choi , J. Choi, W. Jun , J. Kim , Y.W. Kim , S. Ko , H. Lee , J. Lee , J. Lee , B.H. Oh , S.B. Oh , H. Seo , U.K. Yang, I. Yoon

University of Seoul, Seoul, Korea

W. Jang , D.Y. Kang, S. Kim , B. Ko, J.S.H. Lee , Y. Lee , I.C. Park , Y. Roh, I.J. Watson 

Yonsei University, Department of Physics, Seoul, Korea

G. Cho, S. Ha , K. Hwang , B. Kim , K. Lee , H.D. Yoo 

Sungkyunkwan University, Suwon, Korea

M. Choi , M.R. Kim , H. Lee, Y. Lee , I. Yu 

College of Engineering and Technology, American University of the Middle East (AUM),

Dasman, KuwaitT. Beyrouthy , Y. Gharbia **Kuwait University - College of Science - Department of Physics, Safat, Kuwait**F. Alazemi **Riga Technical University, Riga, Latvia**K. Dreimanis , A. Gaile , C. Munoz Diaz , D. Osite , G. Pikurs , A. Potrebko , M. Seidel , D. Sidiropoulos Kontos **University of Latvia (LU), Riga, Latvia**N.R. Strautnieks **Vilnius University, Vilnius, Lithuania**M. Ambrozas , A. Juodagalvis , A. Rinkevicius , G. Tamulaitis **National Centre for Particle Physics, Universiti Malaya, Kuala Lumpur, Malaysia**I. Yusuff⁵⁶ , Z. Zolkapli**Universidad de Sonora (UNISON), Hermosillo, Mexico**J.F. Benitez , A. Castaneda Hernandez , H.A. Encinas Acosta, L.G. Gallegos Maríñez, M. León Coello , J.A. Murillo Quijada , A. Sehrawat , L. Valencia Palomo **Centro de Investigacion y de Estudios Avanzados del IPN, Mexico City, Mexico**G. Ayala , H. Castilla-Valdez , H. Crotte Ledesma , E. De La Cruz-Burelo , I. Heredia-De La Cruz⁵⁷ , R. Lopez-Fernandez , J. Mejia Guisao , A. Sánchez Hernández **Universidad Iberoamericana, Mexico City, Mexico**C. Oropeza Barrera , D.L. Ramirez Guadarrama, M. Ramírez García **Benemerita Universidad Autonoma de Puebla, Puebla, Mexico**I. Bautista , F.E. Neri Huerta , I. Pedraza , H.A. Salazar Ibarguen , C. Uribe Estrada **University of Montenegro, Podgorica, Montenegro**I. Bubanja , N. Raicevic **University of Canterbury, Christchurch, New Zealand**P.H. Butler **National Centre for Physics, Quaid-I-Azam University, Islamabad, Pakistan**A. Ahmad , M.I. Asghar , A. Awais , M.I.M. Awan, H.R. Hoorani , W.A. Khan **AGH University of Krakow, Krakow, Poland**V. Avati, A. Bellora⁵⁸ , L. Forthomme , L. Grzanka , M. Malawski , K. Piotrzkowski **National Centre for Nuclear Research, Swierk, Poland**H. Bialkowska , M. Bluj , M. Górski , M. Kazana , M. Szleper , P. Zalewski **Institute of Experimental Physics, Faculty of Physics, University of Warsaw, Warsaw, Poland**K. Bunkowski , K. Doroba , A. Kalinowski , M. Konecki , J. Krolikowski , A. Muhammad **Warsaw University of Technology, Warsaw, Poland**P. Fokow , K. Pozniak , W. Zabolotny **Laboratório de Instrumentação e Física Experimental de Partículas, Lisboa, Portugal**M. Araujo , D. Bastos , C. Beirão Da Cruz E Silva , A. Boletti , M. Bozzo , T. Camporesi , G. Da Molin , P. Faccioli , M. Gallinaro , J. Hollar , N. Leonardo 

G.B. Marozzo [ID](#), A. Petrilli [ID](#), M. Pisano [ID](#), J. Seixas [ID](#), J. Varela [ID](#), J.W. Wulff [ID](#)

Faculty of Physics, University of Belgrade, Belgrade, Serbia

P. Adzic [ID](#), P. Milenovic [ID](#)

VINCA Institute of Nuclear Sciences, University of Belgrade, Belgrade, Serbia

D. Devetak [ID](#), M. Dordevic [ID](#), J. Milosevic [ID](#), L. Nadderd [ID](#), V. Rekovic, M. Stojanovic [ID](#)

Centro de Investigaciones Energéticas Medioambientales y Tecnológicas (CIEMAT), Madrid, Spain

J. Alcaraz Maestre [ID](#), Cristina F. Bedoya [ID](#), J.A. Brochero Cifuentes [ID](#), Oliver M. Carretero [ID](#), M. Cepeda [ID](#), M. Cerrada [ID](#), N. Colino [ID](#), B. De La Cruz [ID](#), A. Delgado Peris [ID](#), A. Escalante Del Valle [ID](#), D. Fernández Del Val [ID](#), J.P. Fernández Ramos [ID](#), J. Flix [ID](#), M.C. Fouz [ID](#), O. Gonzalez Lopez [ID](#), S. Goy Lopez [ID](#), J.M. Hernandez [ID](#), M.I. Josa [ID](#), J. Llorente Merino [ID](#), C. Martin Perez [ID](#), E. Martin Viscasillas [ID](#), D. Moran [ID](#), C. M. Morcillo Perez [ID](#), Á. Navarro Tobar [ID](#), C. Perez Dengra [ID](#), A. Pérez-Calero Yzquierdo [ID](#), J. Puerta Pelayo [ID](#), I. Redondo [ID](#), J. Sastre [ID](#), J. Vazquez Escobar [ID](#)

Universidad Autónoma de Madrid, Madrid, Spain

J.F. de Trocóniz [ID](#)

Universidad de Oviedo, Instituto Universitario de Ciencias y Tecnologías Espaciales de Asturias (ICTEA), Oviedo, Spain

B. Alvarez Gonzalez [ID](#), J. Cuevas [ID](#), J. Fernandez Menendez [ID](#), S. Folgueras [ID](#), I. Gonzalez Caballero [ID](#), P. Leguina [ID](#), E. Palencia Cortezon [ID](#), J. Prado Pico [ID](#), V. Rodríguez Bouza [ID](#), A. Soto Rodríguez [ID](#), A. Trapote [ID](#), C. Vico Villalba [ID](#), P. Vischia [ID](#)

Instituto de Física de Cantabria (IFCA), CSIC-Universidad de Cantabria, Santander, Spain

S. Blanco Fernández [ID](#), I.J. Cabrillo [ID](#), A. Calderon [ID](#), J. Duarte Campderros [ID](#), M. Fernandez [ID](#), G. Gomez [ID](#), C. Lasosa García [ID](#), R. Lopez Ruiz [ID](#), C. Martinez Rivero [ID](#), P. Martinez Ruiz del Arbol [ID](#), F. Matorras [ID](#), P. Matorras Cuevas [ID](#), E. Navarrete Ramos [ID](#), J. Piedra Gomez [ID](#), L. Scodellaro [ID](#), I. Vila [ID](#), J.M. Vizan Garcia [ID](#)

University of Colombo, Colombo, Sri Lanka

B. Kailasapathy⁵⁹ [ID](#), D.D.C. Wickramarathna [ID](#)

University of Ruhuna, Department of Physics, Matara, Sri Lanka

W.G.D. Dharmaratna⁶⁰ [ID](#), K. Liyanage [ID](#), N. Perera [ID](#)

CERN, European Organization for Nuclear Research, Geneva, Switzerland

D. Abbaneo [ID](#), C. Amendola [ID](#), E. Auffray [ID](#), J. Baechler, D. Barney [ID](#), A. Bermúdez Martínez [ID](#), M. Bianco [ID](#), A.A. Bin Anuar [ID](#), A. Bocci [ID](#), L. Borgonovi [ID](#), C. Botta [ID](#), A. Bragagnolo [ID](#), E. Brondolin [ID](#), C.E. Brown [ID](#), C. Caillol [ID](#), G. Cerminara [ID](#), N. Chernyavskaya [ID](#), D. d'Enterria [ID](#), A. Dabrowski [ID](#), A. David [ID](#), A. De Roeck [ID](#), M.M. Defranchis [ID](#), M. Deile [ID](#), M. Dobson [ID](#), W. Funk [ID](#), S. Giani, D. Gigi, K. Gill [ID](#), F. Glege [ID](#), M. Glowacki, J. Hegeman [ID](#), J.K. Heikkilä [ID](#), B. Huber [ID](#), V. Innocente [ID](#), T. James [ID](#), P. Janot [ID](#), O. Kaluzinska [ID](#), O. Karacheban²⁷ [ID](#), G. Karathanasis [ID](#), S. Laurila [ID](#), P. Lecoq [ID](#), E. Leutgeb [ID](#), C. Lourenço [ID](#), M. Magherini [ID](#), L. Malgeri [ID](#), M. Mannelli [ID](#), M. Matthewman, A. Mehta [ID](#), F. Meijers [ID](#), S. Mersi [ID](#), E. Meschi [ID](#), M. Migliorini [ID](#), V. Milosevic [ID](#), F. Monti [ID](#), F. Moortgat [ID](#), M. Mulders [ID](#), I. Neutelings [ID](#), S. Orfanelli, F. Pantaleo [ID](#), G. Petrucciani [ID](#), A. Pfeiffer [ID](#), M. Pierini [ID](#), M. Pitt [ID](#), H. Qu [ID](#), D. Rabady [ID](#), B. Ribeiro Lopes [ID](#), F. Riti [ID](#), M. Rovere [ID](#), H. Sakulin [ID](#), R. Salvatico [ID](#), S. Sanchez Cruz [ID](#), S. Scarfi [ID](#), M. Selvaggi [ID](#), A. Sharma [ID](#), K. Shchelina [ID](#), P. Silva [ID](#), P. Sphicas⁶¹ [ID](#), A.G. Stahl Leiton [ID](#), A. Steen [ID](#), S. Summers [ID](#), D. Treille [ID](#), P. Tropea [ID](#), D. Walter [ID](#)

J. Wanczyk⁶² , J. Wang, S. Wuchterl , P. Zehetner , P. Zejdl , W.D. Zeuner 

PSI Center for Neutron and Muon Sciences, Villigen, Switzerland

T. Bevilacqua⁶³ , L. Caminada⁶³ , A. Ebrahimi , W. Erdmann , R. Horisberger , Q. Ingram , H.C. Kaestli , D. Kotlinski , C. Lange , M. Missiroli⁶³ , L. Noehte⁶³ , T. Rohe , A. Samalan 

ETH Zurich - Institute for Particle Physics and Astrophysics (IPA), Zurich, Switzerland

T.K. Aarrestad , M. Backhaus , G. Bonomelli , A. Calandri , C. Cazzaniga , K. Datta , P. De Bryas Dexmiers D'archiac⁶² , A. De Cosa , G. Dissertori , M. Dittmar, M. Donegà , F. Eble , M. Galli , K. Gedia , F. Glessgen , C. Grab , N. Härringer , T.G. Harte , D. Hits , W. Lustermann , A.-M. Lyon , R.A. Manzoni , M. Marchegiani , L. Marchese , A. Mascellani⁶² , F. Nessi-Tedaldi , F. Pauss , V. Perovic , S. Pigazzini , B. Ristic , R. Seidita , J. Steggemann⁶² , A. Tarabini , D. Valsecchi , R. Wallny 

Universität Zürich, Zurich, Switzerland

C. Amsler⁶⁴ , P. Bärtschi , M.F. Canelli , G. Celotto , K. Cormier , M. Huwiler , W. Jin , A. Jofrehei , B. Kilminster , S. Leontsinis , S.P. Liechti , A. Macchiolo , P. Meiring , F. Meng , J. Motta , A. Reimers , P. Robmann, M. Senger , E. Shokr , F. Stäger , R. Tramontano 

National Central University, Chung-Li, Taiwan

C. Adloff⁶⁵ , D. Bhowmik, C.M. Kuo, W. Lin , P.K. Rout , P.C. Tiwari³⁷ 

National Taiwan University (NTU), Taipei, Taiwan

L. Ceard, K.F. Chen , Z.g. Chen, A. De Iorio , W.-S. Hou , Th. Hsu, Y.w. Kao, S. Karmakar , G. Kole , Y.y. Li , R.-S. Lu , E. Paganis , X.f. Su , J. Thomas-Wilsker , L.s. Tsai, D. Tsionou, H.y. Wu , E. Yazgan 

High Energy Physics Research Unit, Department of Physics, Faculty of Science, Chulalongkorn University, Bangkok, Thailand

C. Asawatangtrakuldee , N. Srimanobhas , V. Wachirapusanand 

Tunis El Manar University, Tunis, Tunisia

Y. Maghrbi 

Çukurova University, Physics Department, Science and Art Faculty, Adana, Turkey

D. Agyel , F. Boran , F. Dolek , I. Dumanoglu⁶⁶ , E. Eskut , Y. Guler⁶⁷ , E. Gurpinar Guler⁶⁷ , C. Isik , O. Kara , A. Kayis Topaksu , Y. Komurcu , G. Onengut , K. Ozdemir⁶⁸ , A. Polatoz , B. Tali⁶⁹ , U.G. Tok , E. Uslan , I.S. Zorbakir 

Middle East Technical University, Physics Department, Ankara, Turkey

M. Yalvac⁷⁰ 

Bogazici University, Istanbul, Turkey

B. Akgun , I.O. Atakisi , E. Gümmez , M. Kaya⁷¹ , O. Kaya⁷² , S. Tekten⁷³ 

Istanbul Technical University, Istanbul, Turkey

A. Cakir , K. Cankocak^{66,74} , S. Sen⁷⁵ 

Istanbul University, Istanbul, Turkey

O. Aydilek⁷⁶ , B. Hacisahinoglu , I. Hos⁷⁷ , B. Kaynak , S. Ozkorucuklu , O. Potok , H. Sert , C. Simsek , C. Zorbilmez 

Yildiz Technical University, Istanbul, Turkey

S. Cerci [ID](#), B. Isildak⁷⁸ [ID](#), D. Sunar Cerci [ID](#), T. Yetkin [ID](#)

Institute for Scintillation Materials of National Academy of Science of Ukraine, Kharkiv, Ukraine

A. Boyaryntsev [ID](#), B. Grynyov [ID](#)

National Science Centre, Kharkiv Institute of Physics and Technology, Kharkiv, Ukraine

L. Levchuk [ID](#)

University of Bristol, Bristol, United Kingdom

D. Anthony [ID](#), J.J. Brooke [ID](#), A. Bundock [ID](#), F. Bury [ID](#), E. Clement [ID](#), D. Cussans [ID](#), H. Flacher [ID](#), J. Goldstein [ID](#), H.F. Heath [ID](#), M.-L. Holmberg [ID](#), L. Kreczko [ID](#), S. Paramesvaran [ID](#), L. Robertshaw, V.J. Smith [ID](#), K. Walkingshaw Pass

Rutherford Appleton Laboratory, Didcot, United Kingdom

A.H. Ball, K.W. Bell [ID](#), A. Belyaev⁷⁹ [ID](#), C. Brew [ID](#), R.M. Brown [ID](#), D.J.A. Cockerill [ID](#), C. Cooke [ID](#), A. Elliot [ID](#), K.V. Ellis, K. Harder [ID](#), S. Harper [ID](#), J. Linacre [ID](#), K. Manolopoulos, M. Moallemi [ID](#), D.M. Newbold [ID](#), E. Olaiya [ID](#), D. Petyt [ID](#), T. Reis [ID](#), A.R. Sahasransu [ID](#), G. Salvi [ID](#), T. Schuh, C.H. Shepherd-Themistocleous [ID](#), I.R. Tomalin [ID](#), K.C. Whalen [ID](#), T. Williams [ID](#)

Imperial College, London, United Kingdom

I. Andreou [ID](#), R. Bainbridge [ID](#), P. Bloch [ID](#), O. Buchmuller, C.A. Carrillo Montoya [ID](#), G.S. Chahal⁸⁰ [ID](#), D. Colling [ID](#), J.S. Dancu, I. Das [ID](#), P. Dauncey [ID](#), G. Davies [ID](#), M. Della Negra [ID](#), S. Fayer, G. Fedi [ID](#), G. Hall [ID](#), A. Howard, G. Iles [ID](#), C.R. Knight [ID](#), P. Krueper [ID](#), J. Langford [ID](#), K.H. Law [ID](#), J. León Holgado [ID](#), L. Lyons [ID](#), A.-M. Magnan [ID](#), B. Maier [ID](#), S. Mallios, M. Mieskolainen [ID](#), J. Nash⁸¹ [ID](#), M. Pesaresi [ID](#), P.B. Pradeep [ID](#), B.C. Radburn-Smith [ID](#), A. Richards, A. Rose [ID](#), L. Russell [ID](#), K. Savva [ID](#), C. Seez [ID](#), R. Shukla [ID](#), A. Tapper [ID](#), K. Uchida [ID](#), G.P. Uttley [ID](#), T. Virdee²⁹ [ID](#), M. Vojinovic [ID](#), N. Wardle [ID](#), D. Winterbottom [ID](#)

Brunel University, Uxbridge, United Kingdom

J.E. Cole [ID](#), A. Khan, P. Kyberd [ID](#), I.D. Reid [ID](#)

Baylor University, Waco, Texas, USA

S. Abdullin [ID](#), A. Brinkerhoff [ID](#), E. Collins [ID](#), M.R. Darwish [ID](#), J. Dittmann [ID](#), K. Hatakeyama [ID](#), V. Hegde [ID](#), J. Hiltbrand [ID](#), B. McMaster [ID](#), J. Samudio [ID](#), S. Sawant [ID](#), C. Sutantawibul [ID](#), J. Wilson [ID](#)

Catholic University of America, Washington, DC, USA

R. Bartek [ID](#), A. Dominguez [ID](#), A.E. Simsek [ID](#), S.S. Yu [ID](#)

The University of Alabama, Tuscaloosa, Alabama, USA

B. Bam [ID](#), A. Buchot Perraguin [ID](#), R. Chudasama [ID](#), S.I. Cooper [ID](#), C. Crovella [ID](#), G. Fidalgo [ID](#), S.V. Gleyzer [ID](#), E. Pearson, C.U. Perez [ID](#), P. Rumerio⁸² [ID](#), E. Usai [ID](#), R. Yi [ID](#)

Boston University, Boston, Massachusetts, USA

G. De Castro, Z. Demiragli [ID](#), C. Erice [ID](#), C. Fangmeier [ID](#), C. Fernandez Madrazo [ID](#), E. Fontanesi [ID](#), D. Gastler [ID](#), F. Golf [ID](#), S. Jeon [ID](#), J. O'cain, I. Reed [ID](#), J. Rohlf [ID](#), K. Salyer [ID](#), D. Sperka [ID](#), D. Spitzbart [ID](#), I. Suarez [ID](#), A. Tsatsos [ID](#), A.G. Zecchinelli [ID](#)

Brown University, Providence, Rhode Island, USA

G. Barone [ID](#), G. Benelli [ID](#), D. Cutts [ID](#), S. Ellis [ID](#), L. Gouskos [ID](#), M. Hadley [ID](#), U. Heintz [ID](#), K.W. Ho [ID](#), J.M. Hogan⁸³ [ID](#), T. Kwon [ID](#), G. Landsberg [ID](#), K.T. Lau [ID](#), J. Luo [ID](#), S. Mondal [ID](#), T. Russell [ID](#), S. Sagir⁸⁴ [ID](#), X. Shen [ID](#), M. Stamenkovic [ID](#), N. Venkatasubramanian [ID](#)

University of California, Davis, Davis, California, USA

S. Abbott [ID](#), B. Barton [ID](#), C. Brainerd [ID](#), R. Breedon [ID](#), H. Cai [ID](#), M. Calderon De La Barca Sanchez [ID](#), M. Chertok [ID](#), M. Citron [ID](#), J. Conway [ID](#), P.T. Cox [ID](#), R. Erbacher [ID](#), F. Jensen [ID](#), O. Kukral [ID](#), G. Mocellin [ID](#), M. Mulhearn [ID](#), S. Ostrom [ID](#), W. Wei [ID](#), S. Yoo [ID](#)

University of California, Los Angeles, California, USA

K. Adamidis, M. Bachtis [ID](#), D. Campos, R. Cousins [ID](#), A. Datta [ID](#), G. Flores Avila [ID](#), J. Hauser [ID](#), M. Ignatenko [ID](#), M.A. Iqbal [ID](#), T. Lam [ID](#), Y.f. Lo [ID](#), E. Manca [ID](#), A. Nunez Del Prado [ID](#), D. Saltzberg [ID](#), V. Valuev [ID](#)

University of California, Riverside, Riverside, California, USA

R. Clare [ID](#), J.W. Gary [ID](#), G. Hanson [ID](#)

University of California, San Diego, La Jolla, California, USA

A. Aportela [ID](#), A. Arora [ID](#), J.G. Branson [ID](#), S. Cittolin [ID](#), S. Cooperstein [ID](#), D. Diaz [ID](#), J. Duarte [ID](#), L. Giannini [ID](#), Y. Gu, J. Guiang [ID](#), R. Kansal [ID](#), V. Krutelyov [ID](#), R. Lee [ID](#), J. Letts [ID](#), M. Masciovecchio [ID](#), F. Mokhtar [ID](#), S. Mukherjee [ID](#), M. Pieri [ID](#), D. Primosch, M. Quinnan [ID](#), V. Sharma [ID](#), M. Tadel [ID](#), E. Vourliotis [ID](#), F. Würthwein [ID](#), Y. Xiang [ID](#), A. Yagil [ID](#)

University of California, Santa Barbara - Department of Physics, Santa Barbara, California, USA

A. Barzdukas [ID](#), L. Brennan [ID](#), C. Campagnari [ID](#), K. Downham [ID](#), C. Grieco [ID](#), M.M. Hussain, J. Incandela [ID](#), J. Kim [ID](#), A.J. Li [ID](#), P. Masterson [ID](#), H. Mei [ID](#), J. Richman [ID](#), S.N. Santpur [ID](#), U. Sarica [ID](#), R. Schmitz [ID](#), F. Setti [ID](#), J. Sheplock [ID](#), D. Stuart [ID](#), T.A. Vámi [ID](#), X. Yan [ID](#), D. Zhang [ID](#)

California Institute of Technology, Pasadena, California, USA

A. Albert [ID](#), S. Bhattacharya [ID](#), A. Bornheim [ID](#), O. Cerri, J. Mao [ID](#), H.B. Newman [ID](#), G. Reales Gutiérrez, M. Spiropulu [ID](#), J.R. Vlimant [ID](#), S. Xie [ID](#), R.Y. Zhu [ID](#)

Carnegie Mellon University, Pittsburgh, Pennsylvania, USA

J. Alison [ID](#), S. An [ID](#), P. Bryant [ID](#), M. Cremonesi, V. Dutta [ID](#), T. Ferguson [ID](#), T.A. Gómez Espinosa [ID](#), A. Harilal [ID](#), A. Kallil Tharayil, M. Kanemura, C. Liu [ID](#), T. Mudholkar [ID](#), S. Murthy [ID](#), P. Palit [ID](#), K. Park [ID](#), M. Paulini [ID](#), A. Roberts [ID](#), A. Sanchez [ID](#), W. Terrill [ID](#)

University of Colorado Boulder, Boulder, Colorado, USA

J.P. Cumalat [ID](#), W.T. Ford [ID](#), A. Hart [ID](#), A. Hassani [ID](#), N. Manganelli [ID](#), J. Pearkes [ID](#), C. Savard [ID](#), N. Schonbeck [ID](#), K. Stenson [ID](#), K.A. Ulmer [ID](#), S.R. Wagner [ID](#), N. Zipper [ID](#), D. Zuolo [ID](#)

Cornell University, Ithaca, New York, USA

J. Alexander [ID](#), X. Chen [ID](#), D.J. Cranshaw [ID](#), J. Dickinson [ID](#), J. Fan [ID](#), X. Fan [ID](#), J. Grassi [ID](#), S. Hogan [ID](#), P. Kotamnives [ID](#), J. Monroy [ID](#), G. Niendorf [ID](#), M. Oshiro [ID](#), J.R. Patterson [ID](#), M. Reid [ID](#), A. Ryd [ID](#), J. Thom [ID](#), P. Wittich [ID](#), R. Zou [ID](#)

Fermi National Accelerator Laboratory, Batavia, Illinois, USA

M. Albrow [ID](#), M. Alyari [ID](#), O. Amram [ID](#), G. Apollinari [ID](#), A. Apresyan [ID](#), L.A.T. Bauerick [ID](#), D. Berry [ID](#), J. Berryhill [ID](#), P.C. Bhat [ID](#), K. Burkett [ID](#), J.N. Butler [ID](#), A. Canepa [ID](#), G.B. Cerati [ID](#), H.W.K. Cheung [ID](#), F. Chlebana [ID](#), C. Cosby [ID](#), G. Cummings [ID](#), I. Dutta [ID](#), V.D. Elvira [ID](#), J. Freeman [ID](#), A. Gandrakota [ID](#), Z. Gecse [ID](#), L. Gray [ID](#), D. Green, A. Grumer [ID](#), S. Grünendahl [ID](#), D. Guerrero [ID](#), O. Gutsche [ID](#), R.M. Harris [ID](#), T.C. Herwig [ID](#), J. Hirschauer [ID](#), B. Jayatilaka [ID](#), S. Jindariani [ID](#), M. Johnson [ID](#), U. Joshi [ID](#), T. Klijnsma [ID](#),

B. Klima [ID](#), K.H.M. Kwok [ID](#), S. Lammel [ID](#), C. Lee [ID](#), D. Lincoln [ID](#), R. Lipton [ID](#), T. Liu [ID](#), K. Maeshima [ID](#), D. Mason [ID](#), P. McBride [ID](#), P. Merkel [ID](#), S. Mrenna [ID](#), S. Nahn [ID](#), J. Ngadiuba [ID](#), D. Noonan [ID](#), S. Norberg, V. Papadimitriou [ID](#), N. Pastika [ID](#), K. Pedro [ID](#), C. Pena⁸⁵ [ID](#), F. Ravera [ID](#), A. Reinsvold Hall⁸⁶ [ID](#), L. Ristori [ID](#), M. Safdari [ID](#), E. Sexton-Kennedy [ID](#), N. Smith [ID](#), A. Soha [ID](#), L. Spiegel [ID](#), S. Stoynev [ID](#), J. Strait [ID](#), L. Taylor [ID](#), S. Tkaczyk [ID](#), N.V. Tran [ID](#), L. Uplegger [ID](#), E.W. Vaandering [ID](#), C. Wang [ID](#), I. Zoi [ID](#)

University of Florida, Gainesville, Florida, USA

C. Aruta [ID](#), P. Avery [ID](#), D. Bourilkov [ID](#), P. Chang [ID](#), V. Cherepanov [ID](#), R.D. Field, C. Huh [ID](#), E. Koenig [ID](#), M. Kolosova [ID](#), J. Konigsberg [ID](#), A. Korytov [ID](#), K. Matchev [ID](#), N. Menendez [ID](#), G. Mitselmakher [ID](#), K. Mohrman [ID](#), A. Muthirakalayil Madhu [ID](#), N. Rawal [ID](#), S. Rosenzweig [ID](#), Y. Takahashi [ID](#), J. Wang [ID](#)

Florida State University, Tallahassee, Florida, USA

T. Adams [ID](#), A. Al Kadhim [ID](#), A. Askew [ID](#), S. Bower [ID](#), R. Hashmi [ID](#), R.S. Kim [ID](#), S. Kim [ID](#), T. Kolberg [ID](#), G. Martinez [ID](#), H. Prosper [ID](#), P.R. Prova, M. Wulansatiti [ID](#), R. Yohay [ID](#), J. Zhang

Florida Institute of Technology, Melbourne, Florida, USA

B. Alsufyani [ID](#), S. Butalla [ID](#), S. Das [ID](#), T. Elkafrawy⁸⁷ [ID](#), M. Hohlmann [ID](#), E. Yanes

University of Illinois Chicago, Chicago, Illinois, USA

M.R. Adams [ID](#), A. Baty [ID](#), C. Bennett [ID](#), R. Cavanaugh [ID](#), R. Escobar Franco [ID](#), O. Evdokimov [ID](#), C.E. Gerber [ID](#), H. Gupta [ID](#), M. Hawksworth, A. Hingrajiya, D.J. Hofman [ID](#), J.h. Lee [ID](#), D. S. Lemos [ID](#), C. Mills [ID](#), S. Nanda [ID](#), B. Ozek [ID](#), D. Pilipovic [ID](#), R. Pradhan [ID](#), E. Prifti, P. Roy, T. Roy [ID](#), S. Rudrabhatla [ID](#), N. Singh, M.B. Tonjes [ID](#), N. Varelas [ID](#), M.A. Wadud [ID](#), Z. Ye [ID](#), J. Yoo [ID](#)

The University of Iowa, Iowa City, Iowa, USA

M. Alhusseini [ID](#), D. Blend [ID](#), K. Dilsiz⁸⁸ [ID](#), L. Emediato [ID](#), G. Karaman [ID](#), O.K. Köseyan [ID](#), J.-P. Merlo, A. Mestvirishvili⁸⁹ [ID](#), O. Neogi, H. Ogul⁹⁰ [ID](#), Y. Onel [ID](#), A. Penzo [ID](#), C. Snyder, E. Tiras⁹¹ [ID](#)

Johns Hopkins University, Baltimore, Maryland, USA

B. Blumenfeld [ID](#), L. Corcodilos [ID](#), J. Davis [ID](#), A.V. Gritsan [ID](#), L. Kang [ID](#), S. Kyriacou [ID](#), P. Maksimovic [ID](#), M. Roguljic [ID](#), J. Roskes [ID](#), S. Sekhar [ID](#), M. Swartz [ID](#)

The University of Kansas, Lawrence, Kansas, USA

A. Abreu [ID](#), L.F. Alcerro Alcerro [ID](#), J. Anguiano [ID](#), S. Arteaga Escatel [ID](#), P. Baringer [ID](#), A. Bean [ID](#), Z. Flowers [ID](#), D. Grove [ID](#), J. King [ID](#), G. Krintiras [ID](#), M. Lazarovits [ID](#), C. Le Mahieu [ID](#), J. Marquez [ID](#), M. Murray [ID](#), M. Nickel [ID](#), S. Popescu⁹² [ID](#), C. Rogan [ID](#), C. Royon [ID](#), S. Sanders [ID](#), E. Schmitz [ID](#), C. Smith [ID](#), G. Wilson [ID](#)

Kansas State University, Manhattan, Kansas, USA

B. Allmond [ID](#), R. Guju Gurunadha [ID](#), A. Ivanov [ID](#), K. Kaadze [ID](#), Y. Maravin [ID](#), J. Natoli [ID](#), D. Roy [ID](#), G. Sorrentino [ID](#)

University of Maryland, College Park, Maryland, USA

A. Baden [ID](#), A. Belloni [ID](#), J. Bistany-riebman, S.C. Eno [ID](#), N.J. Hadley [ID](#), S. Jabeen [ID](#), R.G. Kellogg [ID](#), T. Koeth [ID](#), B. Kronheim, S. Lascio [ID](#), P. Major [ID](#), A.C. Mignerey [ID](#), S. Nabili [ID](#), C. Palmer [ID](#), C. Papageorgakis [ID](#), M.M. Paranjape, E. Popova⁹³ [ID](#), A. Shevelev [ID](#), L. Wang [ID](#), L. Zhang [ID](#)

Massachusetts Institute of Technology, Cambridge, Massachusetts, USA

C. Baldenegro Barrera [ID](#), J. Bendavid [ID](#), S. Bright-Thonney [ID](#), I.A. Cali [ID](#), P.c. Chou [ID](#),

M. D'Alfonso [ID](#), J. Eysermans [ID](#), C. Freer [ID](#), G. Gomez-Ceballos [ID](#), M. Goncharov, G. Grossos [ID](#), P. Harris, D. Hoang [ID](#), D. Kovalskyi [ID](#), J. Krupa [ID](#), L. Lavezzi [ID](#), Y.-J. Lee [ID](#), K. Long [ID](#), C. McGinn [ID](#), A. Novak [ID](#), M.I. Park [ID](#), C. Paus [ID](#), C. Reissel [ID](#), C. Roland [ID](#), G. Roland [ID](#), S. Rothman [ID](#), G.S.F. Stephans [ID](#), Z. Wang [ID](#), B. Wyslouch [ID](#), T. J. Yang [ID](#)

University of Minnesota, Minneapolis, Minnesota, USA

B. Crossman [ID](#), C. Kapsiak [ID](#), M. Krohn [ID](#), D. Mahon [ID](#), J. Mans [ID](#), B. Marzocchi [ID](#), M. Revering [ID](#), R. Rusack [ID](#), R. Saradhy [ID](#), N. Strobbe [ID](#)

University of Nebraska-Lincoln, Lincoln, Nebraska, USA

K. Bloom [ID](#), D.R. Claes [ID](#), G. Haza [ID](#), J. Hossain [ID](#), C. Joo [ID](#), I. Kravchenko [ID](#), A. Rohilla [ID](#), J.E. Siado [ID](#), W. Tabb [ID](#), A. Vagnerini [ID](#), A. Wightman [ID](#), F. Yan [ID](#), D. Yu [ID](#)

State University of New York at Buffalo, Buffalo, New York, USA

H. Bandyopadhyay [ID](#), L. Hay [ID](#), H.W. Hsia [ID](#), I. Iashvili [ID](#), A. Kalogeropoulos [ID](#), A. Kharchilava [ID](#), M. Morris [ID](#), D. Nguyen [ID](#), S. Rappoccio [ID](#), H. Rejeb Sfar, A. Williams [ID](#), P. Young [ID](#)

Northeastern University, Boston, Massachusetts, USA

G. Alverson [ID](#), E. Barberis [ID](#), J. Bonilla [ID](#), B. Bylsma, M. Campana [ID](#), J. Dervan [ID](#), Y. Haddad [ID](#), Y. Han [ID](#), I. Israr [ID](#), A. Krishna [ID](#), P. Levchenko [ID](#), J. Li [ID](#), M. Lu [ID](#), R. McCarthy [ID](#), D.M. Morse [ID](#), T. Orimoto [ID](#), A. Parker [ID](#), L. Skinnari [ID](#), C.S. Thoreson [ID](#), E. Tsai [ID](#), D. Wood [ID](#)

Northwestern University, Evanston, Illinois, USA

S. Dittmer [ID](#), K.A. Hahn [ID](#), D. Li [ID](#), Y. Liu [ID](#), M. McGinnis [ID](#), Y. Miao [ID](#), D.G. Monk [ID](#), M.H. Schmitt [ID](#), A. Taliercio [ID](#), M. Velasco [ID](#)

University of Notre Dame, Notre Dame, Indiana, USA

G. Agarwal [ID](#), R. Band [ID](#), R. Bucci, S. Castells [ID](#), A. Das [ID](#), R. Goldouzian [ID](#), M. Hildreth [ID](#), K. Hurtado Anampa [ID](#), T. Ivanov [ID](#), C. Jessop [ID](#), K. Lannon [ID](#), J. Lawrence [ID](#), N. Loukas [ID](#), L. Lutton [ID](#), J. Mariano [ID](#), N. Marinelli, I. McAlister, T. McCauley [ID](#), C. McGrady [ID](#), C. Moore [ID](#), Y. Musienko²² [ID](#), H. Nelson [ID](#), M. Osherson [ID](#), A. Piccinelli [ID](#), R. Ruchti [ID](#), A. Townsend [ID](#), Y. Wan, M. Wayne [ID](#), H. Yockey, M. Zarucki [ID](#), L. Zygalas [ID](#)

The Ohio State University, Columbus, Ohio, USA

A. Basnet [ID](#), M. Carrigan [ID](#), L.S. Durkin [ID](#), C. Hill [ID](#), M. Joyce [ID](#), M. Nunez Ornelas [ID](#), K. Wei, D.A. Wenzl, B.L. Winer [ID](#), B. R. Yates [ID](#)

Princeton University, Princeton, New Jersey, USA

H. Bouchamaoui [ID](#), K. Coldham, P. Das [ID](#), G. Dezoort [ID](#), P. Elmer [ID](#), P. Fackeldey [ID](#), A. Frankenthal [ID](#), B. Greenberg [ID](#), N. Haubrich [ID](#), K. Kennedy, G. Kopp [ID](#), S. Kwan [ID](#), Y. Lai [ID](#), D. Lange [ID](#), A. Loeliger [ID](#), D. Marlow [ID](#), I. Ojalvo [ID](#), J. Olsen [ID](#), F. Simpson [ID](#), D. Stickland [ID](#), C. Tully [ID](#), L.H. Vage [ID](#)

University of Puerto Rico, Mayaguez, Puerto Rico, USA

S. Malik [ID](#), R. Sharma [ID](#)

Purdue University, West Lafayette, Indiana, USA

A.S. Bakshi [ID](#), S. Chandra [ID](#), R. Chawla [ID](#), A. Gu [ID](#), L. Gutay, M. Jones [ID](#), A.W. Jung [ID](#), M. Liu [ID](#), G. Negro [ID](#), N. Neumeister [ID](#), G. Paspalaki [ID](#), S. Piperov [ID](#), J.F. Schulte [ID](#), A. K. Virdi [ID](#), F. Wang [ID](#), A. Wildridge [ID](#), W. Xie [ID](#), Y. Yao [ID](#)

Purdue University Northwest, Hammond, Indiana, USA

J. Dolen [ID](#), N. Parashar [ID](#), A. Pathak [ID](#)

Rice University, Houston, Texas, USA

D. Acosta , A. Agrawal , T. Carnahan , K.M. Ecklund , P.J. Fernández Manteca , S. Freed, P. Gardner, F.J.M. Geurts , T. Huang , I. Krommydas , W. Li , J. Lin , O. Miguel Colin , B.P. Padley , R. Redjimi , J. Rotter , E. Yigitbasi , Y. Zhang 

University of Rochester, Rochester, New York, USA

A. Bodek , P. de Barbaro , R. Demina , J.L. Dulemba , A. Garcia-Bellido , O. Hindrichs , A. Khukhunaishvili , N. Parmar , P. Parygin⁹³ , R. Taus 

Rutgers, The State University of New Jersey, Piscataway, New Jersey, USA

B. Chiarito, J.P. Chou , S.V. Clark , D. Gadkari , Y. Gershtein , E. Halkiadakis , M. Heindl , C. Houghton , D. Jaroslawski , S. Konstantinou , I. Laflotte , A. Lath , J. Martins , R. Montalvo, K. Nash, J. Reichert , P. Saha , S. Salur , S. Schnetzer, S. Somalwar , R. Stone , S.A. Thayil , S. Thomas, J. Vora 

University of Tennessee, Knoxville, Tennessee, USA

D. Ally , A.G. Delannoy , S. Fiorendi , S. Higginbotham , T. Holmes , A.R. Kanuganti , N. Karunaratna , L. Lee , E. Nibigira , S. Spanier 

Texas A&M University, College Station, Texas, USA

D. Aebi , M. Ahmad , T. Akhter , K. Androsov , A. Bolshov, O. Bouhali⁹⁴ , R. Eusebi , J. Gilmore , T. Kamon , H. Kim , S. Luo , R. Mueller , A. Safonov 

Texas Tech University, Lubbock, Texas, USA

N. Akchurin , J. Damgov , Y. Feng , N. Gogate , Y. Kazhykarim, K. Lamichhane , S.W. Lee , C. Madrid , A. Mankel , T. Peltola , I. Volobouev 

Vanderbilt University, Nashville, Tennessee, USA

E. Appelt , Y. Chen , S. Greene, A. Gurrola , W. Johns , R. Kunawalkam Elayavalli , A. Melo , D. Rathjens , F. Romeo , P. Sheldon , S. Tuo , J. Velkovska , J. Viinikainen 

University of Virginia, Charlottesville, Virginia, USA

B. Cardwell , H. Chung , B. Cox , J. Hakala , R. Hirosky , A. Ledovskoy , C. Mantilla , C. Neu , C. Ramón Álvarez 

Wayne State University, Detroit, Michigan, USA

S. Bhattacharya , P.E. Karchin 

University of Wisconsin - Madison, Madison, Wisconsin, USA

A. Aravind , S. Banerjee , K. Black , T. Bose , E. Chavez , S. Dasu , P. Everaerts , C. Galloni, H. He , M. Herndon , A. Herve , C.K. Koraka , A. Lanaro, R. Loveless , A. Mallampalli , A. Mohammadi , S. Mondal, G. Parida , L. Pétré , D. Pinna , A. Savin, V. Shang , V. Sharma , W.H. Smith , D. Teague, H.F. Tsoi , W. Vetens , A. Warden 

Authors affiliated with an international laboratory covered by a cooperation agreement with CERN

S. Afanasiev , V. Alexakhin , Yu. Andreev , T. Aushev , D. Budkouski , M. Danilov⁹⁵ , T. Dimova⁹⁵ , A. Ershov⁹⁵ , I. Golutvin[†] , I. Gorbunov , A. Gribushin⁹⁵ , V. Karjavine , V. Klyukhin⁹⁵ , O. Kodolova^{96,93} , V. Korenkov , A. Kozyrev⁹⁵ , A. Lanev , A. Malakhov , V. Matveev⁹⁵ , A. Nikitenko^{97,96} , V. Palichik , V. Perelygin , S. Petrushanko⁹⁵ , O. Radchenko⁹⁵ , M. Savina , V. Shalaev , S. Shmatov , S. Shulha , Y. Skovpen⁹⁵ , V. Smirnov , O. Teryaev , I. Tlisova⁹⁵ , A. Toropin , N. Voytishin , B.S. Yuldashev⁺⁹⁸ , A. Zarubin , I. Zhizhin 

Authors affiliated with an institute formerly covered by a cooperation agreement with CERN

G. Gavrilov , V. Golovtcov , Y. Ivanov , V. Kim⁹⁵ , V. Murzin , V. Oreshkin , D. Sosnov , V. Sulimov , L. Uvarov , A. Vorobyev[†], A. Dermenev , S. Gninenko , N. Golubev , A. Karneyeu , D. Kirpichnikov , M. Kirsanov , N. Krasnikov , K. Ivanov , V. Gavrilov , N. Lychkovskaya , V. Popov , A. Zhokin , R. Chistov⁹⁵ , S. Polikarpov⁹⁵ , V. Andreev , M. Azarkin , M. Kirakosyan, A. Terkulov , E. Boos , V. Bunichev , M. Dubinin⁸⁵ , L. Dudko , M. Perfilov , V. Savrin , V. Blinov⁹⁵, V. Kachanov , S. Slabospitskii , A. Uzunian , A. Babaev , V. Borshch , D. Druzhkin

[†]: Deceased

¹Also at Yerevan State University, Yerevan, Armenia

²Also at TU Wien, Vienna, Austria

³Also at Ghent University, Ghent, Belgium

⁴Also at Universidade do Estado do Rio de Janeiro, Rio de Janeiro, Brazil

⁵Also at FACAMP - Faculdades de Campinas, Sao Paulo, Brazil

⁶Also at Universidade Estadual de Campinas, Campinas, Brazil

⁷Also at Federal University of Rio Grande do Sul, Porto Alegre, Brazil

⁸Also at University of Chinese Academy of Sciences, Beijing, China

⁹Also at China Center of Advanced Science and Technology, Beijing, China

¹⁰Also at University of Chinese Academy of Sciences, Beijing, China

¹¹Also at China Spallation Neutron Source, Guangdong, China

¹²Now at Henan Normal University, Xinxiang, China

¹³Also at University of Shanghai for Science and Technology, Shanghai, China

¹⁴Now at The University of Iowa, Iowa City, Iowa, USA

¹⁵Also at Cairo University, Cairo, Egypt

¹⁶Also at British University in Egypt, Cairo, Egypt

¹⁷Now at Helwan University, Cairo, Egypt

¹⁸Also at Suez University, Suez, Egypt

¹⁹Also at Purdue University, West Lafayette, Indiana, USA

²⁰Also at Université de Haute Alsace, Mulhouse, France

²¹Also at Istinye University, Istanbul, Turkey

²²Also at an institute formerly covered by a cooperation agreement with CERN

²³Also at The University of the State of Amazonas, Manaus, Brazil

²⁴Also at University of Hamburg, Hamburg, Germany

²⁵Also at RWTH Aachen University, III. Physikalisches Institut A, Aachen, Germany

²⁶Also at Bergische University Wuppertal (BUW), Wuppertal, Germany

²⁷Also at Brandenburg University of Technology, Cottbus, Germany

²⁸Also at Forschungszentrum Jülich, Juelich, Germany

²⁹Also at CERN, European Organization for Nuclear Research, Geneva, Switzerland

³⁰Also at HUN-REN ATOMKI - Institute of Nuclear Research, Debrecen, Hungary

³¹Now at Universitatea Babes-Bolyai - Facultatea de Fizica, Cluj-Napoca, Romania

³²Also at MTA-ELTE Lendület CMS Particle and Nuclear Physics Group, Eötvös Loránd University, Budapest, Hungary

³³Also at HUN-REN Wigner Research Centre for Physics, Budapest, Hungary

³⁴Also at Physics Department, Faculty of Science, Assiut University, Assiut, Egypt

³⁵Also at Punjab Agricultural University, Ludhiana, India

³⁶Also at University of Visva-Bharati, Santiniketan, India

³⁷Also at Indian Institute of Science (IISc), Bangalore, India

³⁸Also at Amity University Uttar Pradesh, Noida, India

³⁹Also at UPES - University of Petroleum and Energy Studies, Dehradun, India

⁴⁰Also at IIT Bhubaneswar, Bhubaneswar, India

⁴¹Also at Institute of Physics, Bhubaneswar, India

⁴²Also at University of Hyderabad, Hyderabad, India

⁴³Also at Deutsches Elektronen-Synchrotron, Hamburg, Germany

⁴⁴Also at Isfahan University of Technology, Isfahan, Iran

⁴⁵Also at Sharif University of Technology, Tehran, Iran

⁴⁶Also at Department of Physics, University of Science and Technology of Mazandaran, Behshahr, Iran

⁴⁷Also at Department of Physics, Faculty of Science, Arak University, ARAK, Iran

⁴⁸Also at Italian National Agency for New Technologies, Energy and Sustainable Economic Development, Bologna, Italy

⁴⁹Also at Centro Siciliano di Fisica Nucleare e di Struttura Della Materia, Catania, Italy

⁵⁰Also at Università degli Studi Guglielmo Marconi, Roma, Italy

⁵¹Also at Scuola Superiore Meridionale, Università di Napoli 'Federico II', Napoli, Italy

⁵²Also at Fermi National Accelerator Laboratory, Batavia, Illinois, USA

⁵³Also at Lulea University of Technology, Lulea, Sweden

⁵⁴Also at Consiglio Nazionale delle Ricerche - Istituto Officina dei Materiali, Perugia, Italy

⁵⁵Also at Institut de Physique des 2 Infinis de Lyon (IP2I), Villeurbanne, France

⁵⁶Also at Department of Applied Physics, Faculty of Science and Technology, Universiti Kebangsaan Malaysia, Bangi, Malaysia

⁵⁷Also at Consejo Nacional de Ciencia y Tecnología, Mexico City, Mexico

⁵⁸Also at INFN Sezione di Torino, Università di Torino, Torino, Italy; Università del Piemonte Orientale, Novara, Italy

⁵⁹Also at Trincomalee Campus, Eastern University, Sri Lanka, Nilaveli, Sri Lanka

⁶⁰Also at Saegis Campus, Nugegoda, Sri Lanka

⁶¹Also at National and Kapodistrian University of Athens, Athens, Greece

⁶²Also at Ecole Polytechnique Fédérale Lausanne, Lausanne, Switzerland

⁶³Also at Universität Zürich, Zurich, Switzerland

⁶⁴Also at Stefan Meyer Institute for Subatomic Physics, Vienna, Austria

⁶⁵Also at Laboratoire d'Annecy-le-Vieux de Physique des Particules, IN2P3-CNRS, Annecy-le-Vieux, France

⁶⁶Also at Near East University, Research Center of Experimental Health Science, Mersin, Turkey

⁶⁷Also at Konya Technical University, Konya, Turkey

⁶⁸Also at Izmir Bakircay University, Izmir, Turkey

⁶⁹Also at Adiyaman University, Adiyaman, Turkey

⁷⁰Also at Bozok Universitetesi Rektörlüğü, Yozgat, Turkey

⁷¹Also at Marmara University, Istanbul, Turkey

⁷²Also at Milli Savunma University, Istanbul, Turkey

⁷³Also at Kafkas University, Kars, Turkey

⁷⁴Now at Istanbul Okan University, Istanbul, Turkey

⁷⁵Also at Hacettepe University, Ankara, Turkey

⁷⁶Also at Erzincan Binali Yıldırım University, Erzincan, Turkey

⁷⁷Also at Istanbul University - Cerrahpasa, Faculty of Engineering, Istanbul, Turkey

⁷⁸Also at Yildiz Technical University, Istanbul, Turkey

⁷⁹Also at School of Physics and Astronomy, University of Southampton, Southampton, United Kingdom

⁸⁰Also at IPPP Durham University, Durham, United Kingdom

⁸¹Also at Monash University, Faculty of Science, Clayton, Australia

⁸²Also at Università di Torino, Torino, Italy

⁸³Also at Bethel University, St. Paul, Minnesota, USA

⁸⁴Also at Karamanoğlu Mehmetbey University, Karaman, Turkey

⁸⁵Also at California Institute of Technology, Pasadena, California, USA

⁸⁶Also at United States Naval Academy, Annapolis, Maryland, USA

⁸⁷Also at Ain Shams University, Cairo, Egypt

⁸⁸Also at Bingol University, Bingol, Turkey

⁸⁹Also at Georgian Technical University, Tbilisi, Georgia

⁹⁰Also at Sinop University, Sinop, Turkey

⁹¹Also at Erciyes University, Kayseri, Turkey

⁹²Also at Horia Hulubei National Institute of Physics and Nuclear Engineering (IFIN-HH), Bucharest, Romania

⁹³Now at another institute formerly covered by a cooperation agreement with CERN

⁹⁴Also at Texas A&M University at Qatar, Doha, Qatar

⁹⁵Also at another institute formerly covered by a cooperation agreement with CERN

⁹⁶Also at Yerevan Physics Institute, Yerevan, Armenia

⁹⁷Also at Imperial College, London, United Kingdom

⁹⁸Also at Institute of Nuclear Physics of the Uzbekistan Academy of Sciences, Tashkent, Uzbekistan